Università degli Studi di Padova
Dipartimento di Scienze Chimiche
Corso di Laurea Magistrale in Chimica

Tesi di Laurea Magistrale

Light-triggered Catalytic Asymmetric Allylic Benzylation of Isatin-derived MBH Carbonates

Relatore: Dott. Luca Dell'Amico
Supervisore: Dott. Xavier Companyó
Controrelatore: Prof. Donatella Carbonera

Laureanda: Michela Marcon

Anno Accademico 2018/2019

È facile comprendere le vicende umane se si tiene conto che gran parte dei trionfi e delle tragedie della storia non sono causati da uomini irrimediabilmente buoni o cattivi, ma da uomini che sono irrimediabilmente umani.

— *Terry Pratchett & Neil Gaiman*

Prefazione

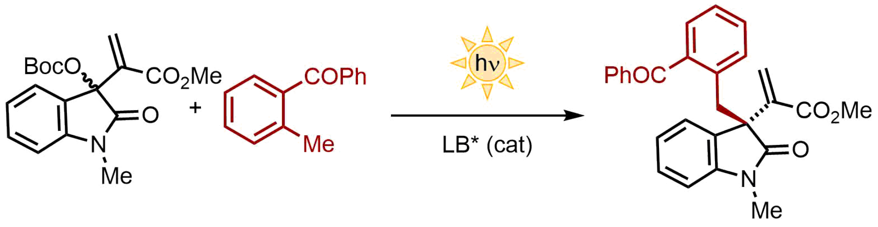

In sintesi organica, tra i più floridi ambiti di ricerca vi è la creazione di nuovi legami carbonio-carbonio. Il controllo della formazione di legami C-C fornisce infatti nuove e sempre più complesse classi di molecole. Un'ulteriore sfida è lo sviluppo di nuovi metodi sintetici che forniscano, in maniera enantioselettiva, centri chirali *all-carbon*. Questi centri sono spesso il punto chiave per l'accesso alle sintesi totali di molecole complesse e di grande valore, quali sono i prodotti naturali. Il crescente interesse verso la tutela dell'ambiente sta dirigendo sempre più la ricerca verso soluzioni che rispettino i principi della Green Chemistry: atom economy, solventi meno inquinanti, condizioni di reazione più blande e utilizzo di risorse rinnovabili. La fotochimica e l'organocatalisi, co-protagoniste di questo progetto di tesi, sono in pieno accordo con i principi della Green Chemistry. Lo sviluppo di nuove trasformazioni attivate dalla luce, assieme all'impiego di catalizzatori organici permettono infatti di lavorare in condizioni più blande e con meno sprechi di energia. Questo progetto di tesi è incentrato sull'ottimizzazione della reazione di alchilazione allilica, con l'utilizzo di un nucleofilo non stabilizzato che viene attivato dalla luce. Al momento esistono pochissimi esempi di alchilazione allilica asimmetrica con nucleofili non stabilizzati, e nessuno di questi organocatalizzato. Gli elettrofili utilizzati per questo progetto sono i carbonati Morita-Baylis-Hillman (MBH) derivati dall'isatina, una molecola naturale bioattiva. A partire dal carbonato racemico, si forma un nuovo centro quaternario *all-carbon* in maniera enantioselettiva attraverso una doppia attivazione. L'organocatalizzatore chirale attiva l'elettrofilo e trasferisce l'informazione chirale, mentre la luce attiva il derivato del 2-metilbenzofenone per formare l'intermedio come nucleofilo al carbonio non stabilizzato. Inoltre, la reazione è stata ottimizzata in reattore microfluidico per la sintesi continua in flusso.

Abstract

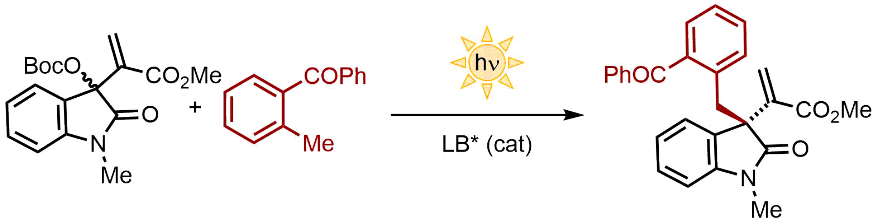

The formation of new C-C bonds is among the most thriving fields of research in synthetic organic chemistry. In fact, novel C-C bond-forming transformations give access to new, unprecedented carbon backbones. An even more challenging goal is the development of synthetic methods able to forge quaternary *all-carbon* centres in an enantioselective fashion, that allow the synthesis of complex, valuable molecules like natural products. The growing attention to environment is now directing research towards greener chemical solutions: atom economy, environmentally friendly solvents, mild reaction conditions, and the use of renewable resources. Photochemistry and organocatalysis, the two co-protagonists of this thesis project, are in full agreement with the principles of Green Chemistry. The development of light-triggered transformations along with the employment of purely organic chiral catalysts allow milder reaction conditions, thus energy saving. This thesis project is focused on the development and the optimisation of the asymmetric allylic alkylation reaction, using non-stabilised, photo-generated nucleophiles. To the best of our knowledge, only very few examples of asymmetric allylic alkylation with non-stabilised nucleophiles have been reported, and none of them through an organocatalysed strategy. For this purpose, Morita-Baylis-Hillman (MBH) carbonates derived from isatin, a biologically active molecule, are selected as electrophiles. Starting from racemic MBH carbonates, quaternary *all-carbon* stereocentres are created in an enantioselective fashion via a dual activation strategy. The chiral organocatalyst activates the electrophile and is responsible for the stereoinduction event, while light irradiation activates the 2-methylbenzophenone derivative to form the photoenol intermediate as non-stabilised C-nucleophile. In addition, the reaction is also optimised under a microfluidic photoreactor for *in-flow* continuous synthesis.

Contents

1 Introduction 11
- 1.1 Asymmetric Synthesis . . . 12
- 1.2 Catalysis and Organocatalysis . . . 15
  - 1.2.1 Cinchona Alkaloids . . . 17
- 1.3 Asymmetric Allylic Alkylation . . . 18
- 1.4 Photochemistry . . . 20
  - 1.4.1 Photoenol . . . 22
- 1.5 Microfluidics in Photochemical Reactions . . . 25

2 Results and Discussion 27
- 2.1 Development of the Reaction . . . 27
- 2.2 Synthesis of the Starting Materials . . . 28
- 2.3 Optimisation of the Reaction in Batch . . . 29
- 2.4 Characterisation of the Catalytic Intermediate . . . 37
- 2.5 Optimisation of the Reaction in Flow . . . 46
- 2.6 Scope . . . 49

3 Conclusions 53

4 Experimental 55
- 4.1 General procedure for preparation of substituted 2-methylbenzophenones . . . 55
- 4.2 General procedure for preparation of N-methyl-isatins . . . 56
- 4.3 General procedure for preparation of MBH alcohols . . . 57
- 4.4 General procedure for preparation of MBH carbonates . . . 58
- 4.5 General procedure for allylic benzylation . . . 60
- 4.6 Screening of the reaction conditions for microfluidic setup . . . 61
  - 4.6.1 Upscaling of flow reaction . . . 62
- 4.7 Characterisation of the benzylated products . . . 62
- 4.8 Synthesis and characterisation of intermediates IIIa and IIIa' . . . 67
- 4.9 X-Ray Structure and Absolute Configuration of Compound 4a . . . 68
- 4.10 NMR Spectra . . . 71
- 4.11 HPLC Traces . . . 84

References 97

Acknowledgements 99

Chapter 1

Introduction

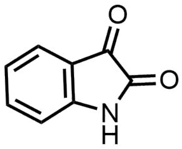

Heterocyclic compounds are an important class of organic compounds having a crucial role in both biological and pharmacological fields. Isatin (1H-indole-2,3-dione) is a heterocyclic molecule formed by a six-membered ring fused to a five-membered ring bearing a ketone in $\alpha$to an amide group. Both rings are planar. The six-membered ring presents aromatic character, whereas the five-membered ring possesses an anti-aromatic character. Isatin was first discovered by Erdmann and Laurent as the oxidation product of indigo. It is found in humans and other mammals as an endogenous molecule, though its metabolic pathway is not yet fully understood.[1]

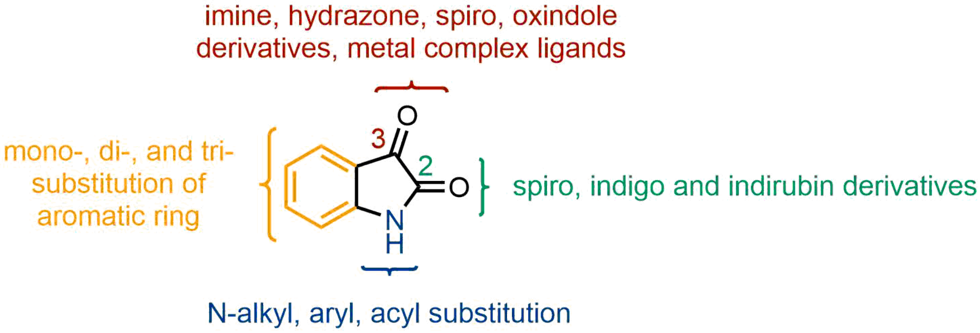
imine, hydrazone, spiro, oxindole derivatives, metal complex ligands
mono-, di-, and tri-substitution of aromatic ring
3
2
spiro, indigo and indirubin derivatives
N-alkyl, aryl, acyl substitution

Figure 1.1: The different functionalisation sites of isatin.[2]

As shown in *Figure 1.1*, isatin can be easily functionalised, due to the diversity of its functionalisation sites, thus a large variety of new compounds can be synthesized from it. Isatin and its derivatives are known to be biologically active molecules and are widely used in industry as dyes and for electronics applications.[2,3] In particular, 3,3-disubstituted oxindoles are of great value for their biological activity and structural complexity, and they already found application in the pharmaceutical field,[4,5] as shown in *Figure 1.2*. Moreover, it has been demonstrated that the 3D arrangement of a molecule, intended as the sp^3 character of the carbon centres, results in an enhancement of bioactivity. The well-defined 3D structure along with the enhanced conformational rigidity offer distinctive features for new drug candidates, such as enhanced drug-target recognition or improved physico-chemical properties. A bigger library of structural isomers and stereoisomers becomes also available, allowing a better fine-tuning of the ligand/receptor complementarity, thus affording a better targeting with less side effects.[6]

Being isatin a versatile and inexpensive compound, I selected it as starting material to develop new types of reactivity along with novel functionalisations that can result, ideally, in a new class of useful compounds.

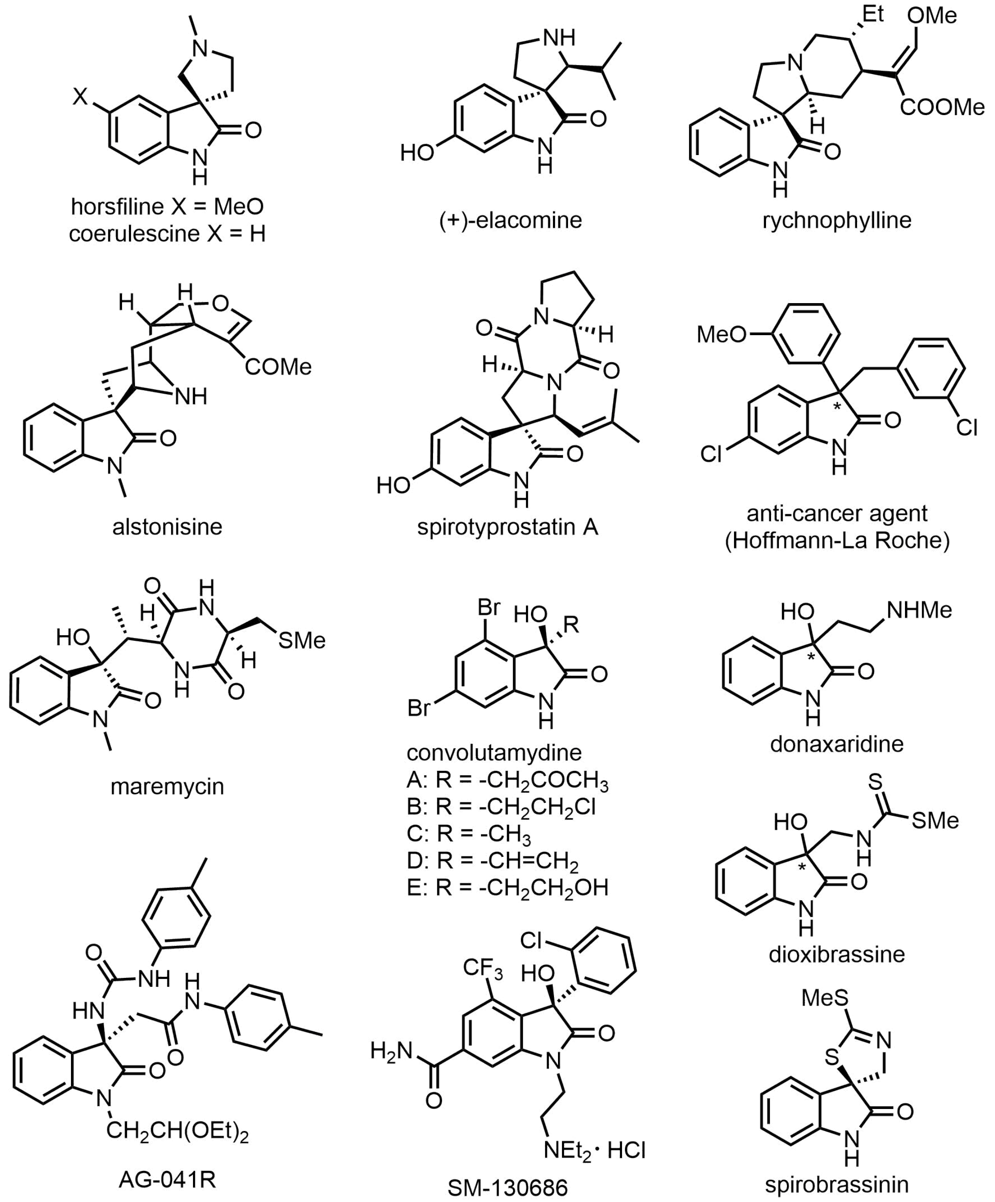
horsfiline X = MeO
coerulescine X = H
(+)-elacomine
rychnophylline
alstonisine
spirotyprostatin A
anti-cancer agent
(Hoffmann-La Roche)
maremycin
convolutamydine
A: R = -CH2COCH3
B: R = -CH2CH2Cl
C: R = -CH3
D: R = -CH=CH2
E: R = -CH2CH2OH
donaxaridine
dioxibrassine
AG-041R
SM-130686
spirobrassinin

Figure 1.2: Some examples of bioactive 3,3-disubstituted oxindoles[5]

1.1 Asymmetric Synthesis

Asymmetric synthesis consists in the selective synthesis of one of the two enantiomers of a chiral molecule. It is of great importance for preparing the precursors for the total synthesis of natural products, and for the production of efficient pharmaceuticals. A chiral molecule is any molecule that does not present a plane of symmetry, and therefore is not superimposable with its mirror image.[7] These two mirror images are called enantiomers and show, in achiral environment, exactly the same properties. Conversely, in a chiral environment they present different properties, owing to the interactions with other chiral molecules, called *diastereomeric interactions.* Later on, in 1832 Jean Baptiste Biot observed the optical activity of natural D-tartaric acid. Another form of tartaric acid was also known with the same properties but no optical activity, and it was called *racemic acid*. In 1848 Louis Pasteur separated manually the crystals of synthetic L- and D-tartrate salts. He observed that the two types of crystals yielded opposite rotation of plane polarised light, while the mixture of the two would cancel the optical activity reciprocally. So, chirality was discovered. Chiral molecules that are the main building blocks of living organisms, such as aminoacids and carbohydrates, are present in nature in only one of the two enantiomeric forms. This fact causes the overall intrinsic asymmetry of the living beings, from the right-handedness of the DNA, to the left position of the heart in human beings.[7] Therefore, knowledge and control on the interactions of chiral molecules in a chiral environment is of vital importance, since it regards ourselves and everyday life, for instance to develop new and more efficient bioactive compounds. It is well known that the distinct diastereomeric interactions of the two enantiomers of a drug with the chiral receptors present in our body can result in inactivity or even in detrimental side effects for one of the two enantiomers.[8]

A sadly famous example of the different biological activity of two enantiomers is the case of thalidomide (shown in *Figure 1.3*), an antiemetic drug for pregnant women that was commercialised in the late ‘50s as a racemic mixture. While the *(R)*-enantiomer gave the expected effect, the *(S)*-enantiomer was discovered to be a teratogenic agent, causing thousands of cases of malformation in new-born babies.[9] Thus, this case raised the attention of the organic chemists on the importance of producing enantiopure pharmaceuticals. The use of asymmetric synthesis plays nowadays a crucial role, and developments are constantly arising. There are different strategies towards asymmetric synthesis (shown in *Figure 1.4*): chiral resolution, synthesis from the chiral pool, the use of chiral auxiliaries and asymmetric catalysis.

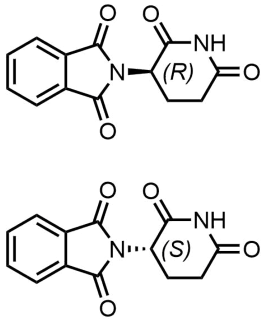

Figure 1.3: The two enantiomers of thalidomide, the *(R)*- with antiemetic effect (top) and the *(S)*- causing phocomelia in newborn babies (bottom)

Chiral resolution It consists in the separation of a racemic mixture by exploiting the different physicochemical properties (i.e. solubility) of the diastereomeric salts of the racemic compound with an enantiopure compound (resolving agent). This method is useful if both enantiomers are needed, otherwise it has a huge limitation: since it starts from a racemic mixture, the maximum theoretical yield of one enantiomer is 50%, while the other 50% is wasted.

Chiral pool A second approach is to start from a readily available enantiopure compound, known as the *chiral pool*, and derivatise it by using stereospecific transformations. This method also presents important limitations, since there may not be suitable starting materials for the product of interest or the number of required steps could be very high, reducing the overall yield of the desired final product.

Chiral auxiliary The third strategy is the use of chiral auxiliaries, enantiopure molecules that can be easily attached to the achiral substrate, affording an enantiopure adduct. Then, the intended diastereoselective reaction forges a new stereocentre, furnishing preferably one of the two possible diastereoisomers. Subsequently, the chiral auxiliary is removed, affording the enantioenriched product.[7] The limita-

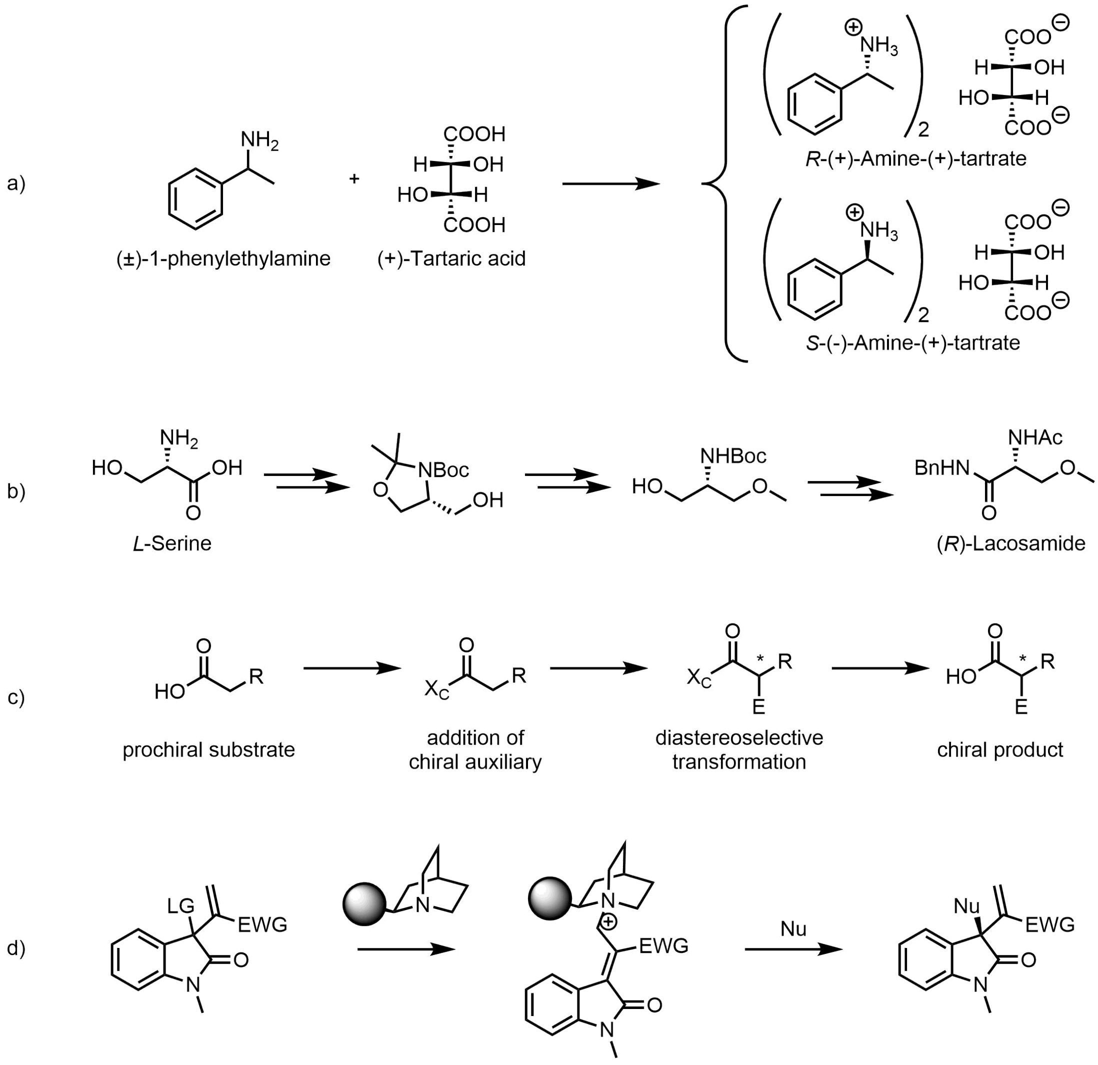
a)
NH2
(±)-1-phenylethylamine
+
COOH
H OH
HO H
COOH
(+)-Tartaric acid
NH3
2
COO
R-(+)-Amine-(+)-tartrate
S-(-)-Amine-(+)-tartrate
b)
NH2
HO
OH
O
L-Serine
NBoc
O
OH
NHBoc
HO
O
NHAc
BnHN
(R)-Lacosamide
c)
HO
R
X_C
*
E
prochiral substrate
addition of chiral auxiliary
diastereoselective transformation
chiral product
d)
LG
EWG
N
O
Nu

Figure 1.4: Representative examples of chiral resolution (a) and asymmetric synthesis: from the chiral pool (b), with chiral auxiliary (c) and asymmetric catalysis (this work, d)

tion of this method is the need of a stoichiometric quantity of the chiral auxiliary. Moreover, two additional steps are required: the addition of the chiral auxiliary and the removal after the reaction is completed. These two steps contribute to lower the overall yield as well as the chemical efficiency of the process.

Asymmetric catalysis The last method consists in the use of a substoichiometric amount of a chiral compound that has the dual function of substrate activation and transfer of the chiral information. The enantiopure catalyst interacts with the inactive substrate, activating it and directing the bond-formation event. Once the transformation has occurred, the chiral catalyst unbinds and is ready for a new transformation, affording an enantiomerically enriched product in a single step, making it possible to amplify the chiral information. This method has many advantages: it is more general and thus can be applied to a larger variety of substrates, and the theoretical yield and enantiomeric excess can reach up to 100%. Thus, modern organic synthesis is now focusing on this greener and more efficient approach to asymmetric synthesis.

1.2 Catalysis and Organocatalysis

Catalysis consists in the enhancement of the rate of a reaction due to a substoichiometric amount of a catalyst, that is ideally recovered unaffected at the end of the reaction.[10] The action of the catalyst consists in lowering the activation energy of the reaction through a more advantageous reaction pathway with respect to the non-catalysed reaction. Catalysts can be broadly divided into:

- Transition-metals based catalysts: historically the most widely used, for the diversity of metal centres and the possibility to finetune the metals' properties by changing their ligands. There are some issues regarding the lability, the toxicity and the waste disposal for this type of catalysts.
- Biocatalysis: the most selective and efficient since they work at physiological conditions. However, it is the most difficult to use from a synthetic perspective due to their cost, as well as their great mechanistic complexity.
- Organocatalysis: consists in the use of small purely organic molecules to activate substrates, such as phosphines, secondary and tertiary amines, carbenes, thioureas or phosphoric acids, amongst others.

Organocatalysis is a relatively recent field, even though it is known that it had a key role in the formation of prebiotic molecules and in the generation of homochirality in living beings.[10] The main goal of modern organocatalysis is the use of organic catalysts in asymmetric synthesis. Asymmetric catalysis makes use of enantiopure catalysts that create diastereomeric interactions with the substrate, so that the formation of one of the two enantiomers will be kinetically favoured, resulting in an enantiomeric enrichment of the desired product. The origins of organocatalysis can be dated back to 1912, when Bredig reported the addition of HCN to aromatic aldehydes **10** catalysed by cinchona alkaloids (*Figure 1.5*). The cyanohydrin product **12** was obtained in opposite asymmetric induction by switching from quinine (**8**) to quinidine (**9**), albeit in low enantiomeric excesses (<10% ee).[11]

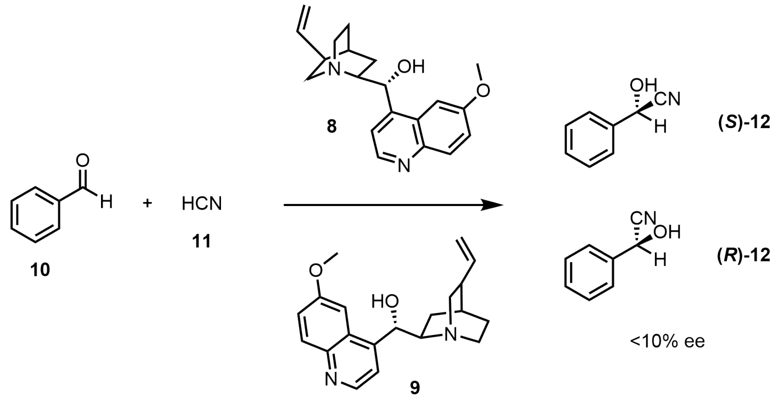

Figure 1.5: The organocatalysed addition of HCN to aldehydes, discovered by Bredig and Fiske in 1912.

In recent years, asymmetric organocatalysis has experienced a fast-growing interest for its numerous advantages. Organic catalysts are generally more stable and less toxic with respect to their organometallic counterparts. In addition, they are usually commercially available and less expensive. Stability, in particular, makes the reaction conditions more accessible, increasing the reproducibility and operational simplicity.[12]

Furthermore, since either they are mostly obtained from the chiral pool and they are easily modified in order to fine-tune their stereoelectronic properties, organocatalysts are particularly suitable for asymmetric synthesis. For instance, the addition of bulky groups commonly increases the efficiency of the asymmetric induction via steric shielding; the addition of hydrogen-bond donor or acceptor moieties improves the directionality and the tightness of the interaction in the transition state; while electron-donating or electron-withdrawing groups might enhance the nucleophilicity and electrophilicity of the catalyst, respectively. A paradigmatic example of organocatalyst is L-proline, a natural aminoacid which contains a pyrrolidine ring. The nucleophilic secondary amine moiety is able to condense with carbonyls to form the reactive enamine intermediate, while the chiral carboxylic acid residue is able to transfer the chiral information during the bon-formation event. The availability of both enantiomers and the numerous possibilities of functionalisation has made proline one of the most used organocatalysts, since its first appearance in 1971 in the Hajos-Parrish-Eder-Sauer-Wiechert reaction.[13,14]
In 2000, List, Lerner and Barbas used proline as catalyst for the intermolecular asymmetric aldol reactions between aromatic aldehydes and α-enolisable ketones. Further, they postulated the dual activation of proline to both the nucleophile and the electrophile, operated by the secondary amine and the carboxylic acid respectedly.[15]

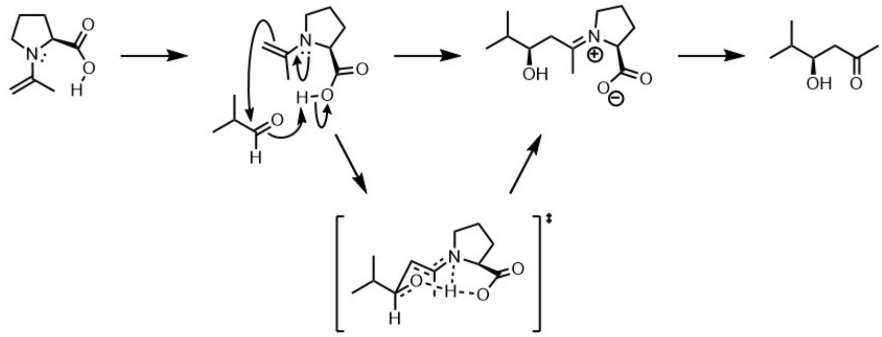

Figure 1.6: The mechanism of activation of the asymmetric aldol reaction by proline.

In the same year, MacMillan's group developed an imidazolidinone catalyst derived from phenylalanine, for a highly enantioselective Diels-Alder cycloaddition between α,β-unsaturated aldehydes with dienes.[16]

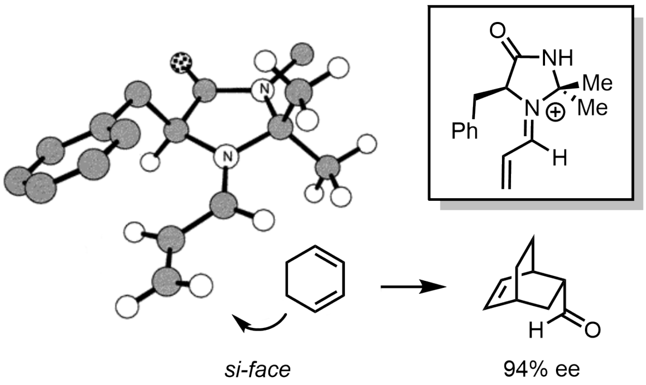

Figure 1.7: Structure of the chiral activated iminium ion, formed upon condensation between the α,β-unsaturated aldehyde with the imidazolidinone catalyst.[16]

In this case, the catalyst forms a hindered chiral iminium ion, directing preferentially the nucleophilic attack by the *Si*-face of the electrophilic conjugated π-system. In *Figure 1.7* is shown the original example reported by MacMillan and co-workers. Remarkably, these two reports are currently considered as the birth of modern organocatalysts. Further, they set the basis of the two main activation modes in covalent aminocatalysis: the HOMO-rising[15] and the LUMO-lowering[16] strategies. Another remarkable advantage of organocatalysis is predictability: there are few, well-known activation mechanisms, and they are generalisable to a large number of different reactions.[17] Although they can be grouped using different criteria, the most common classification is according the nature of the interaction between the substrate and the catalyst, between covalent and non-covalent activation.[18]

- Covalent activation: the catalyst binds covalently to the substrate generating the activated species. After the bond-formation step, the activated species is hydrolysed forming the final product while releasing the catalyst. This class of activation includes enamine activation (HOMO-rising), iminium ion activation (LUMO-lowering) or SOMO activation, amongst others.

- Non-covalent activation: the catalyst activates the substrate and directs the bond-formation event via non-covalent interaction such as hydrogen-bonding or ion pairing. Examples of non-covalent catalysts are chiral thioureas and squaramides, phase-transfer catalysis or chiral Brønsted acid.

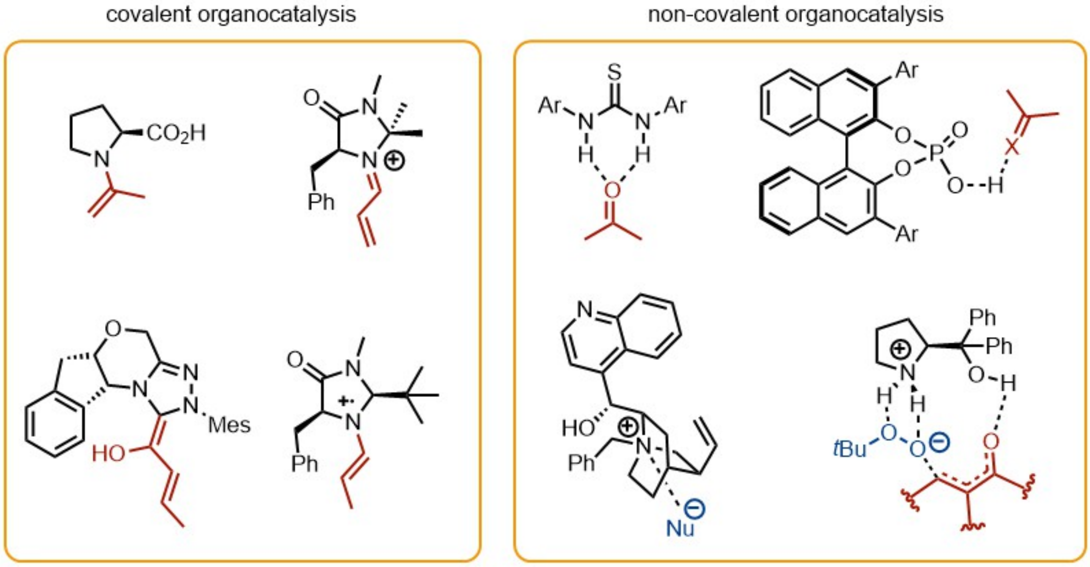

Figure 1.8: Examples of covalent and non-covalent activation in organocatalysis.[19]

It should be noticed that many organocatalysts present multiple active sites and consequently can simultaneously activate both the nucleophile and the electrophile, as already mentioned for proline (see *Figure 1.6*). These are known as multifunctional catalysts.[20] Moreover the same catalyst can work under different activation modes, depending on the substrate.

1.2.1 Cinchona Alkaloids

Cinchona alkaloids are natural bioactive molecules, extracted from the bark of the Cinchona trees, historically used as medicaments. They are constituted by two main parts: a quinoline ring and a substituted chiral 1-azabicyclo[2.2.2]octane moiety, joined together through a stereogenic carbon that bears a secondary alcohol.[21] In organic synthesis they are often employed as chiral Brønsted and Lewis bases. They are available as two pseudoenantiomeric forms, that usually provide opposite enantiomers with almost identical enantioselectivity.[22] Their high versatility brought to a great library of synthetic derivatives. Of particular interest is the β-isoquinidine **2c**, that contains an oxazatwistane ring. This ring, having less conformational flexibility, presents reduced steric hindrance at the quinuclidine nitrogen, thus increasing the basicity and the nucleophilicity of the tertiary amine.[22] Moreover, the removal of the methyl group in **2c** affords β-isocupreidine **2a**, that contains an aromatic hydroxy group that either can hydrogen-bond with the substrate or can be further functionalised to tune the catalyst properties. Thus, β-isocupreidineis a multifunctional catalyst which presents a highly nucleophilic tertiary amine and a hydrogen-bond donor site. In the present thesis work, β-isocupreidine has been proven as the best performing catalyst.

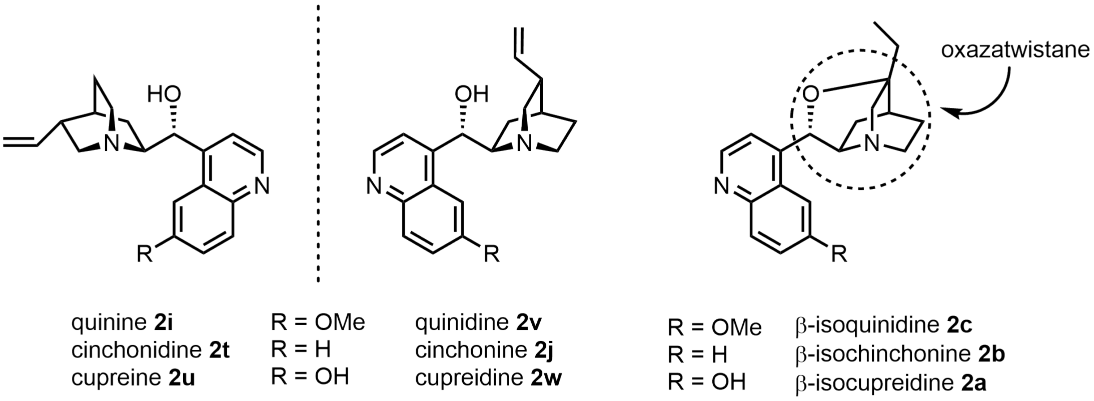
HO
N
N
R
OH
N
N
R
oxazatwistane
O
N
N
R
quinine **2i**
cinchonidine **2t**
cupreine **2u**
R = OMe
R = H
R = OH
quinidine **2v**
cinchonine **2j**
cupreidine **2w**
R = OMe
R = H
R = OH
β-isoquinidine **2c**
β-isochinchonine **2b**
β-isocupreidine **2a**

Figure 1.9: Natural cinchona alkaloids and their synthetic derivatives.

1.3 Asymmetric Allylic Alkylation

Asymmetric allylic alkylation is considered nowadays one of the most powerful strategies to make C-C bonds enantioselectively. It was first developed in 1965 by Tsuji and co-workers, using a stoichiometric allylpalladium complex as the activated electrophile.[23] Subsequently, the group of Trost[24] improved the method adding triphenylphosphine as a ligand on palladium, making the transformation catalytic. Further, in 1977 the same group developed the first asymmetric version,[25] by using Pd together with a chiral phosphine ligand.

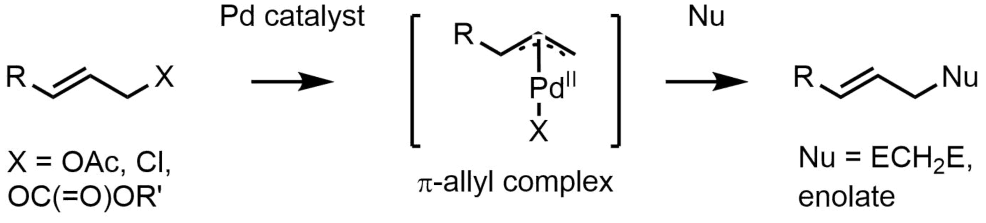
Pd catalyst
R
X
X = OAc, Cl,
OC(=O)OR'
R
Pd^II
X
π-allyl complex
Nu
R
Nu
Nu = ECH2E,
enolate

Figure 1.10: The Tsuji-Trost reaction.

The great innovation with respect to other asymmetric metal-catalysed reactions lies in the fact that, from racemic, achiral or prochiral starting materials, the transformation converges quantitatively to only one enantiomer of the product.[26] This is due to the loss of the stereocentre in the formation of the electrophilic π-allyl complex.

Thus, the stereoinducing event is controlled by the chiral palladium complex catalysts. Trost also identified two different mechanisms according to the different nature of the nucleophile: stabilised or "soft" nucleophiles maintain the stereochemistry of the complex, because they directly attack the allylic position, while unstabilised, or "hard" nucleophiles attack the palladium centre, resulting in an inversion of the stereochemistry with respect to the starting material (*Figure 1.11*). Several synthetically useful transformations have been established using stabilised nucleophiles, while the efficient use of non-stabilised nucleophiles is much more challenging and to date only very few examples are reported.

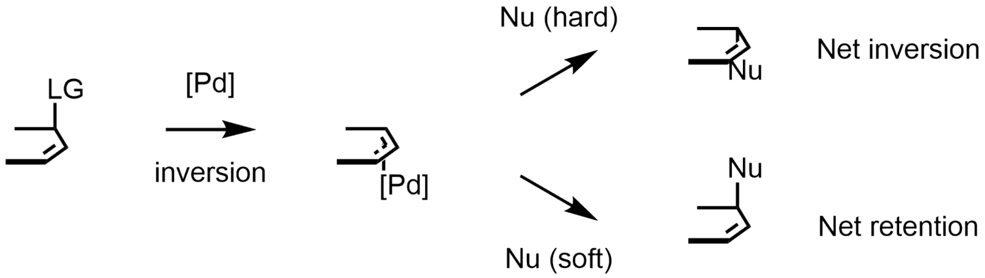

Figure 1.11: The different mechanisms of Pd-catalysed allylic alkylation, according to the nature of the nucleophile.

In 2002 the first organocatalytic asymmetric allylic substitution was reported by Kim,[27] using Baylis-Hillman acetates as the allylic electrophiles, and cinchona alkaloids as chiral catalysts (*Figure 1.12*). Interestingly, a double selectivity is operative in this transformation. Firstly, the kinetic resolution in the formation of the diastereomeric salt **XIII** with the chiral catalyst, and subsequently the asymmetric induction in the nucleophile addition step to **XIII**, that generates the alcohol **14**. Two years later, Krische reported the deracemisation of MBH acetates using a chiral phosphine as catalyst, obtaining therefore a dynamic resolution in the first step.[28]

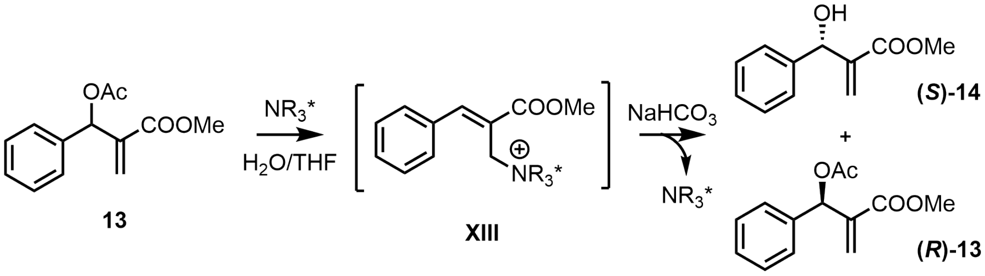

Figure 1.12: The first enantioselective catalytic allylic substitution.

The mechanism, summarised in *Figure 1.13*, starts with the attack of the tertiary amine on the alkene moiety of the MBH carbonate **15**, ionising the leaving group *via* an S_N2' mechanism and forming the electrophilic catalytic intermediate **XV**. Subsequently, the nucleophile performs a second S_N2' to the allylic position of the catalytic species, releasing the catalyst which is ready for a new catalytic turnover while furnishing the final product.[29]

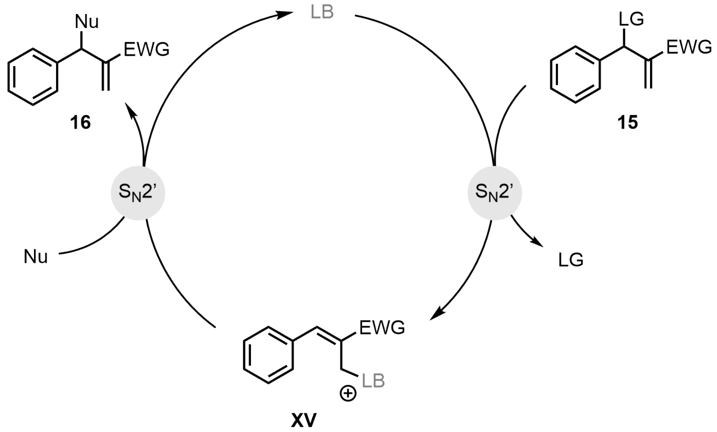

Nu
EWG
16
LB
LG
EWG
15
S_N2'
S_N2'
Nu
LG
EWG
LB
XV

Figure 1.13: The S_N2'-S_N2' mechanism of the organocatalytic asymmetric allylic alkylation.

Since then, extensive study has been done. MBH derivatives are suitable for asymmetric allylic alkylation and their carbonates and acetates have been widely studied, because of the facile transformation of the allylic alcohol into a better leaving group. Chen and co-workers were the first to report in 2010 a highly stereo- and enantioselective allylic alkylation of isatin-derived MBH carbonates, using β-isocupreidine as the chiral Lewis base (*Figure 1.14*).[30] Many stabilised nucleophiles have been tested on MBH carbonates with good results: N-nucleophiles[31] also with less nucleophilic partners, like aromatic amines,[32] O-nucleophiles and C-nucleophiles.[33–35] So far, only few attempts with non-stabilised nucleophiles have been reported, all with metal catalysis,[36,37] while there are no reports in organocatalysis.

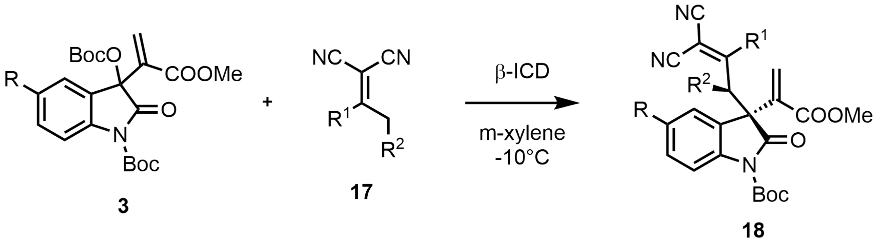

BocO
COOMe
R
O
N
Boc
3
+
NC
CN
R1
R2
17
β-ICD
m-xylene
-10°C
NC
NC
R1
R2
R
COOMe
O
N
Boc
18

Figure 1.14: The first organocatalytic asymmetric allylic alkylation forging a quaternary *all-carbon* stereocentre, by Chen and co-workers.

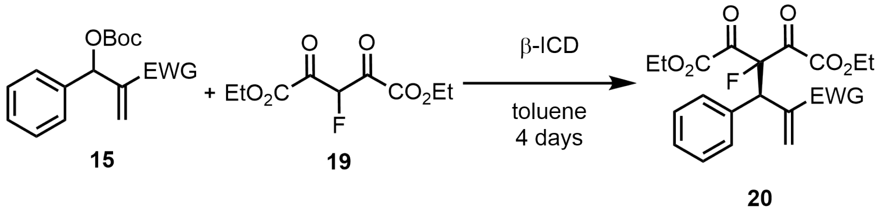

OBoc
EWG
15
+ EtO2C
O
O
CO2Et
F
19
β-ICD
toluene
4 days
O
O
EtO2C
CO2Et
F
EWG
20

Figure 1.15: Example of asymmetric allylic alkylation with 2-fluoromalonate **19**, a stabilised C-nucleophile.[34]

1.4 Photochemistry

Photochemistry is intended as the study of chemical reactions and physical changes resulting from interactions between matter and visible or ultraviolet light.[38] The first photochemical organic reactions were developed by Paternò in 1909 (*Figure 1.16*) and Ciamician in 1912 (*Figure 1.17*). Ciamician already foresaw the necessity of a replacement of coal and non-renewable resources with the way greener sunlight. His numerous studies included the reactivity of alcohols and ketones under light irradiation and the light degradation of terpenes and alkaloids.[39]

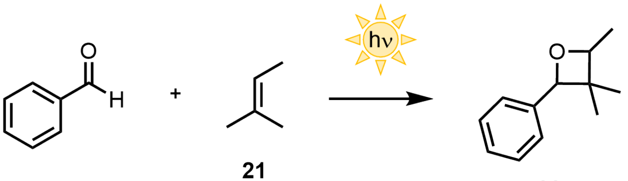

Figure 1.16: The Paternò-Büchi reaction, synthesising an oxetane ring from benzaldehyde and an alkene.

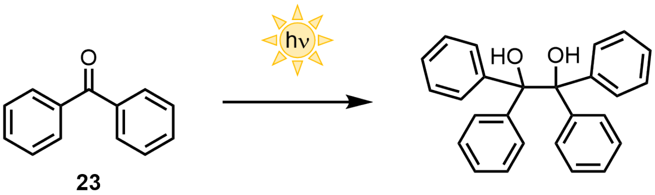

Figure 1.17: The photo-induced coupling of benzophenone, discovered by Ciamician.

Photochemistry is a useful tool in organic synthesis, because light irradiation can generate highly reactive species under mild conditions and with minimum generation of waste, in accordance with the Green Chemistry principles.[40]

The main difference between light activation and thermal activation lies in the way the reactive intermediate is reached. An electronically excited state has approximately the same configuration of the nuclei as the ground state, but different electronic distribution and different polarisation, or eventually radical nature. Thus, compared to the ground state, the excited state is much more energetic. Once excited by light, the molecule can either undergo back conversion to the ground state or conversion to a different intermediate, thus exploring different energetic levels and different configurations. On the other hand, thermal generation of an intermediate is usually a slow step, that requires to overcome a high activation barrier. Thus, generally, more harsh conditions are required, such as high/low pH, high temperature, high pressure, etc. Instead, a photochemical reaction starts already from a highly energetic state (the electronically excited state of the molecule), and the process of formation of the intermediate is just an exothermic decay with a very low energy barrier (*Figure 1.18*). In fact, photochemical reactions are not generally influenced by experimental conditions, provided that the experimental conditions themselves do not change the nature of the excited state. This feature is particularly useful because the intermediates can be generated and reacted in cryogenic conditions, and even labile compounds can react, due to the fact that nor heat neither harsh chemicals are commonly needed for photochemical substrate activation.[41] Nevertheless, photochemistry presents some disadvantages, since light is a new reaction variable to be controlled. Thus, the main relevant parameters are irradiation wavelength and light intensity. The irradiation wavelength can be carefully controlled relatively easily, using lamps with a broader or sharper emission spectrum, according to reaction requirements. On the other hand, light intensity is a bit more tricky since it depends on the lamp type, that should also be changed frequently in order to grant re-

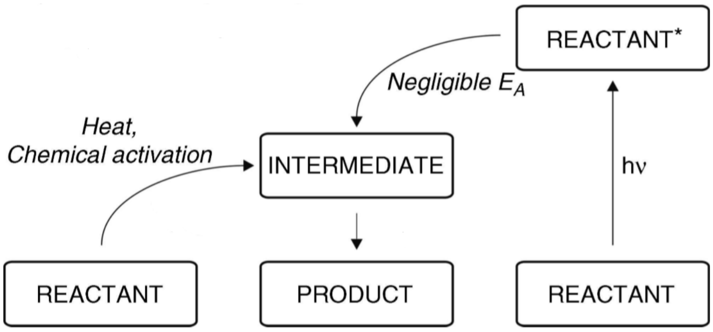

Figure 1.18: Schematic representation of the thermal and photochemical generation of a general reactive intermediate, which subsequently evolves to product formation.

producibility, on the material of the reaction vessel (it is preferable if it is not absorbing at the working wavelength), on the shape of the vessel, on the distance from the light source, on the solvent (which can also absorb at the working wavelength), and on the concentration. According to the Lambert-Beer law $\frac{I}{I_0} = e^{-k_\lambda l}$, the intensity I_0 of light will decrease exponentially with the thickness l of the solution, irradiating efficiently only the most superficial layers, thus making the up-scaling of photochemical reactions an open challenge. Moreover, there could be other species in solution absorbing at the same wavelength, like for instance, the product itself. This is the so called *inner filter effect*, and it is a problem since it reduces the photon flux to the reacting mixture. Also, the product can undergo secondary unwanted side-reactions or light degradation. These problems can be partly resolved by choosing an adequate wavelength at which the product does not absorb, or by subtracting the product from light irradiation as soon as it is formed, for instance with the aid of a microfluidic reactor, which will be introduced in Section 1.5.

1.4.1 Photoenol

The reactivity of photogenerated hydroxy-*o*-quinodimethanes was discovered in 1961 by Yang and Rivas. By irradiation of a 2-methylbenzophenone **1** solution in methanol-d_4 with a Hg arc lamp, deuteration occurred, and the deuterium atoms were only found in the benzylic position, while no deuteration occurred in the case of the reaction in dark.[42] Subsequently, the photoenol intermediate was trapped in a Diels-Alder [4+2] cycloaddition with acetylene dicarboxylate **23** (shown in *Figure 1.19*).

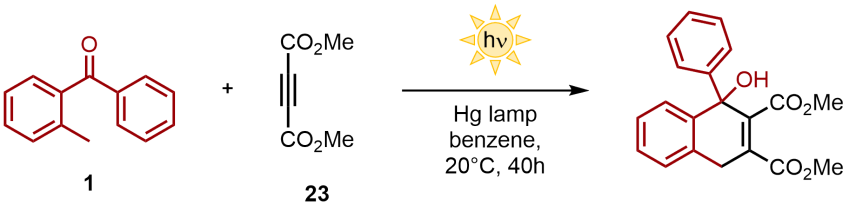

1
23
24

Figure 1.19: The first reaction using a photoenol intermediate, reported by Yang and Rivas in 1961.

Figure 1.20 shows the mechanism of photoexcitation of the 2-methylbenzophenone **1**. Light irradiation generates the diradical excited state that quickly turns from singlet to triplet state *via* inter system crossing. The triplet state decays via intramolecular hydrogen abstraction to two diradical conformers. The (Z)-form is short lived and rapidly undergoes [1,5]-sigmatropic H-shift, affording the initial 2-methylbenzophenone. Conversely, the (E)-form is more stable and as a consequence can react with an electrophile.

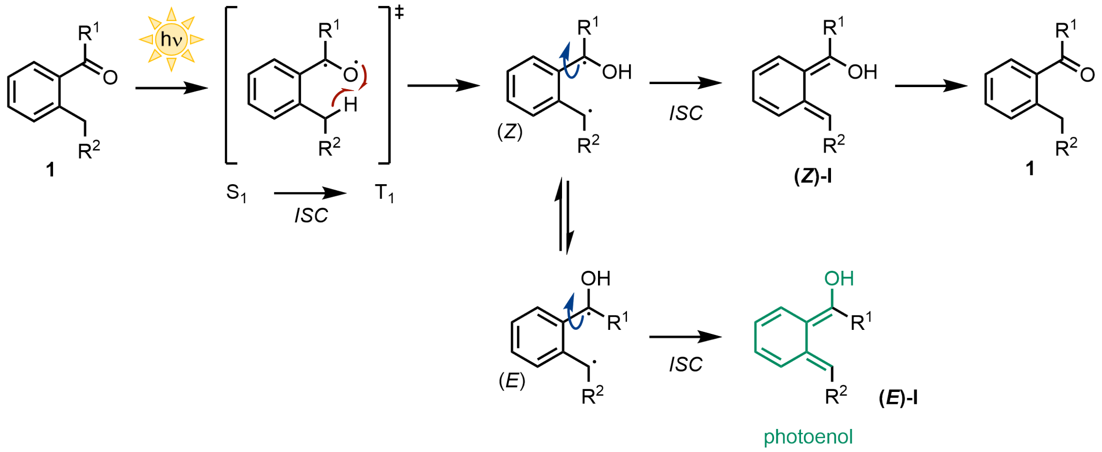

Figure 1.20: The light-triggered photoenol formation of 2-methylbenzophenone.

Photoenol intermediates have only been studied and used in recent years. In 2001 it was used by Jinsung's group for intermolecular and intramolecular cycloadditions. This reaction afforded key building blocks for the total synthesis of hamigerans, which possess bioactive properties.[43]

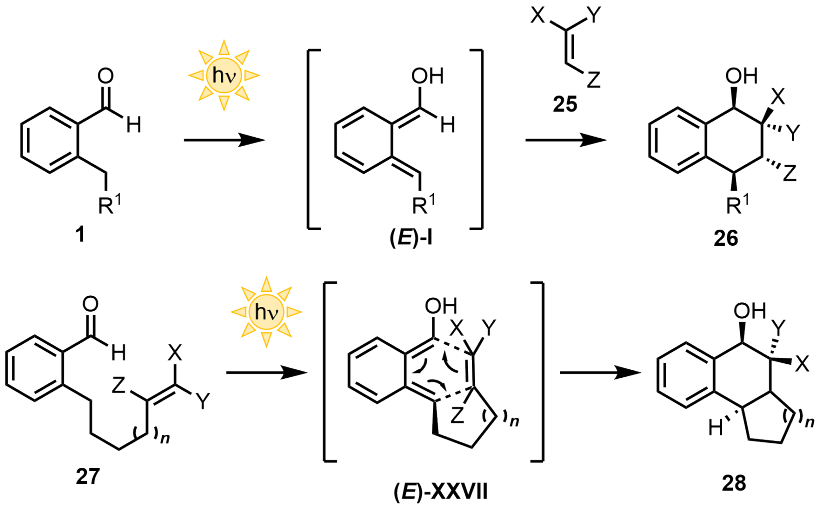

Figure 1.21: Intermolecular and intramolecular cyclisation of the photoenol.

In 2015 Murakami reported a light-driven carboxylation of hydroxy-*o*-quinodimethanes with CO_2. Light irradiation generates the reactive species that is then able to trap CO_2 through a [4+2] transition state, where CO_2 acts as the dienophile. After internal rearrangement, the carboxylated product **29** is formed. Beyond the benefits of CO_2 fixation, these carboxylated products are also valuable building blocks for the synthesis of benzodiazepines.[44]

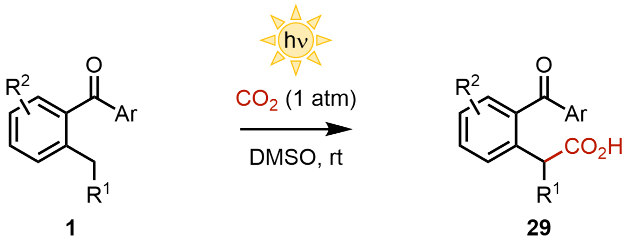

Figure 1.22: Light-driven carboxylation of 2-methylbenzophenones.

In 2016, Melchiorre's group developed the first organocatalytic asymmetric Diels-Alder cycloaddition using the photoenol intermediate as a diene. The authors employed a chiral H-bond donor catalyst in order to make the dienophile more reactive towards cycloaddition, trapping the photogenerated species enantioselectively.[45] The catalyst of choice was a bifunctional thiourea-amine derived from natural cinchona alkaloids. This catalyst was involved in two different mechanisms of stereocontrol: it was responsible of the asymmetric induction and, by partially quenching the photoenol activity, it minimised the background racemic reaction.

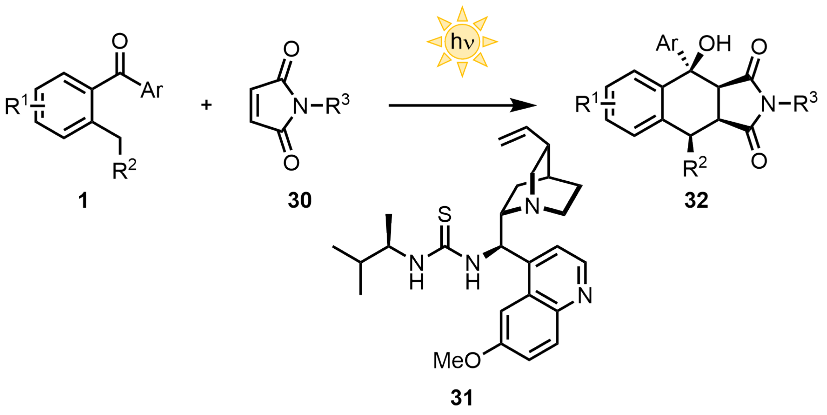

Figure 1.23: The first asymmetric Diels-Alder reaction with a photogenerated hydroxy-*o*-quinodimethane.

One year later, Melchiorre's group again reported the enantioselective conjugate addition of 2-methylbenzophenone **1** to α,β-unsaturated aldehydes **33**.[46] The chiral secondary amine catalyst **34** generates a conjugated iminium ion which then undergoes Michael addition with the photoexcited 2-methylbenzophenone.

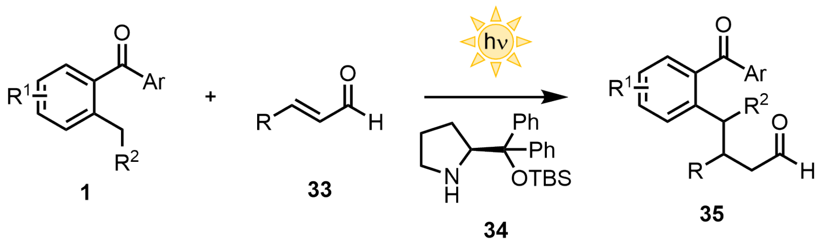

Figure 1.24: The conjugate addition of photogenerated hydroxy-*o*-quinodimethanes to α,β-unsaturated aldehydes.

Later on, Ye and co-workers reported a Michael addition of 2-methylbenzophenone derivatives to enones, that afford new quaternary *all-carbon* stereocentres **38** (*Figure 1.25*).[47] Remarkably, photogenerated hydroxy-*o*-quinodimethanes were proven to trap also activated imines *via* Mannich reaction with moderate enantioselectivity,[48] and can also act as a nucleophile in aldol reactions.[49]

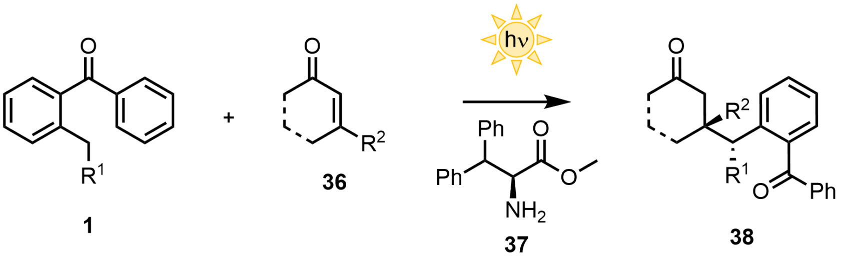
O
R1
1
+
O
R2
36
hν
Ph
O
Ph
O
NH2
37
O
R2
R1
O
Ph
38

Figure 1.25: The Michael addition of photogenerated hydroxy-*o*-quinodimethanes to enones.

However, to the best of our knowledge, photoenol has not yet been used in the asymmetric allylic alkylation reaction.

1.5 Microfluidics in Photochemical Reactions

Microfluidics deals with the behaviour of fluids that are constrained in small capillaries. A microfluidic setup for synthetic applications is typically constituted by eight different parts shown in *Figure 1.26*: fluid and reagent delivery, mixer, the reactor, quenching, back pressure regulation, collection, analysis and purification.[50]

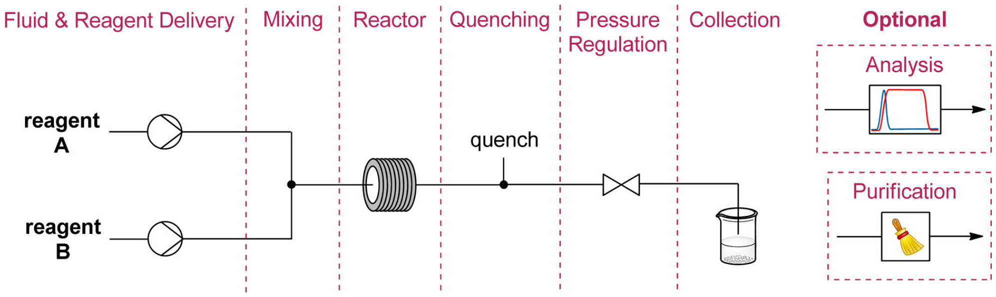
Fluid & Reagent Delivery
Mixing
Reactor
Quenching
Pressure Regulation
Collection
Optional
Analysis
Purification
reagent A
reagent B
quench

Figure 1.26: General scheme of a microfluidic reactor.[50]

Even though not all the reactions are suitable for microfluidic setup, it presents some advantages with respect to the traditional batch setup:

- increased surface to volume ratio
- more efficient heat transfer
- rapid and efficient mixing
- higher pressure that allows high temperature with low-boiling solvents
- easy up-scaling

Further, the implementation of microfluidic reactor in light-triggered transformations becomes a powerful way to enhance the reactivity of photochemical reactions. The additional advantages of microfluidic photoreactor compared to photochemical reactions in batch are:

- better light penetration, granting a uniform illumination
- shorter reaction times
- enhanced reproducibility
- less side reactions
- possibility to avoid detrimental over irradiation

In fact, irradiation can cause to the reaction mixture many side reactions, such as degradation of the product or of the starting material and formation of undesired products. In continuous flow, the reaction mixture is irradiated only for the time it remains inside the reactor. Conversely, in batch the whole reaction mixture is illuminated for the whole time, and slower side reactions can take place in the meantime. Moreover, in the classical batch conditions, illumination reaches only the most superficial molecules, thus giving heterogeneous irradiation to the reaction mixture.[51] The small diameter of the capillary permits a better light penetration on the whole reaction mixture, and pressure ensure a suitable mixing of the reactants. All these properties generally lead to shorter reaction times as well as improved selectivity with respect to batch photoreactions. Also, the continuous flow enables the easy up scaling of the optimised reaction. Furthermore, being the distance between the light and the reaction mixture constant, and being the flow rate controllable, the results are much more accurate and reproducible.

On the other hand, the limitation of microfluidics is the necessity of all reaction components to be soluble in the selected solvent, since the mixture needs to be homogeneous to avoid clog inside the capillary.

Recently, our laboratory has demonstrated how microfluidic conditions enhance the yield of diverse photochemical reactions, reducing the formation of undesired side-products and allowing to scale-up the transformation for grams-scale synthesis without loss in yield.[52,53]

Chapter 2

Results and Discussion

2.1 Development of the Reaction

The aim of this thesis project is the installation of an *all-carbon* quaternary stereocentre at allylic positions of isatin-derived MBG carbonates **3**, trhough the asymmetric allylic alkylation with non-stabilised C-nucleophiles. In order to do this, a dual activation strategy is used: light for the generation of the reactive C-nucleophile **1a** and a chiral catalyst for the stereoselective activation of the electrophile **IIIa**. As previously mentioned in Section 1.3, asymmetric allylic alkylation with non-stabilised nucleophiles (with pKa >25) is still an open challenge, especially in Lewis-base catalysed transformations. Allylic alkylation is a reaction that is particularly suitable for asymmetric synthesis purposes. In fact, from a racemic starting material, the catalyst activation is stereoconvergent towards the common electrophilic intermediate **IIIa**. Thus, the steric hindrance of the chiral Lewis base governs the stereodetermining event to yield the enantioenriched benzylated product **4a**. The activation mechanism of MBH carbonates with tertiary amine catalysts is well documented and it is reported also for isatin-derived MBH carbonates. On the other hand, the light-triggered activation of 2-methylbenzophenone is also reported and already explained in Section 1.4.
Hence, in the present thesis project, the two activation mechanisms are merged in order to develop the dual-activated asymmetric allylic alkylation of MBH carbonates **3** with 2-methylbenzophenone derivatives **1** as non-stabilised C-nucleophiles.

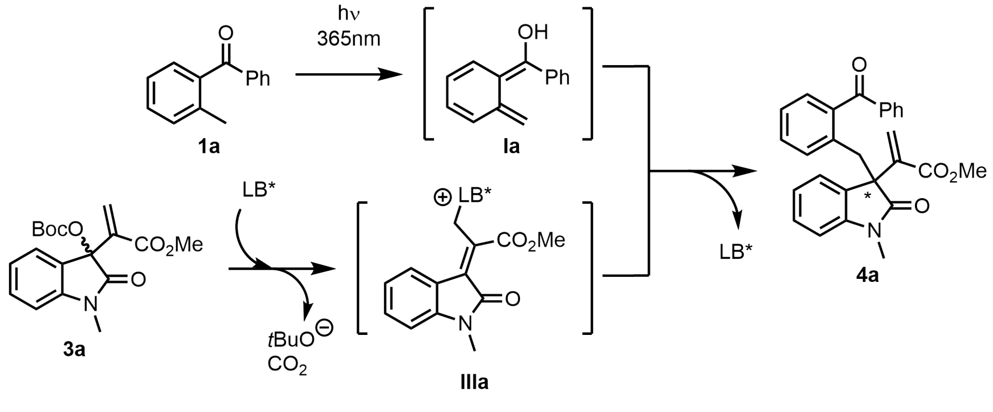

2.2 Synthesis of the Starting Materials

The electrophilic starting materials for this project are synthesised in three steps. The first one is the N-protection of isatin. NaH deprotonation and subsequent addition of the corresponding alkyl halide, affords the protected isatin derivative **5** *via* nucleophilic substitution.

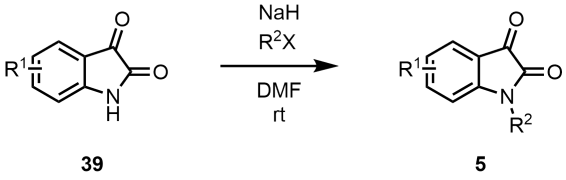
R1
O
O
N
H
NaH
R2X
DMF
rt
R1
O
O
N
R2
39
5

Subsequently, the N-protected isatin is subjected to Morita-Baylis-Hillman reaction with different acrylates catalysed by DABCO (**41**), to obtain the allylic alcohols **6**.

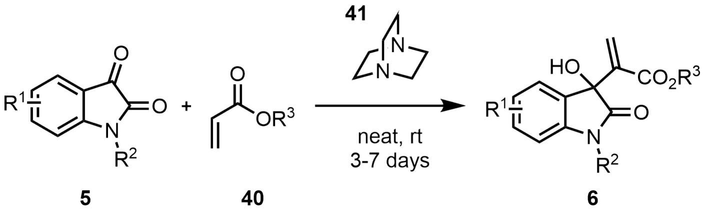
41
N
N
R1
O
O
N
R2
+
O
OR3
neat, rt
3-7 days
HO
CO2R3
R1
O
N
R2
5
40
6

The last step is the conversion of the alcohol group into a good leaving group. Thus, the MBH alcohol **6** is protected with di-*tert*-butyl dicarbonate in the presence of a catalytic amount of DMAP, a nucleophilic amine that activates the anhydride towards the attack of the alcohol.

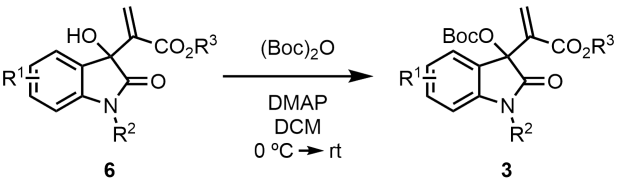
HO
CO2R3
R1
O
N
R2
(Boc)2O
DMAP
DCM
0 °C → rt
BocO
CO2R3
R1
O
N
R2
6
3

On the other hand, the nucleophilic starting materials, are syntehsised in two steps. The first step is Grignard addition to substituted benzaldehyde **42**. The obtained alcohol is directly oxidised to afford the 2-methylbenzophenone derivatives **1**.

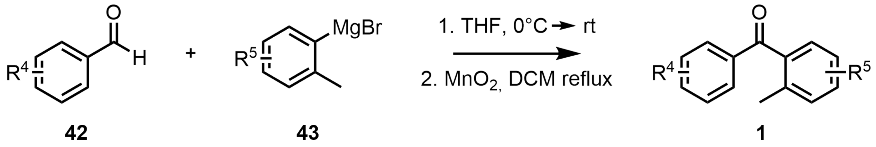
O
R4
H
+
R5
MgBr
1. THF, 0°C → rt
2. MnO2, DCM reflux
O
R4
R5
42
43
1

With the starting materials on hand, the light-triggered catalytic asymmetric allylic benzylation is set up as follows. The isatin-derived MBH carbonate **3** and the catalyst **2** are weighed in a screw-cap vial equipped with a rubber septum and a magnetic stirring bar, and the vial is carefully purged with argon. Removal of oxygen is important because oxygen quenches the triplet state of the excited 2-methylbenzophenone, thus lowering the amount of reactive photoenol intermediate. Subsequently, anhydrous degassed solvent is added through the septum together with the corresponding

2-methylbenzophenone pronucleophile **1**. Finally, the vial is sealed with parafilm and irradiated with the suitable light source for the indicated time.

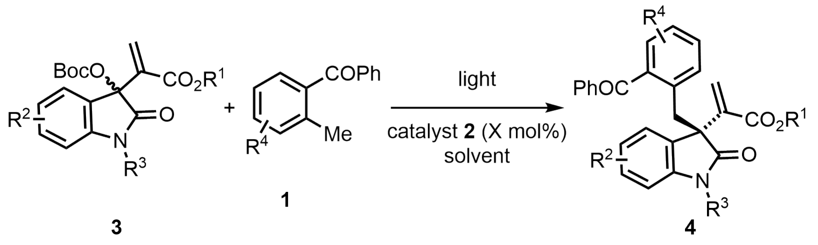

The reaction is initially performed with DABCO as catalyst, in order to synthesise the racemic sample. This allows to establish the feasibility of the transformation and to find the suitable conditions of separation in the chiral HPLC. The two enantiomers should appear as two different peaks with identical area as well as same absorbance spectrum. Injection of the product obtained with the chiral Lewis base in the same conditions, presents the same peaks but with different areas, corresponding to the enantiomeric ratio.

2.3 Optimisation of the Reaction in Batch

Screening of esters and amide-protecting groups in toluene: At the beginning, an initial screening of the esters (R^1) and of the N-protecting groups (R^3) was performed. The selected solvent was toluene, since it was the most widely used in literature for asymmetric allylic alkylation. Selected results are shown in Table 2.1.

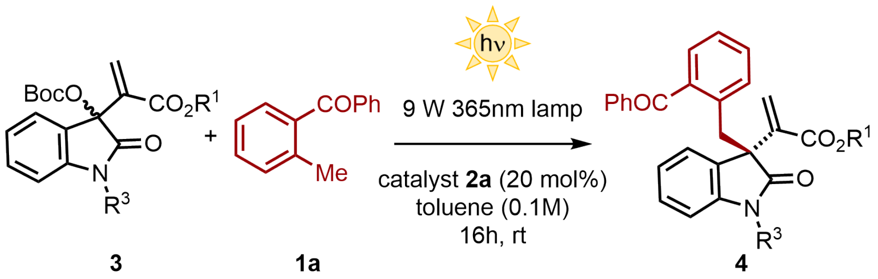

entry	R^1	R^3	**3**	yield (%) of **4**	*er* of **4**
1	Me	Me	**3a**	24	72:28
2	Me	Bn	**3g**	15	75:25
3	Me	Boc	**3h**	traces	n.d.
4	Me	Tr	**3i**	traces	n.d.
5	*t*Bu	Me	**3j**	15	82:18
6	*t*Bu	Bn	**3k**	10	76:24

Table 2.1: Screening of the MBH carbonates with different esters and amide-protecting groups. The yields were calculated by integrating the NMR peaks of the reaction crude using pyrazine as internal standard. The enantiomeric ratio was determined by chiral HPLC analysis. Reaction conditions: 0.1 mmol of **3** (1 equiv.), **1a** (5 equiv.), β-isocupreidine (20 mol%) in 1 mL of MeOH were irradiated at 365 nm for 16h.

Although full conversion of the starting material was observed, the yields were in general low. Moreover, a remarkable difference in yields between **3a** and **3g**, and between

3j and **3k** was observed. The low yields can be attributed to a combination of increased bulkiness of the N-benzyl group and light degradation of both the reagent and the product. The addition of another chromophore, such in the case of the benzyl group in **3k**, increases the absorption of the molecule, leading to faster light-degradation. Since the bulkier amide-protecting groups did not improve the enantiomeric excess, the N-Me protecting group was chosen for further optimisation.

During the setup of the reaction, upon addition of the catalyst and the MBH carbonate in the vial, a rapid change of colour from beige to bright orange was observed, which was attributed to the formation of the activated electrophilic species **IIIa**. This could mean that the formation of the electrophilic intermediate is fast and as a consequence its concentration in the reaction course is relevant. At this point, we attributed the low yields to the degradation of the starting material in the presence of β-isocupreidine **2a**. Therefore, we focused the attention to study and improve the stability of the different reaction components in different solvents.

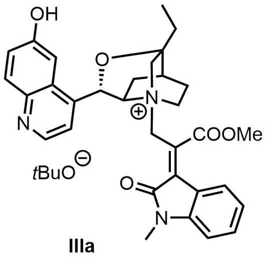

IIIa

Stability tests in different solvents: The MBH carbonate starting materials **3** were mixed with 20 mol% of β-isocupreidine **2a** in different solvents and monitored by semi-continuous NMR experiments. **3k** was proven to be quite stable in toluene, thus the low yield must be attributed to other causes, for instance light decomposition. The exceptional stability in toluene with respect to the other starting materials is attributable to the high steric hindrance of the *tert*-butyl ester that makes the molecule less reactive. Conversely, **3g** was proven to be unstable, with about 80% of remaining starting material after only 4 hours. Also **3a** is unstable in toluene and polar aprotic solvents. Methanol was the only solvent in which **3a** was stable (see *Figure 2.1*), thus it was chosen for further optimisation.

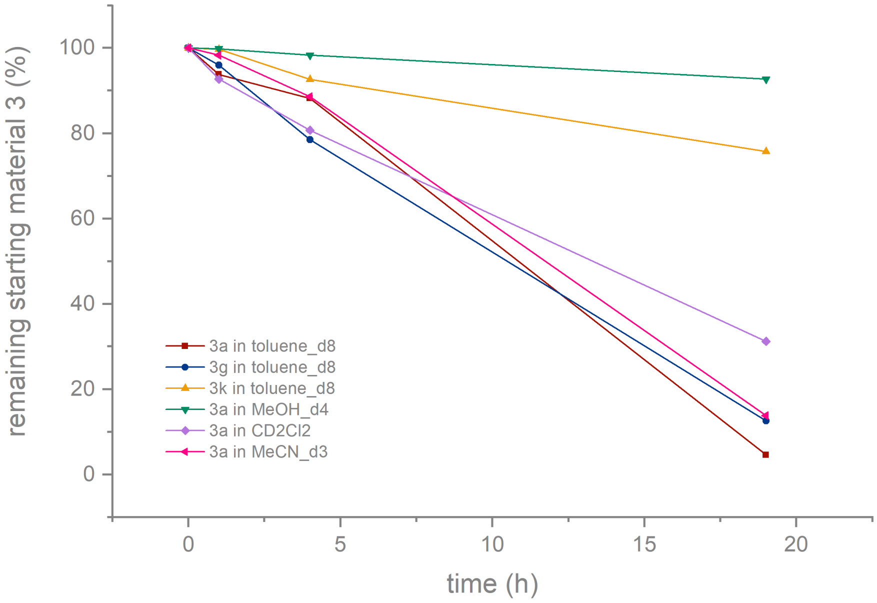

Figure 2.1: The graphic shows the stability of the MBH carbonate with catalytic amounts of β-ICD **2a** versus time in different solvents. Monitored by ^{1}H NMR using pyrazine as internal standard. Reaction conditions: 0.1 mmol of **3** (1 equiv.), β-isocupreidine (20 mol%) in 1 mL of solvent.

Blank tests: The reaction was tested without light and without catalyst. No reactivity was observed, as reported in Table 2.2, thus confirming the proposed dual activation mechanism of the reaction.

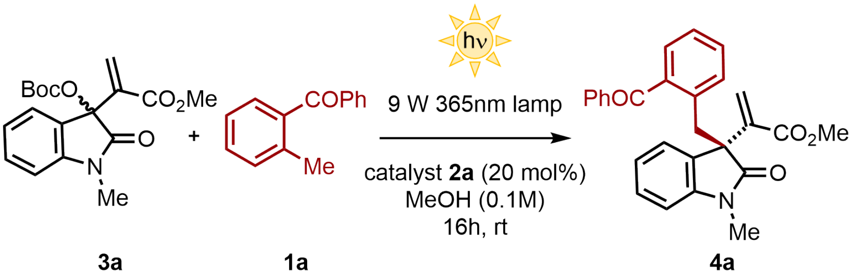
BocO
CO$_2$Me
O
N
Me
+
COPh
Me
hν
9 W 365nm lamp
catalyst 2a (20 mol%)
MeOH (0.1M)
16h, rt
PhOC
CO$_2$Me
O
N
Me
3a
1a
4a

entry	solvent	deviation from standard conditions	yield (%) of **4a**	*er* of **4a**
1	MeOH	no catalyst **2a**	n.r.	n.d.
2	MeOH	no light irradiation	n.r.	n.d.

Table 2.2: Blank reactions. The yields were calculated by integrating the NMR peaks of the reaction crude using pyrazine as internal standard. The enantiomeric ratio was determined by chiral HPLC analysis. Reaction conditions: 0.1 mmol of **3** (1 equiv.), **1a** (5 equiv.), β-isocupreidine (20 mol%) in 1 mL of MeOH were irradiated at 365 nm for 16h.

Screening of chiral Lewis bases: Subsequently, different catalysts were screened, and β-isocupreidine was confirmed to be the best both in terms of reactivity and asymmetric induction. Results are shown in Table 2.3.

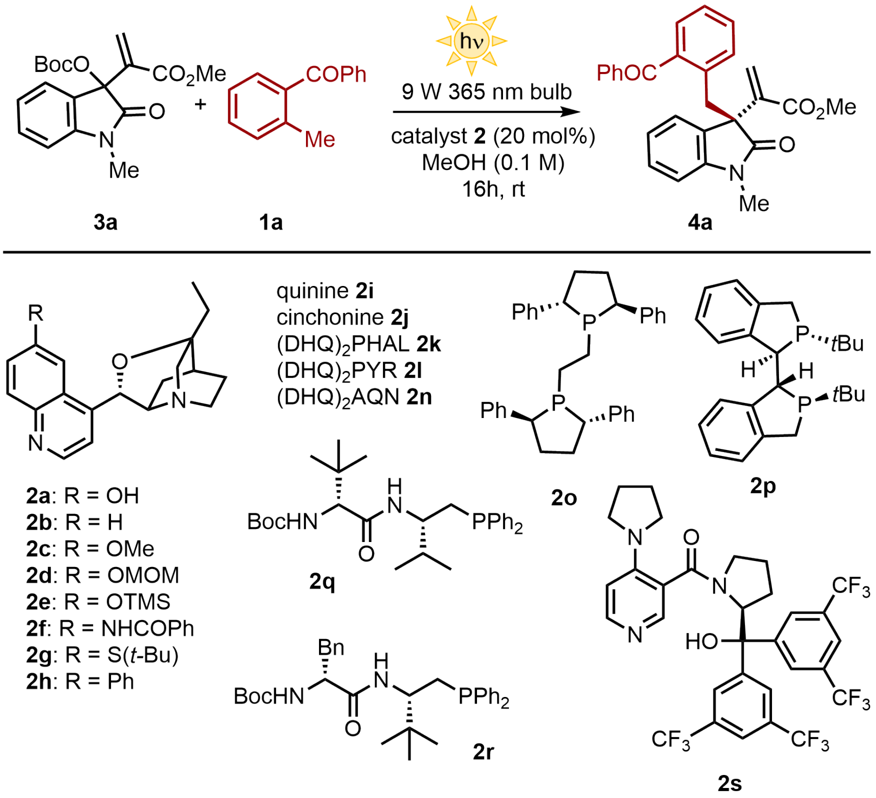
BocO
CO$_2$Me
O
N
Me
+
COPh
Me
hν
9 W 365 nm bulb
catalyst 2 (20 mol%)
MeOH (0.1 M)
16h, rt
PhOC
CO$_2$Me
O
N
Me
3a
1a
4a
R
O
N
N
2a: R = OH
2b: R = H
2c: R = OMe
2d: R = OMOM
2e: R = OTMS
2f: R = NHCOPh
2g: R = S(t-Bu)
2h: R = Ph
quinine 2i
cinchonine 2j
(DHQ)$_2$PHAL 2k
(DHQ)$_2$PYR 2l
(DHQ)$_2$AQN 2n
Ph
P
Ph
Ph
P
Ph
2o
P
tBu
H
H
P
tBu
2p
BocHN
H
N
O
PPh$_2$
2q
Bn
BocHN
H
N
O
PPh$_2$
2r
N
O
N
N
HO
CF$_3$
CF$_3$
CF$_3$
CF$_3$
2s

entry	catalyst **2**	yield (%) of **4a**	*er* of **4a**
1	**2a**	66	70:30
2	**2b**	24	65:25
3	**2c**	31	63:37
4	**2d**	55	70:30
5	**2e**	21	70:30
6	**2f**	12	70:30
7	**2g**	23	59:41
8	**2h**	10	53:46
9	**2i**	n.r.	n.d.
10	**2j**	n.r.	n.d.
11	**2k**	n.r.	n.d.
12	**2l**	n.r.	n.d.
13	**2n**	n.r.	n.d.
14	**2o**	n.r.	n.d.
15	**2p**	n.r.	n.d.
15	**2q**[a]	n.r.	n.d.
17	**2r**[a]	n.r.	n.d.
18	**2s**	4	n.d.

Table 2.3: Screening of different catalysts. The yields were calculated by integrating the NMR peaks of the reaction crude using pyrazine as internal standard. The enantiomeric ratio was determined by chiral HPLC analysis. Reaction conditions: 0.1 mmol of **3** (1 equiv.), **1a** (5 equiv.), catalyst **2** (20 mol%) in 1 mL of MeOH were irradiated at 365 nm for 16h. [a]These catalysts were kindly provided by professor Jose L. Vicario.[54]

Screening of other alcoholic solvents: Commonly, in the asymmetric allylic alkylation with activated C-nucleophiles, the $t\mathrm{BuO}^-$ formed upon decomposition of the leaving group deprotonates the C-pronucleophile before the C-C bond forming step, as shown in *Figure 2.2*. Conversely, in this reaction, the $t\mathrm{BuO}^-$ present in solution is quenched after the C-C bond formation. Thus, the reaction was tested in other alcoholic solvents in order to rule out a possible inhibition of the reactivity by the strong base in solution.

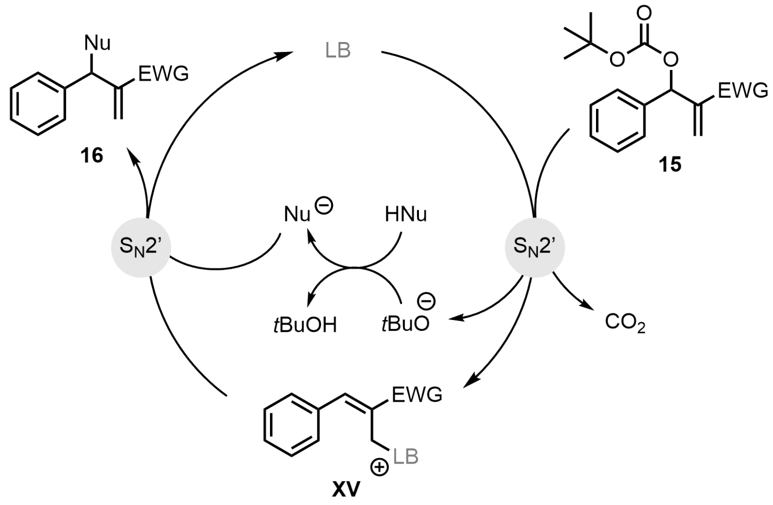

Figure 2.2: General reaction mechanism of asymmetric allylic alkylation with an acidic nucleophile. The tBuOH from the leaving group is necessary to activate the nucleophile.

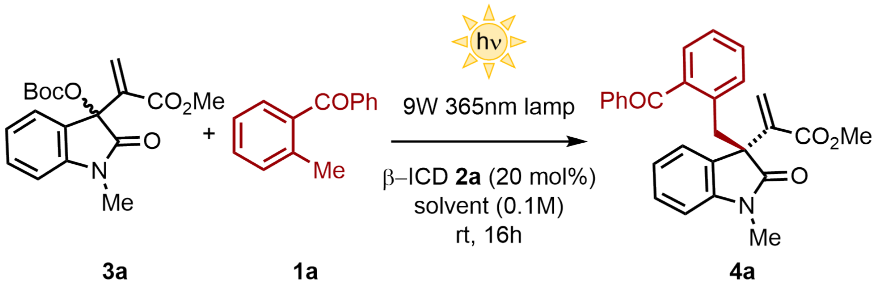
hν
9W 365nm lamp
β–ICD **2a** (20 mol%)
solvent (0.1M)
rt, 16h
BocO
CO_2Me
COPh
Me
N
Me
O
PhOC
3a
1a
4a

entry	solvent	yield (%) of **4a**	*er* of **4a**
1	MeOH	66	70:30
2	*i*PrOH	31	70:30
3	*t*BuOH	45	71:29
4	hexafluoroisopropanol	n.r.	n.d.

Table 2.4: Screening of other alcoholic solvents. The yields were calculated by integrating the NMR peaks of the reaction crude using pyrazine as internal standard. The enantiomeric ratio was determined by chiral HPLC analysis. Reaction conditions: 0.1 mmol of **3** (1 equiv.), **1a** (5 equiv.), β-isocupreidine (20 mol%) in 1 mL of solvent were irradiated at 365 nm for 16h.

Hexafluoroisopropanol is probably too acidic and it can deactivate the catalyst **2a** by protonation of the quinuclidine nitrogen. In fact, no reaction was observed (Table **??**, entry 4). Low reactivity was observed with *i*PrOH and *t*BuOH. Therefore, MeOH was employed for further optimisation.

Effect of temperature: In catalytic asymmetric transformations, temperature usually plays a crucial role in the determination of the enantiomeric excess. Low temperature reduces the energy input to the system, disfavouring the formation of the diastereoisomeric intermediate with higher activation energy. This is verified also in our case, but with no significant improvement in the enantiomeric ratio and, in return, with a considerable loss in yield. The standard conditions (20°C) are used for further investigations.

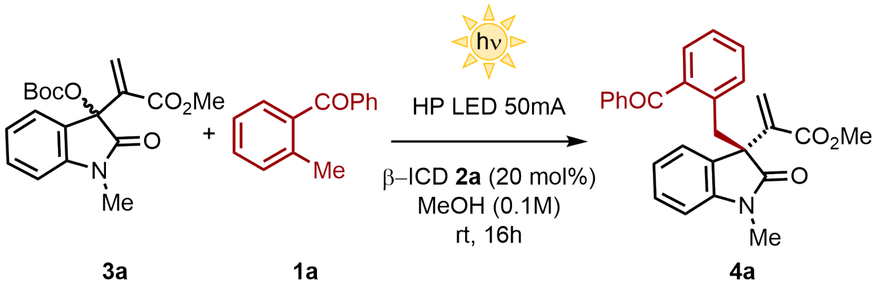
hν
HP LED 50mA
β–ICD **2a** (20 mol%)
MeOH (0.1M)
rt, 16h
BocO
CO_2Me
COPh
Me
N
Me
O
PhOC
3a
1a
4a

entry	temperature	yield (%) of **4a**	*er* of **4a**
1	20°C	66	70:30
2	0°C	42	72:28
3	-12°C	30	75:25

Table 2.5: Effect of temperature. The yields were calculated by integrating the NMR peaks of the reaction crude using pyrazine as internal standard. The enantiomeric ratio was determined by chiral HPLC analysis. Reaction conditions: 0.1 mmol of **3** (1 equiv.), **1a** (5 equiv.), β-isocupreidine (20 mol%) in 1 mL of MeOH were irradiated at 365 nm for 16h.

Screening of miscellaneous reaction parameters: Other relevant parameters such as light source, catalyst loading, and solvent mixtures were investigated. Selected results are shown in Table 2.6.

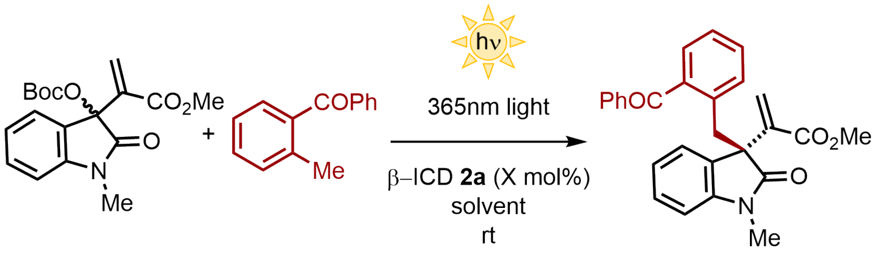

3a **1a** **4a**

entry	**2a** (mol%)	solvent	light	time (h)	yield (%) of **4a**	*er* of **4a**
1	20	MeOH	9W 365nm bulb	16	66	70:30
2	20	MeOH	HP LED 50mA	16	65	70:30
3	20	MeOH	HP LED 350mA	4	81	70:30
4	20	MeOH/Toluene 9:1	HP LED 350mA	4	70	70:30
5	20	MeOH/Cyclohexane 9:1	HP LED 350mA	4	65	71:29
6	20	MeOH/DCM 9:1	HP LED 350mA	4	71	71:29
7	20	MeOH/THF 9:1	HP LED 350mA	4	60	70:30
8	**10**	**MeOH**	**HP LED 350mA**	**3**	**80 [78]**[a]	**70:30**
9	5	MeOH	HP LED 350mA	3	50	70:30
10	1	MeOH	HP LED 350mA	3	12	n.d.
11[b]	20	MeOH	HP LED 350mA	3	51	70:30

Table 2.6: Screening of miscellaneous conditions. The yields were calculated by integrating the NMR peaks of the reaction crude using pyrazine as internal standard. The enantiomeric ratio was determined by chiral HPLC analysis. Reaction conditions: 0.1 mmol of **3** (1 equiv.), **1a** (5 equiv.), β-isocupreidine in 1 mL of solvent were irradiated at 365 nm. [a][Isolated yield]. [b]Using 2 equiv. of **1a**.

As it can be seen in Table 2.6, the best result in terms of yield was obtained using a 10% catalyst loading, with a high-power 365nm LED 350mA of intensity. Being this the best result, and having no remarkable improvements on the enantiomeric excess, the conditions of entry 8 are used for further investigation.

Screening of the ester groups: Various ester groups were examined in MeOH to evaluate whether this substitution has an impact on the enantiomeric excess. Results are shown in Table 2.7.

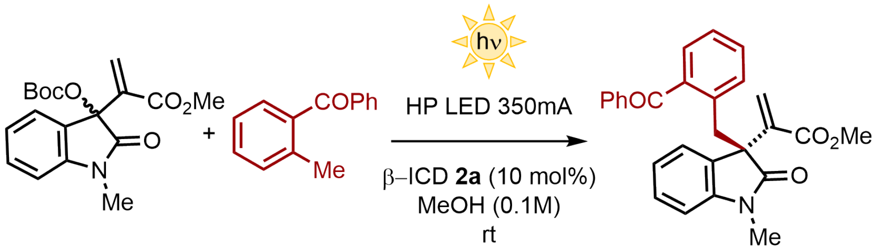

3 **1a** **4**

entry	R^1	**3**	yield (%) of **4**	*er* of **4**
1	Me	**3a**	80 [78]^a	70:30
2	Et	**3e**	61 [57]^a	70:30
3	Hex	**3l**	33	64:36
4	*t*Bu	**3j**	5	85:15
5	Bn	**3m**	34	64:36

Table 2.7: Screening of the ester groups. The yields were calculated by integrating the NMR peaks of the reaction crude using pyrazine as internal standard. The enantiomeric ratio was determined by chiral HPLC analysis. Reaction conditions: 0.1 mmol of **3** (1 equiv.), **1a** (5 equiv.), β-isocupreidine (10 mol%) in 1 mL of MeOH were irradiated at 365 nm. ^{a}[Isolated yield].

Unfortunately, increasing the bulkiness of the ester group only affects the reactivity, and the enantiomeric ratio is increased only with the *t*Bu group. However, the hindrance of the *t*Bu ester derivative **3j** reduces drastically the reactivity, yielding only 5% of product.

After extensive screening of all the variables, the following conclusions were deduced:

- Dual activation of both the nucleophile and the electrophile is needed in order to have the intended reactivity
- A protic solvent is needed to stabilise the reactants
- Steric hindrance of the ester and the amide-protecting group do not affect the asymmetric induction significantly. Only with the *tert*-butyl ester the enantiomeric ratio is improved, but with a considerable loss in yield.
- β-isocupreidine is the best catalyst
- Lower catalyst loading (10%) increases the yield, compared with the initial 20%
- The enantiomeric ratio does not vary significantly upon variation of all the reaction parameters and even the temperature dependence is very slight. The only remarkable variations are obtained upon variation of the chiral catalyst.

Based on literature reports and on the relevant information gained during the extensive optimisation studies, a first hypothesis on the reaction mechanism is formulated (shown in *Figure 2.3*). In this scenario the catalytic resting state is the activated electrophile **IIIa**. The attack of the photogenerated nucleophile **Ia** in the allylic position is the rate determining step. The generated photoenol **Ia** is very low in concentration during the reaction course. In fact, it has a short lifetime and it tends to go back to the initial state **1a**. Therefore, we decided to characterise the intermediate **IIIa**.

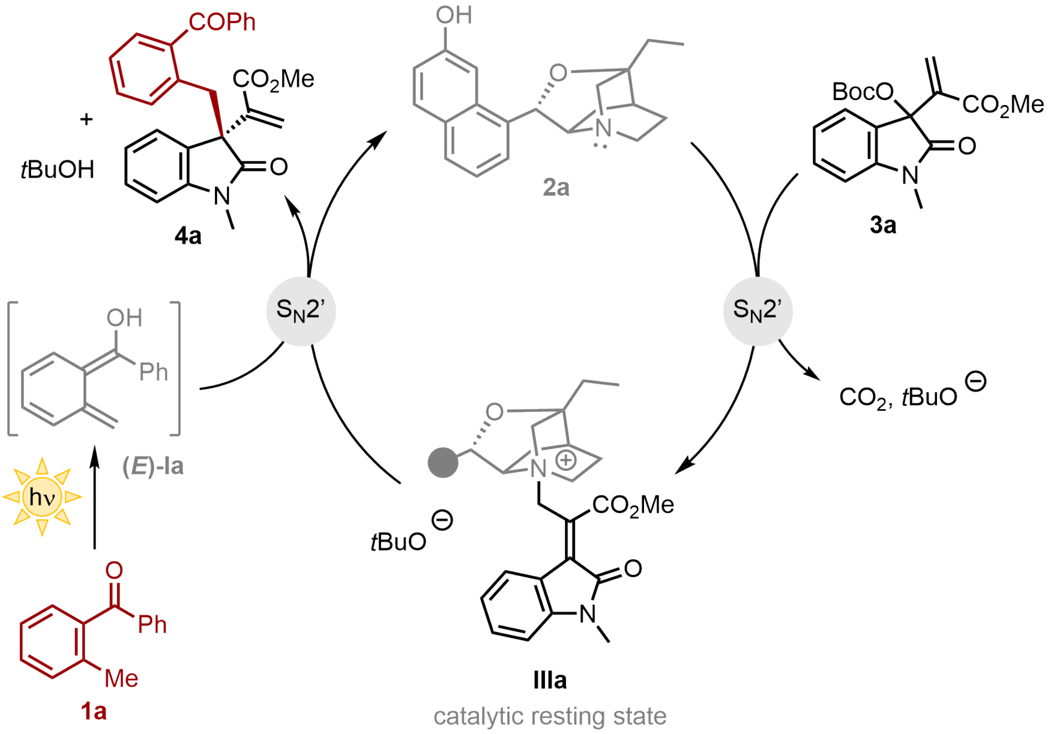
COPh
CO2Me
+
tBuOH
4a
OH
O
N
2a
BocO
CO2Me
O
N
3a
SN2'
SN2'
OH
Ph
(E)-Ia
hν
O
Ph
Me
1a
CO2, tBuO ⊖
tBuO ⊖
O
N ⊕
CO2Me
O
N
IIIa
catalytic resting state

Figure 2.3: Proposed mechanism.

2.4 Characterisation of the Catalytic Intermediate

As highlighted by the previous reports present in literature, the asymmetric allylic alkylation of isatin-derived MBH carbonates **3** catalysed by β-isocupreidine and other cinchona alkaloids usually furnishes good reactivity with excellent enantiomeric excesses.[30,55,56] Conversely, for the present transformation, despite the extensive optimisation studies, the asymmetric induction could not be improved higher than 70:30 er. However, the reaction furnished the product in fair yields up to 78%. In order to understand the reasons of the moderate enantioselectivity, the study on the catalytic intermediate and the reaction mechanism was carried out. The second S_N2' (that is the attack by the photoenol and thus the C-C bond formation) is the rate-determining step, which can be demonstrated by the fact that the catalytic intermediate **IIIa** is the catalytic resting state (its concentration is high and constant during the reaction course). Therefore, the reason for the moderate stereoinduction could be the E/Z isomerisation

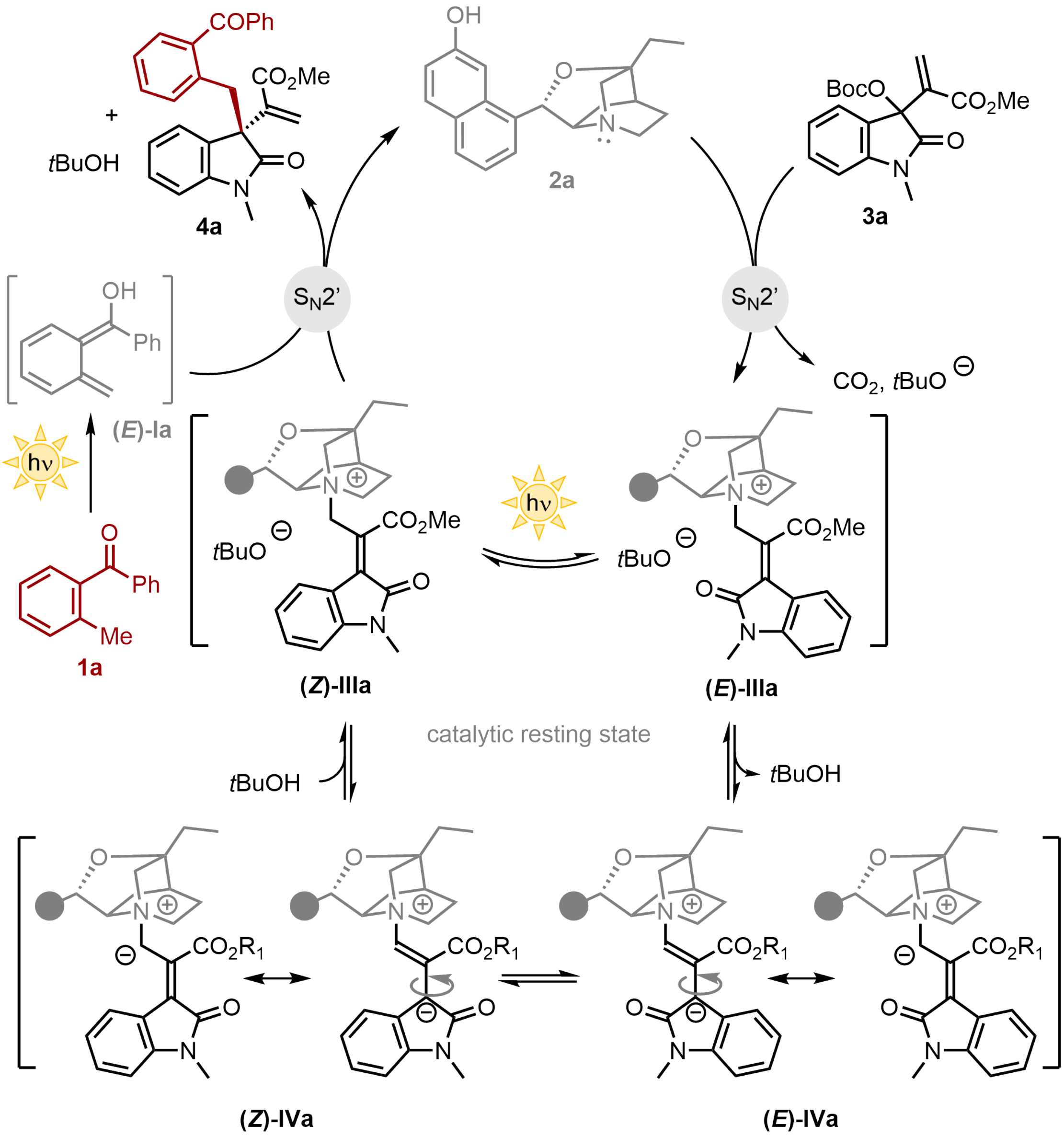
COPh
CO_2Me
+
tBuOH
4a
OH
2a
BocO
CO_2Me
3a
S_N2'
S_N2'
OH
Ph
(E)-Ia
CO_2, tBuO ⊖
hν
O
Ph
Me
1a
tBuO ⊖
CO_2Me
hν
tBuO ⊖
CO_2Me
(Z)-IIIa
(E)-IIIa
catalytic resting state
tBuOH
tBuOH
CO_2R_1
CO_2R_1
CO_2R_1
CO_2R_1
(Z)-IVa
(E)-IVa

Figure 2.4: Proposed mechanism with the possible isomerisation mechanisms.

of the catalytic intermediate **IIIa**: if the catalytic intermediate has the possibility to isomerise, the catalyst will end up shielding the opposite prochiral face, affording the opposite enantiomer. In this scenario, we hypothesise that the isomerisation can be mediated by the *t*BuO$^-$ generated upon leaving group ionisation or owing to the light irradiation. The reaction scheme, with the two possible isomerisation paths, is shown in *Figure 2.4*.

Despite all the attempts to synthesise and isolate the species **IIIa** were unsuccessful, by mixing the MBH carbonate **3a** and β-isocupreidine **2a** in equimolar amount directly inside an NMR tube MeOH-d$_3$ it was possible to form *in situ* the catalytic species**IIIa**. Subsequently, a series of NMR experiments, including ^{1}H NMR, ^{13}C NMR HSQC, HMBC and NOESY NMR were acquired in order to characterise it. The NOESY experiment was acquired both in MeOH-d$_4$ and MeOH-d$_3$. Herein the different characterisation experiments are reported with corresponding assignments.

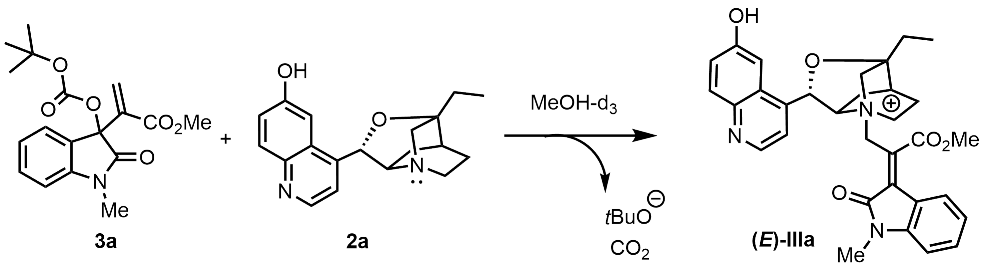

Figure 2.5: *In situ* formation of the catalytic species **IIIa**.

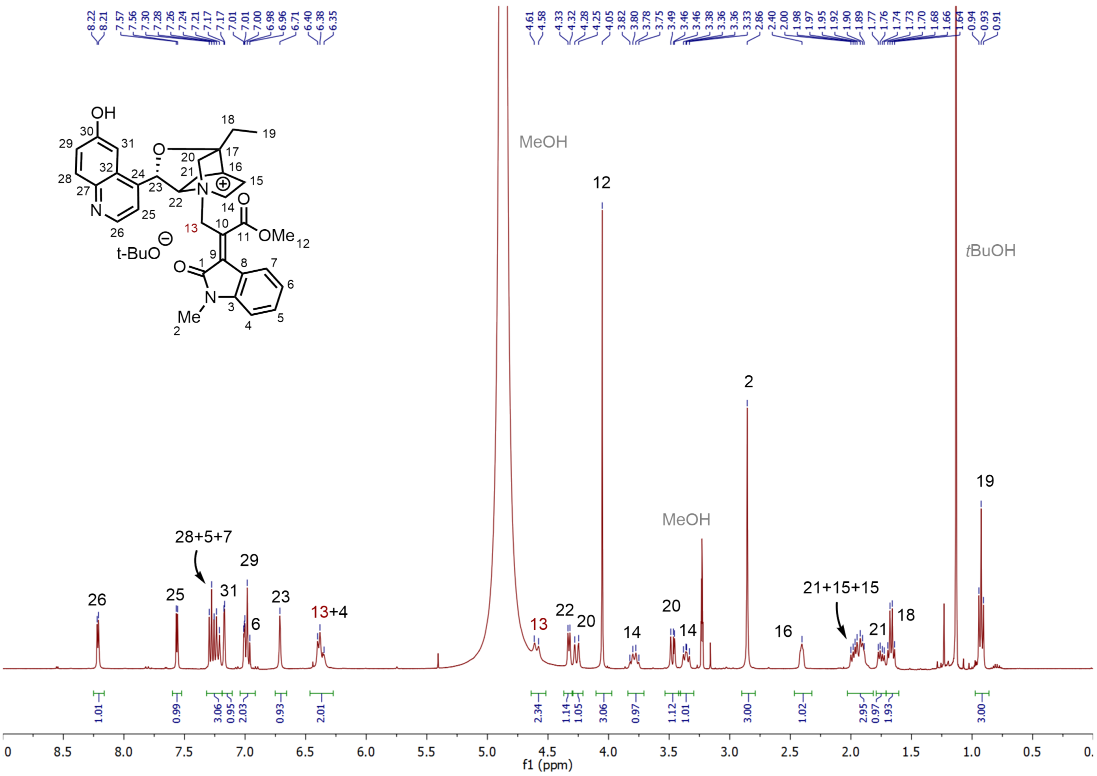

Figure 2.6: Characterisation of the catalytic species **IIIa** in methanol-d$_3$.

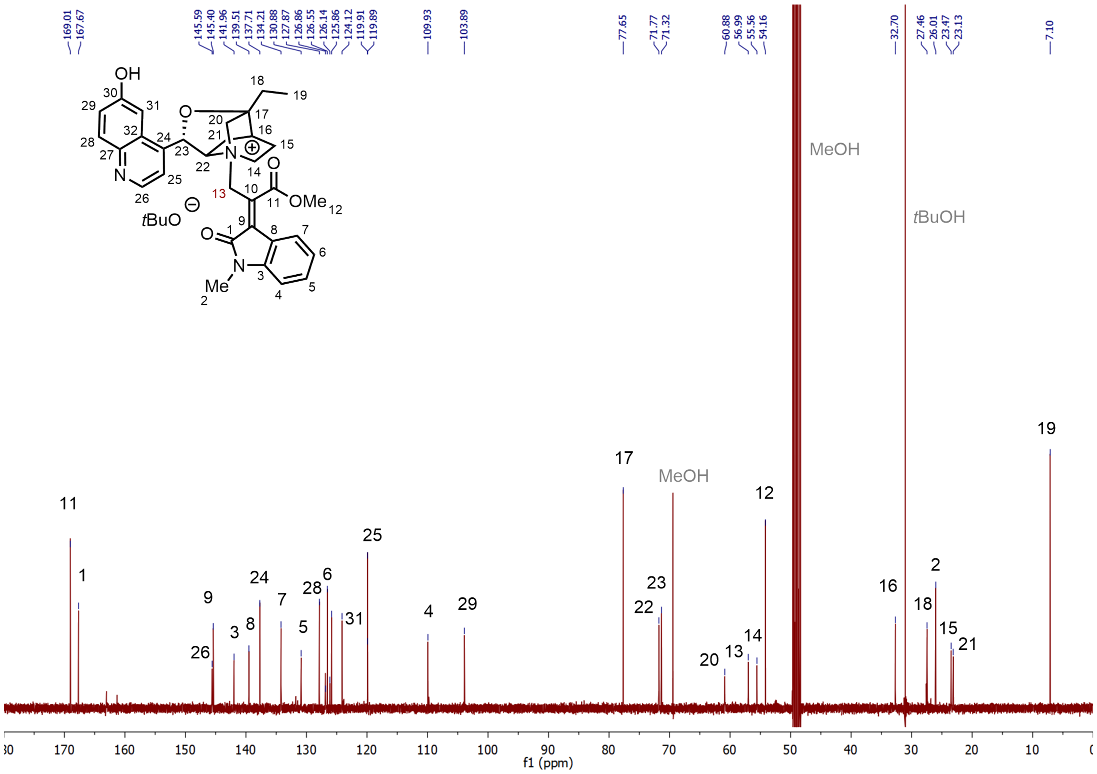

Figure 2.7: Characterisation of the catalytic species **IIIa** in methanol-d$_3$.

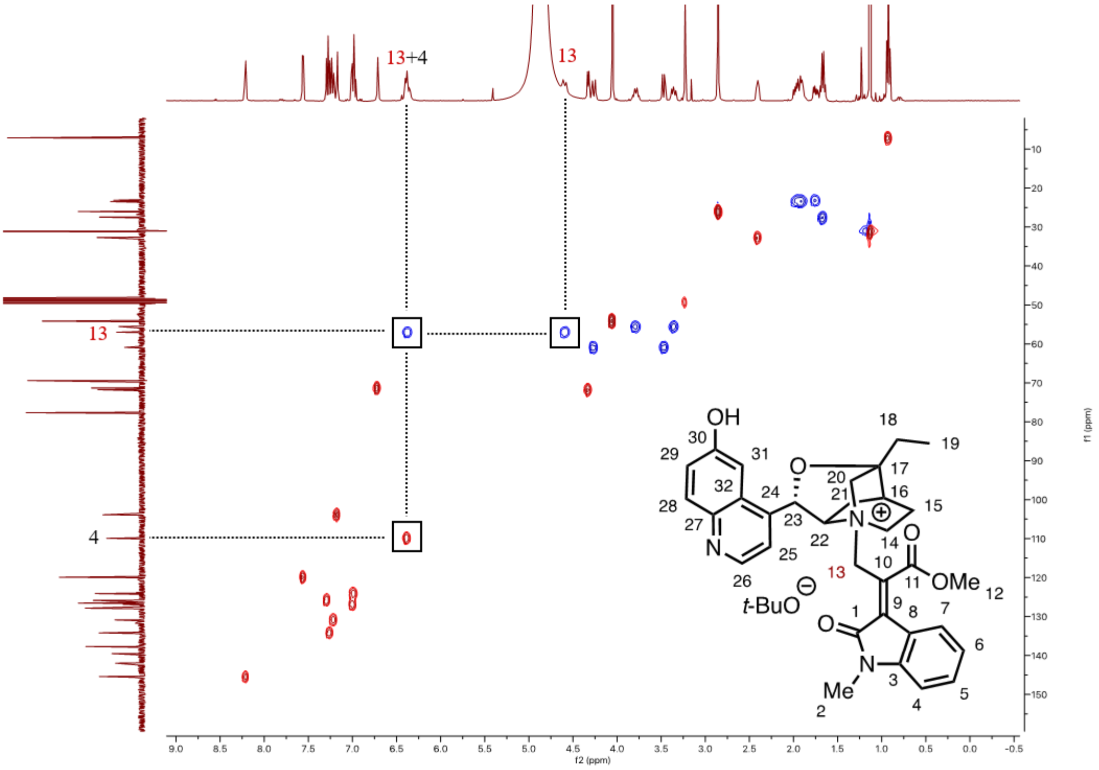

Figure 2.8: HSQC spectrum of **IIIa** in methanol-d$_3$. The HSQC experiment shows the correlation between carbon and hydrogen. In blue CH$_2$, in red CH and CH$_3$. Carbons not showing any correlation peaks are the quaternary carbons.

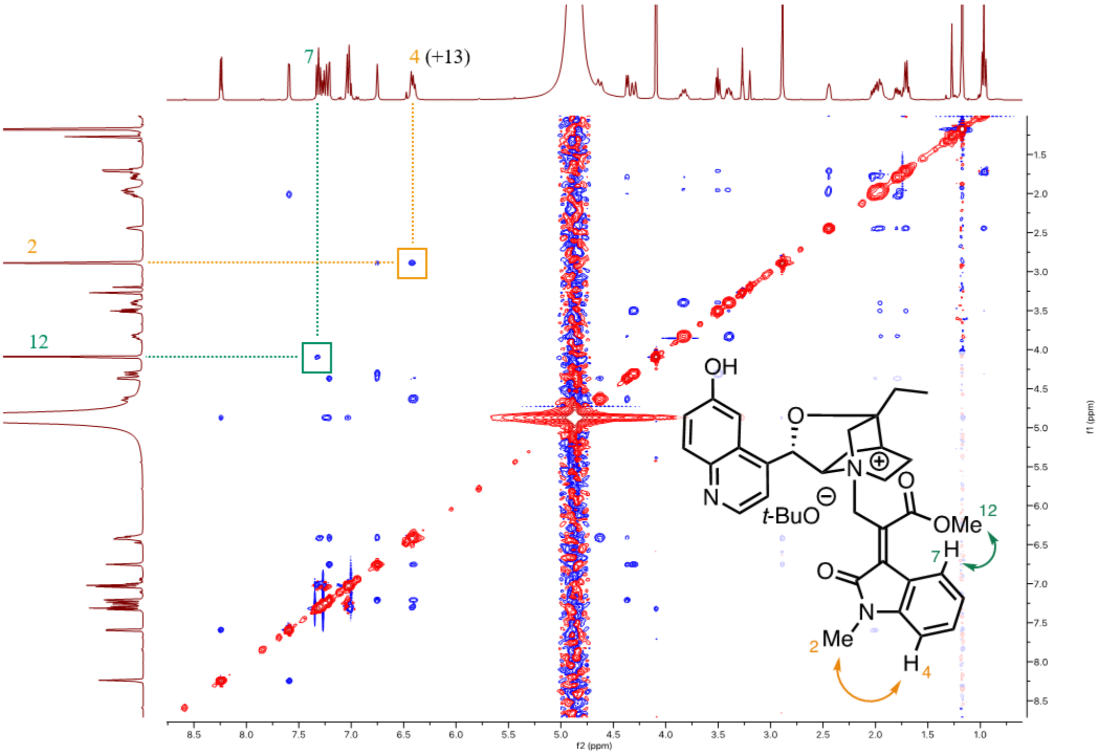

Figure 2.9: NOESY spectrum of **IIIa** in methanol-d$_3$, with assignments. In green the contact between H12 of the methyl ester and H7 is shown.

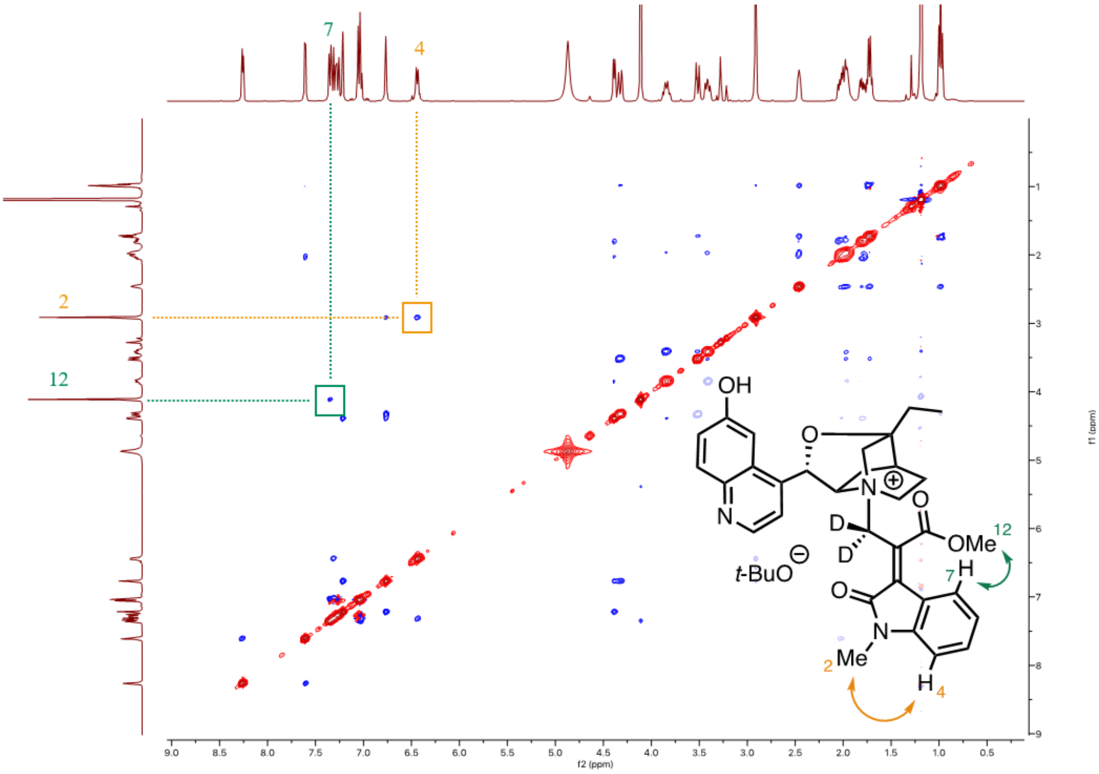

Figure 2.10: NOESY spectrum of **IIIa** in methanol-d$_4$, with assignments. The peak of proton 4, previously hidden by 13, is now visible due to deuteration.

The *Nuclear Overhauser Effect Spectroscopy* experiment shows through-space contacts of protons. Results show that, at least at the initial time, only the (E)-isomer is formed selectively (see the NOESY spectra in *Figure 2.9* and *2.10*). The experiment in methanol-d_4 allows to distinguish the signals arising from proton 4 from the ones of the allylic proton 13. Thus, the NOESY spectra confirm no evidence of formation of the (Z)-**IIIa**. This is consistent with the bulkiness of the catalyst, and with the previous successful reports of asymmetric allylic alkylation with β-isocupreidine as a catalyst. From the HSQC spectrum (*Figure 2.8*, the allylic protons 13 could be correlated with the allylic carbon 13. This carbon has a chemical shift which is typical of the sp^3 character. Thus, the electrophilic intermediate **IIIa** is the species present in solution at equilibrium, rather than the ylide **IVa**. Methanol is acidic enough to protonate the free tBuO$^-$. This explains the bright orange colour of the solution of **IIIa** in methanol, due to the extended conjugation upon nucleophilic attack of the catalyst.

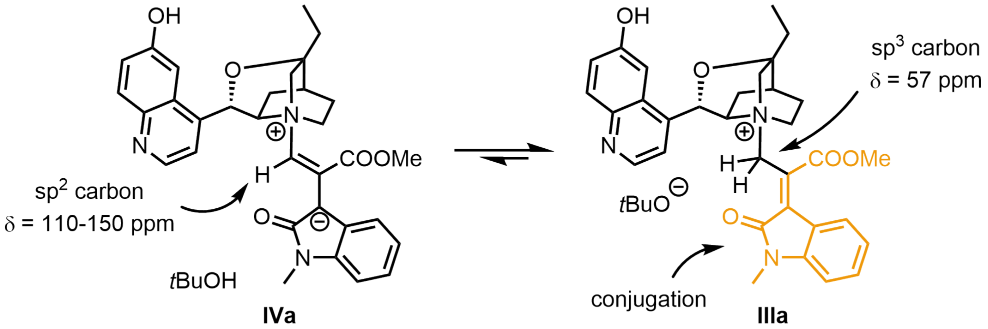

Figure 2.11: Allylic ylide **IVa** (left) and electrophilic catalytic intermediate **IIIa** (right).

Next, the kinetics of formation and isomerisation of the catalytic intermediate **IIIa** was studied. The starting material **3a** and β-isocupreidine **2a** were mixed together in 1:1 ratio in methanol-d_4. ^{1}H NMR spectra were acquired at regular intervals of time. The formation of **IIIa** was monitored by the disappearance of the peak at 1.34 ppm, corresponding to the tBu signal of **3**, along with the appearance of the new peak of the ionised tBuO$^-$ at 1.25 ppm. Once the salt was completely formed, it was irradiated with a 9W 365nm lamp and its evolution was checked by ^{1}H NMR. Two observations can be made:

- The area of the multiple peaks at 6.5 ppm decreases smoothly, until there is only one doublet. In fact, the multiplet is made by two different protons, and one is the allylic proton 13, that exchanges with methanol-d_4, deuterating and disappearing within approximately 180 minutes. The disappearance of the second allylic proton 13 at 4.7 ppm can also be seen in *Figure 2.12*.
- Upon 2h irradiation, no significant change in the chemical shifts is detected (see bottom spectrum of *Figure 2.12*).

The disappearance of the allylic protons 13 of **IIIa** is the proof that there is a proton exchange between the solvent and the allylic protons of **IIIa**. Conversely, light isomerisation could not be detected after irradiation for 2h. Thus, the experiment of irradiation of **IIIa** is repeated, this time in methanol-d_3 in order to avoid deuteration of the allylic protons. **3a** and **2a** are mixed together in stoichiometric amount in the NMR tube, waiting until complete formation of **IIIa** before starting the acquisition. If a substantial change in the chemical shift is detected upon irradiation of the NMR tube, this would be the proof that light is responsible of the isomerisation of the catalytic species. As expected, with methanol-d_3 the allylic protons 13 could be detected. Unfortunately, the catalytic species **IIIa** decomposed under light irradiation before any

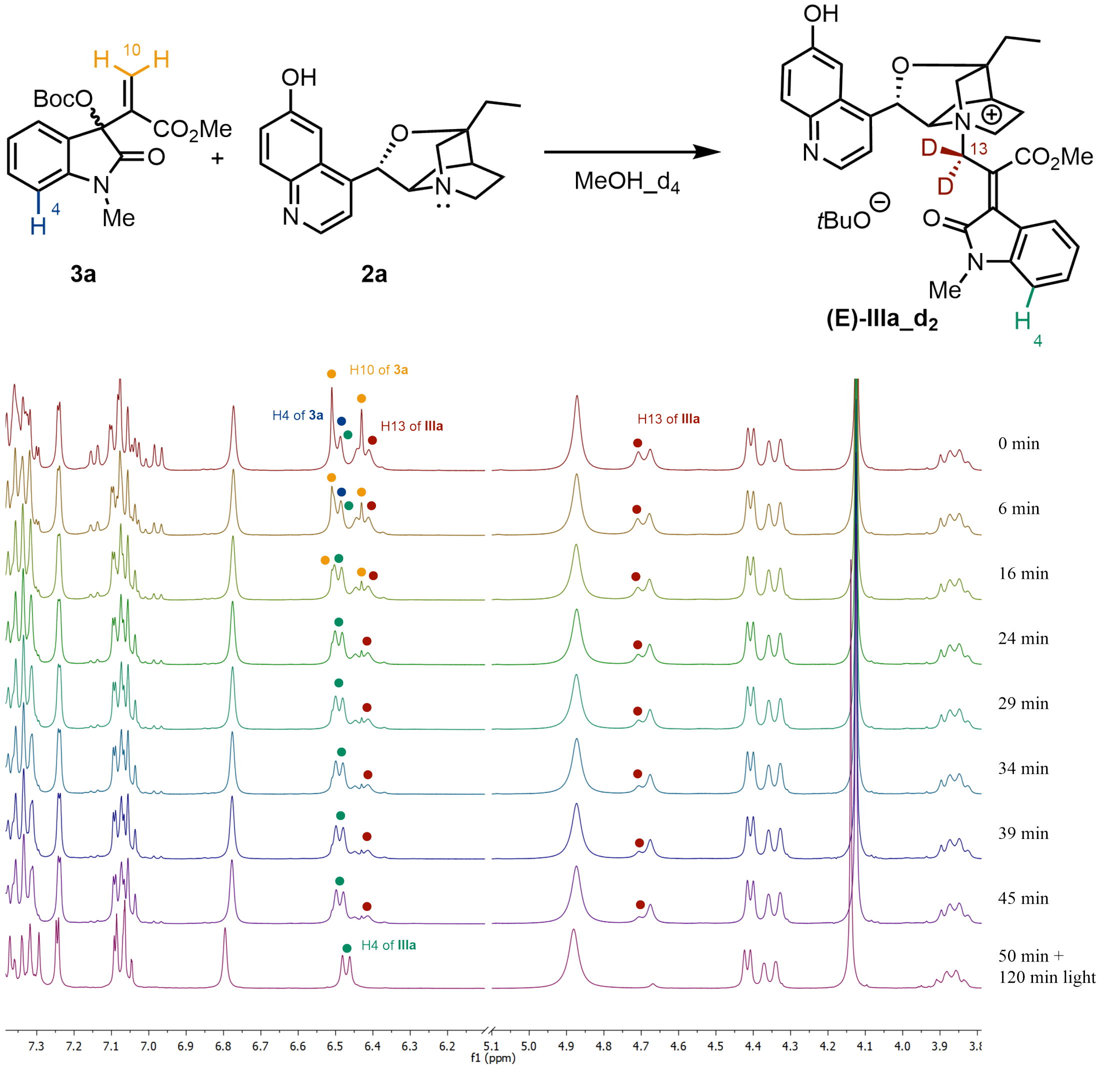

Figure 2.12: ^{1}H NMR spectra of the catalytic intermediate at different times in methanol-d$_4$. In yellow the starting material **3a** can be seen. In blue, H4 of **3a**, that is superimposed with H4 of **IIIa** (green). In red, the disappearance of the allylic protons 13 of **IIIa**, due to deuteration.

light-induced isomerisation could be observed.
From this series of experiments some conclusions can be made:

- There is proton exchange between the acidic proton of methanol and the catalytic intermediate **IIIa**
- Isomerisation happens but it cannot be detected by NMR experiments because the catalytic intermediate decomposes under light
- Base-mediated isomerisation cannot be excluded

Characterisation of the MBH-DABCO bromide salt IIIa': In order to detect the isomerisation of the catalytic species, and to exclude the role of the strong base in the isomerisation of the catalytic intermediate, a similar system with a non-basic counteranion was studied. Adapting the procedure from a reported study,[57] the bromide salt **IIIa'** derived from the isatin MBH alcohol and DABCO (see *Figure 2.13*) was synthesised. The MBH alcohol **6a** was treated with aqueous HBr 48% to yield the bromide (*E*)-**7a** The bromide **7a** was then treated with DABCO and (*E*)-**IIIa'** was isolated in 45% yield as an orange solid.

The salt was fully characterised and its photochemical isomerisation was studied by semi-continuous ^{1}H NMR experiments.

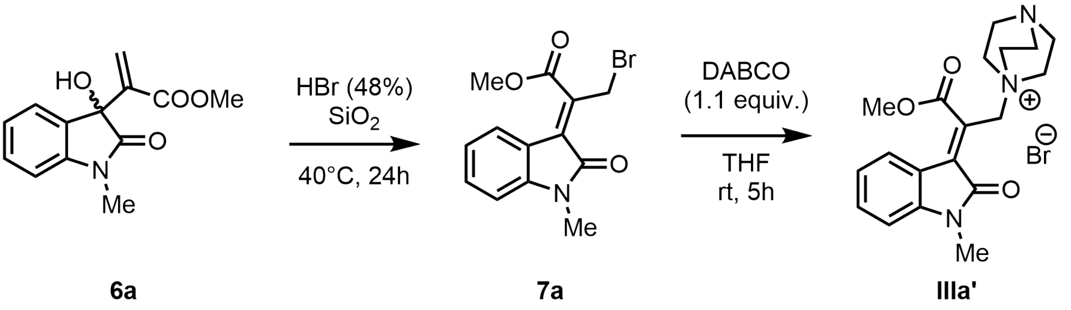

Figure 2.13: Synthesis of the MBH-DABCO bromide salt **(*E*)-IIIa'**.

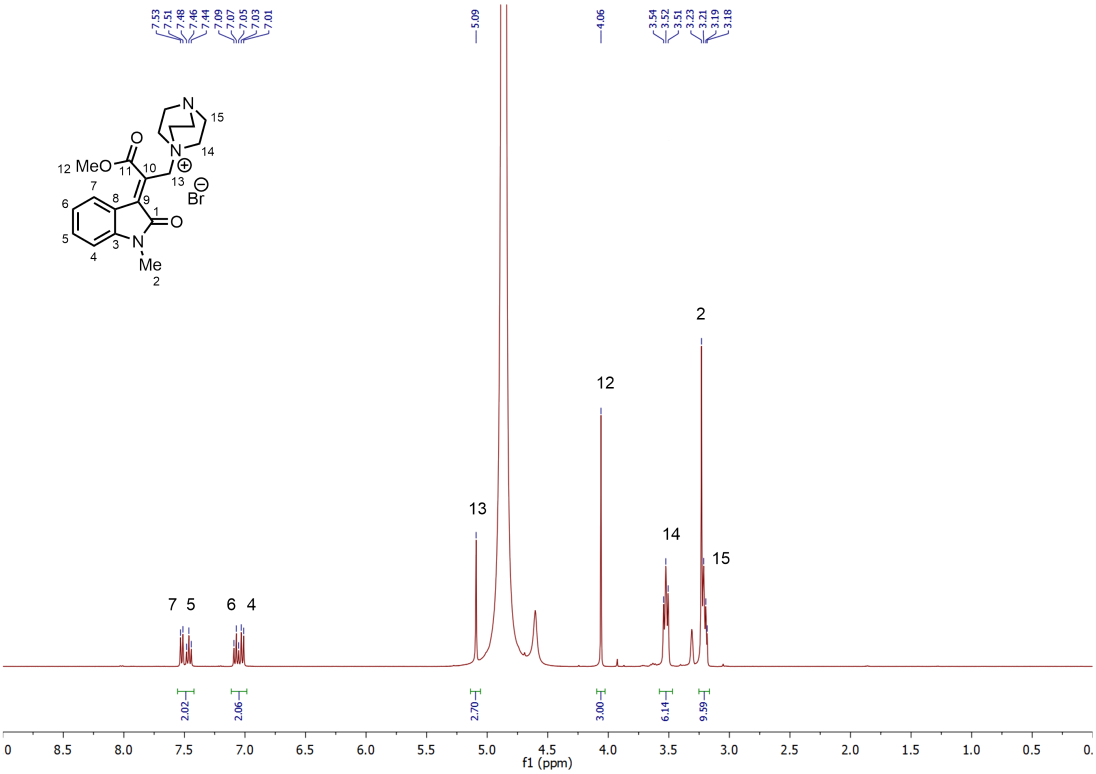

Figure 2.14: ^{1}H NMR characterisation of **IIIa'** in methanol-d$_3$. In the absence of irradiation it is only present as the (*E*)-isomer.

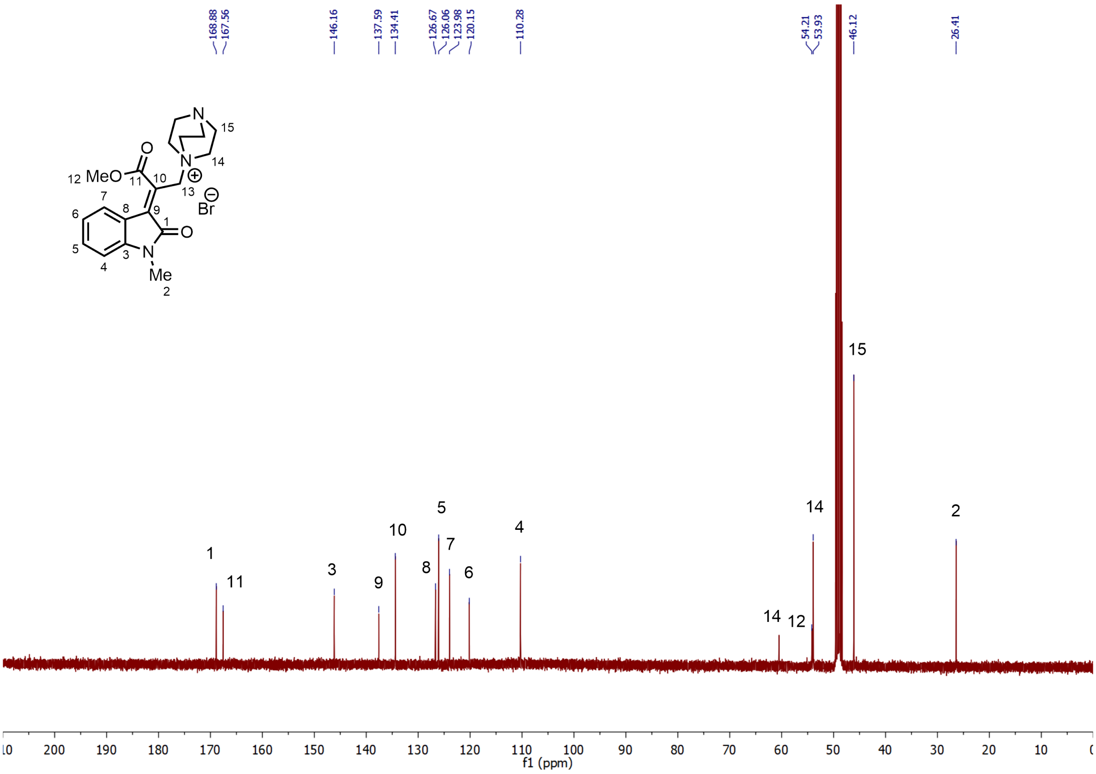

Figure 2.15: ^{13}C NMR characterisation of **IIIa'** in methanol-d$_3$.

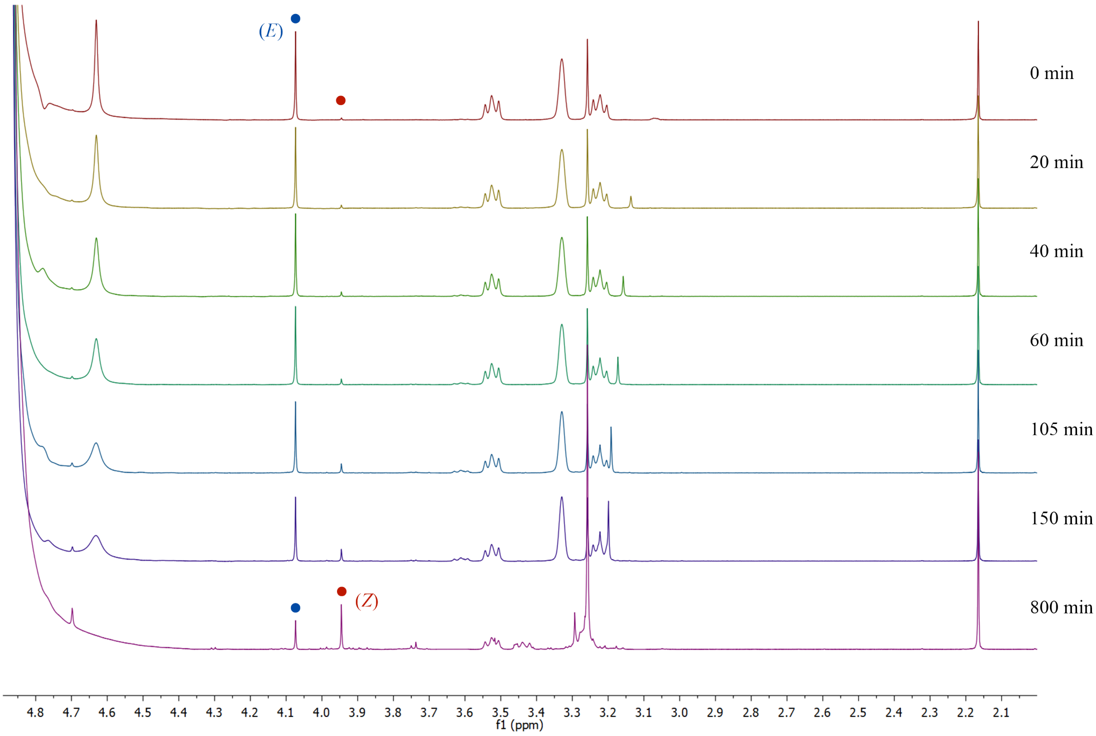

Figure 2.16: Isomerisation of the salt **IIIa'** upon light irradiation, followed by ^{1}H NMR.

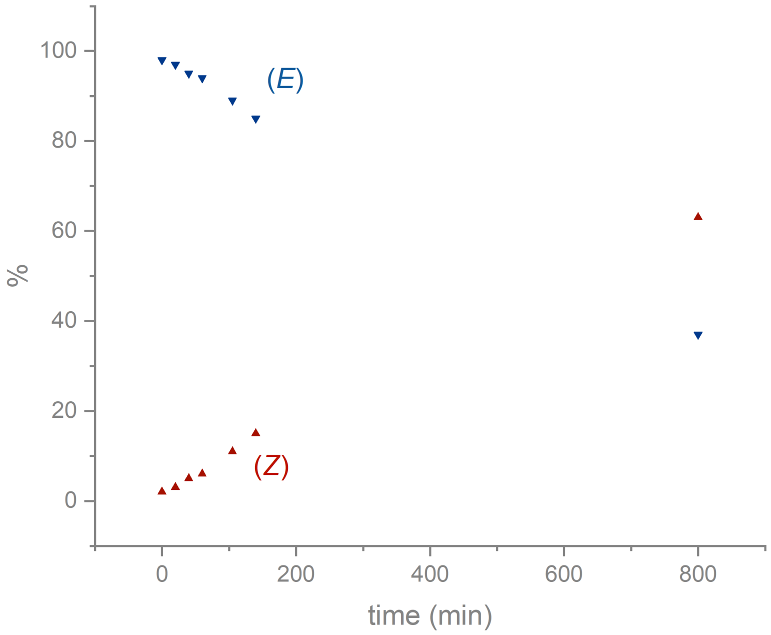

Figure 2.17: Isomerisation of the salt **IIIa'** upon irradiation. In the graph, the area of the peaks corresponding to the methyl ester (H12) are plotted against illumination time.

This time isomerisation between **(*E*)-IIIa'** and **(*Z*)-IIIa'** could be observed. In 140 min of irradiation the diastereomeric ratio changes from $E/Z = 98{:}2$ to 85:15, reaching 37:63 after 13h (shown in *Figure 2.16* and *Figure 2.17*). Remarkably, no isomerisation was observed in the absence of irradiation after 16h, thus confirming the key role of light in the determination of the enantiomeric ratio. It is reasonable to think that, in the reaction conditions, intermediate **IIIa** formed with β-isocupreidine has the same behaviour, although the effect may be mitigated by the increased steric hindrance of β-isocupreidine.

2.5 Optimisation of the Reaction in Flow

Proven that the reaction mixture was homogeneous and stable in methanol without irradiation (as previously shown in *Figure 2.1*, in Section 2.3), the present light-triggered asymmetric allylic benzylation was optimised into a microfluidic photoreactor. The results are shown in Table 2.8.

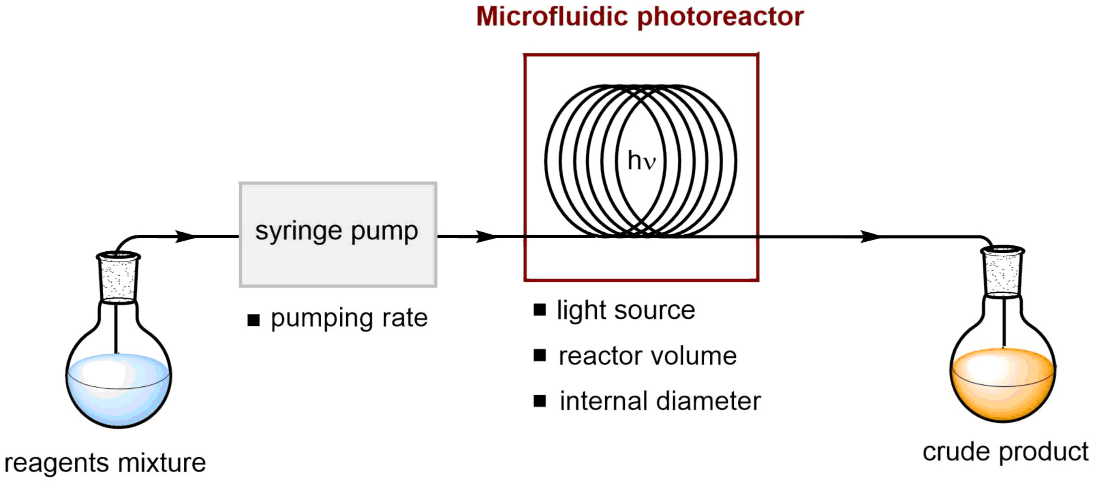
Microfluidic photoreactor
hν
syringe pump
■ pumping rate
■ light source
■ reactor volume
■ internal diameter
reagents mixture
crude product

Figure 2.18: Scheme of the microfluidic photoreactor used in this experiment.

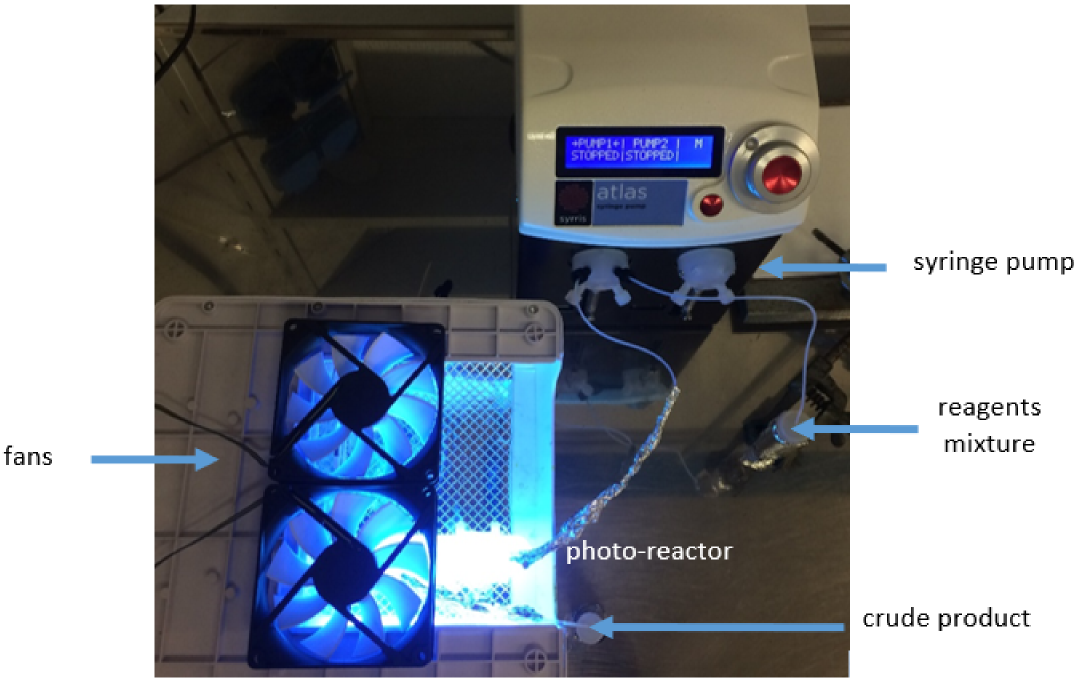
syringe pump
reagents mixture
fans
photo-reactor
crude product

Figure 2.19: Picture of the microfluidic photoreactor used in this experiment.

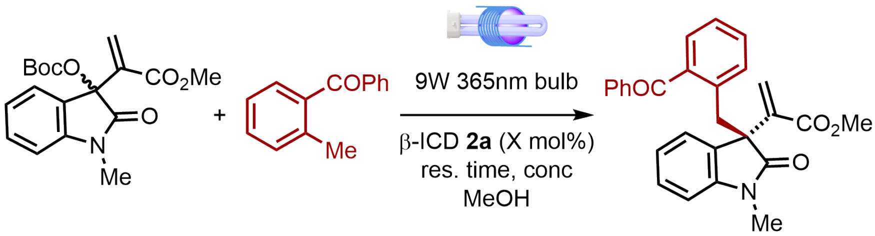

3a **1a** **4a**

Concentration	β-ICD **2a** (mol%)	2-MBP **1a**	Residence time	Conversion	NMR yield
0.1 M	20%	5 eq.	60 min	92%	39%
			40 min	89%	52%
			30 min	86%	50%
0.05 M	20%	5 eq.	40 min	f.c.	47%
			30 min	f.c.	55%
			15 min	71%	46%
			10 min	53%	34%
0.05 M	**10%**	**5 eq.**	50 min	89%	45%
			40 min	91%	44%
			30 min	**67%**	**65% [65%]**[a]
0.05 M	5%	5 eq.	50 min	f.c.%	24%
			40 min	84%	25%
			30 min	68%	29%
			20 min	57%	29%
			10 min	36%	26%
0.05 M	20%	2 eq.	30 min	87%	58%
			25 min	51%	58%
			20 min	60%	39%
			15 min	82%	38%
0.05 M	10%	3 eq.	40 min	60%	46%
			35 min	60%	50%
			30 min	53%	43%
			20 min	48%	37%

Table 2.8: Screening of reaction conditions into a microfluidic photoreactor. Yield and conversion were calculated by integrating the NMR peaks of the reaction crude using pyrazine as internal standard. [a][Isolated yield].

In terms of catalyst loading, the best results were obtained with 10 mol% of **2a**. While a 5 mol% of catalyst loading was not enough to grant the satisfying reaction turnover, 20 mol% of **2a** leads to high conversion values but lower NMR yields. As already seen in the previous section, the electrophilic intermediate **IIIa** decomposes under light irradiation, therefore high catalyst loading causes faster decomposition and reduces the overall efficiency of the transformation. Variation on the concentration of 2-methylbenzophenone also changed the results significantly: being the nucleophilic attack of the photoenol the slow step of the catalytic cycle, the more 2-methylbenzophenone **1a** present in solution, the faster is the reaction. Moreover, higher concentration of **1a** in solution has also the beneficial function of *inner filter*, partially absorbing light irradiation and preventing over irradiation of the catalytic species **IIIa**.

Although, the optimal conditions in the microfluidic photoreactor (shown in bold in Table 2.8) could not improve the 78% yield obtained in batch.

Covalent catalysis is not usually suitable for flow setup, because covalent activation is generally slower than non-covalent activation. In fact, in literature there are very few reports dealing with photoreactions in flow that take place *via* covalent activation. It should be noticed that the use of 10 mol% of catalyst loading means that the catalyst has to make 10 turnovers inside the microfluidic photoreactor.

Another reason could be the different emission spectra of the two lights used for the batch and for the flow, both with the maximum centred on 365nm. While the high-power LED used for batch reactions presents a much sharper emission band, the 9W lamp has a broader spectrum, as shown in *Figure 2.20*. Since both the catalytic intermediate and the product absorb at that given wavelength, it is possible that the product and/or the catalytic intermediate decompose faster under the irradiation of 9W 365nm bulb.

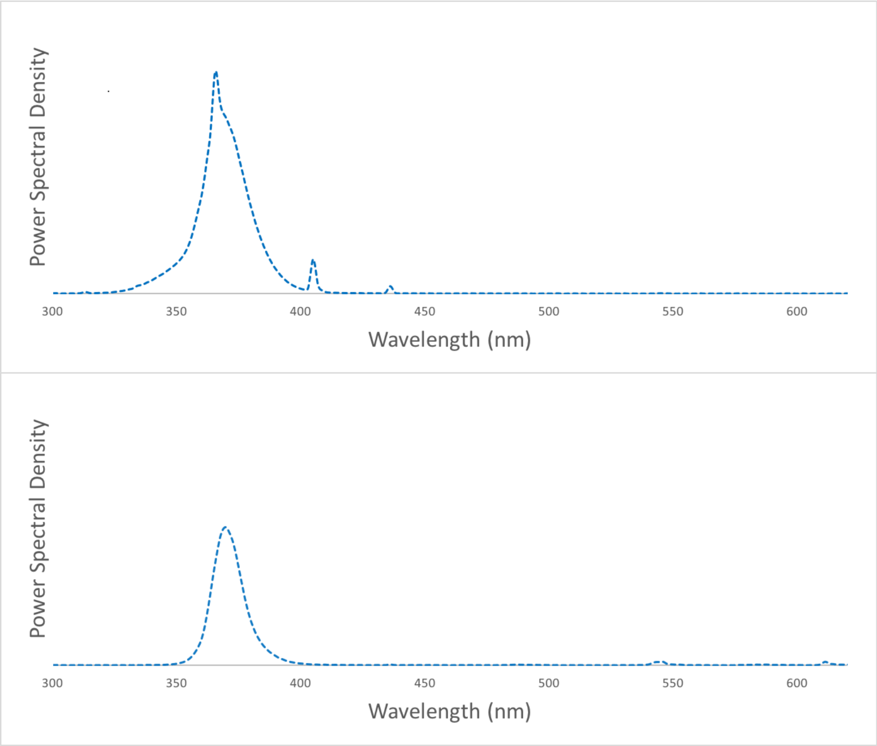

Figure 2.20: Emission spectra of the 9W 365nm lamp used in the flow setup (top) vs High-Power 365nm LED used in the batch setup (bottom).

This hypothesis is supported by the values of conversion: as expected, the quantity of starting material decreases when the residence time is increased (which corresponds to the exposure time to the light). In return, the yield does not increase with the same trend and, conversely, it decreases notably if the residence time is too long. UV-vis spectra were acquired for all the species present in solution (*Figure 2.21*), and both the catalytic species **IIIa** and the product **4a** are absorbing at the working wavelength.
In addition, although the 9W lamp used in the microfluidic setup is about seven times less intense than the HP LED used in batch, the light irradiation is much more efficient in microfluidic conditions. In fact, as already mentioned in the introductory chapter, the capillary grants a more efficient and homogeneous illumination to the whole reacting mixture, but this implies also a faster degradation of the light-sensitive species present in solution.

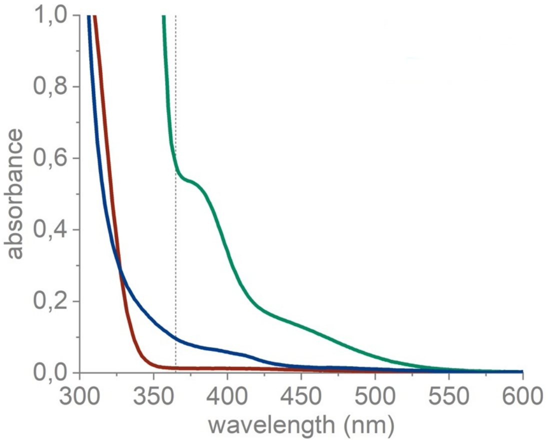

Figure 2.21: Absorption spectra of isatin MBH carbonate **3a** (red, 10^{-3}M), catalytic intermediate **IIIa** (green, 10^{-3}M) and benzylated product **4a** (blue, 10^{-3}M) in MeOH. The operative wavelength used in the present work (365 nm) is shown as a dotted black line.

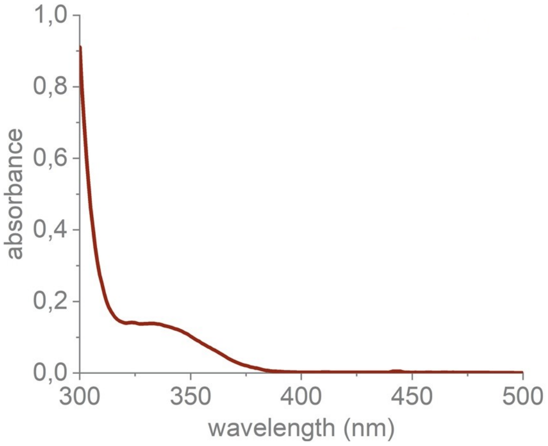

Figure 2.22: Absorption spectrum of 2-methylbenzophenone **1a** (10^{-3}M) in MeOH.

The UV-vis spectrum confirms the high absorbance of the catalytic species **IIIa** at the working wavelength, while **3a** does not absorb at the working wavelength. In addition, the product **4a** is absorbing at the operative wavelength and could also decompose under light exposition. In fact, the benzylated product contains the 2-methylbenzophenone moiety, so the absorbance spectrum will be similar to that of **1a**.

2.6 Scope

The best conditions found during the optimisation of the batch reaction are: 1 equivalent of MBH carbonate **3** (0.1mmol), 5 equivalents of 2-methylbenzophenone derivative **1** and 10% of β-isocupreidine in 1mL degassed methanol (0.1M) at room temperature using HP LED 350mA. With these conditions the generality of the reaction was investigated.

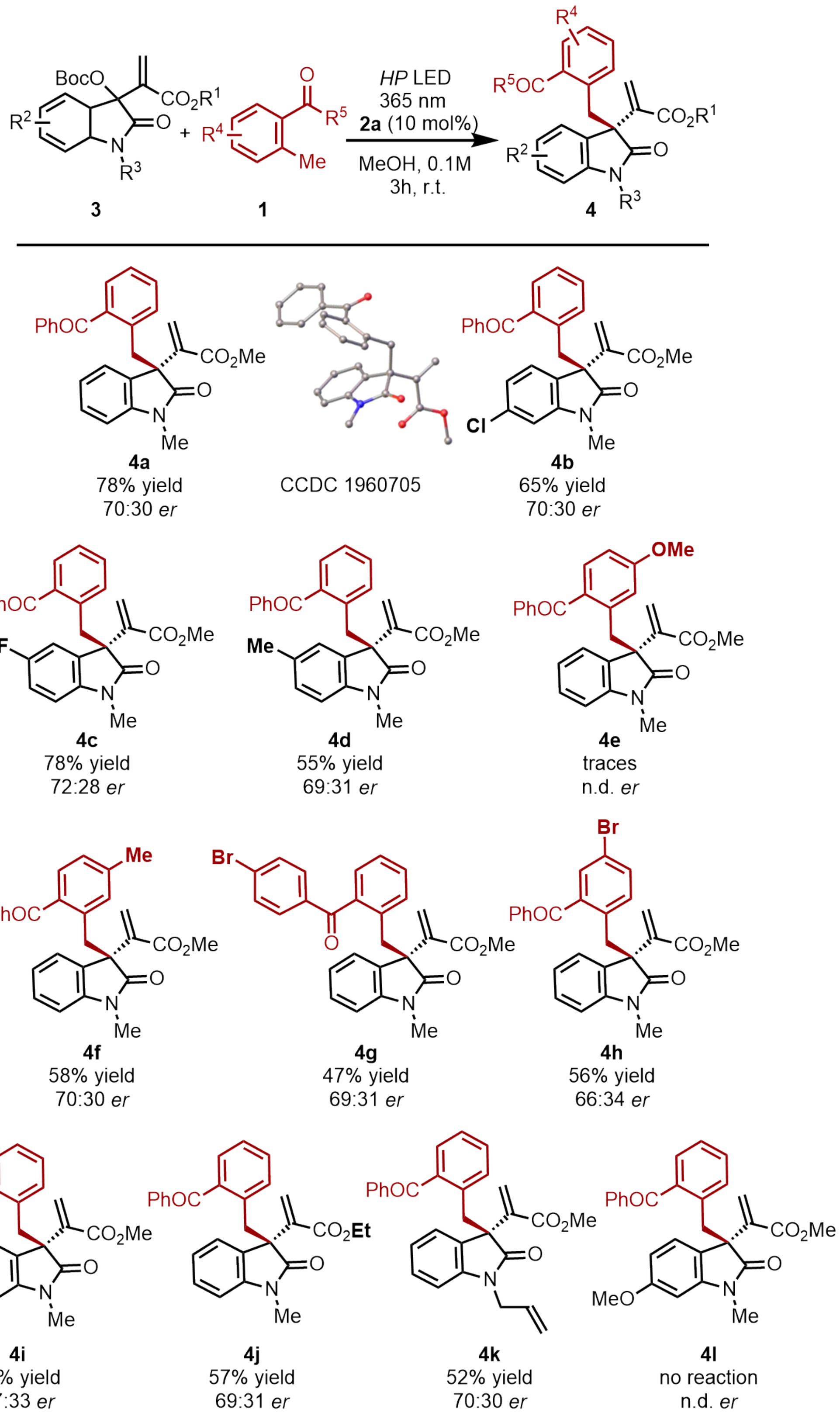
BocO
CO$_2$R^1
R^2
N
R^3
O
R^4
R^5
Me
HP LED
365 nm
2a (10 mol%)
MeOH, 0.1M
3h, r.t.
R^{5}OC
3
1
4
PhOC
CO$_2$Me
CO$_2$Et
Me
Cl
F
OMe
Br
MeO

4a
78% yield
70:30 *er*

CCDC 1960705

4b
65% yield
70:30 *er*

4c
78% yield
72:28 *er*

4d
55% yield
69:31 *er*

4e
traces
n.d. *er*

4f
58% yield
70:30 *er*

4g
47% yield
69:31 *er*

4h
56% yield
66:34 *er*

4i
70% yield
67:33 *er*

4j
57% yield
69:31 *er*

4k
52% yield
70:30 *er*

4l
no reaction
n.d. *er*

Figure 2.23: Scope of the reaction. The enantiomeric ratios were determined by chiral HPLC analysis. Reaction conditions: 0.1 mmol of **3** (1 equiv.), **1** (5 equiv.), β-isocupreidine **2a** (10 mol%) in 1 mL of argon-degassed methanol were irradiated at 365 nm for 3h. ^{a}Irradiated overnight.

The best results were obtained starting from the unsubstituted substrate (product **4a**) and from the 5-F isatin-derived MBH carbonate (product **4c**). It is reasonable to think that these substrates are enough electron-poor towards the nucleophilic attack and therefore the reaction is faster, leading to higher yields. With a chlorine in the 6-position of the aromatic ring of the electrophile the reaction also works quite well (**4b**). Weak electron-donating groups are also tolerated, albeit with lower yield (**4d**). Esters and N-protecting groups only affect the reactivity and not the enantioselectivity, as it can be seen for products **4j** and **4k** and as demonstrated in previous optimisation studies. Conversely, electron-withdrawing groups on the nucleophile decrease both the reactivity and the enantiomeric ratios. The lower reactivity is attributed to the less nucleophilic character of the nucleophiles containing electron-withdrawing groups. Surprisingly, very low reactivity was observed with the extendedly conjugated 4'-MeO-2-methylbenzophenone (product **4e**) which in principle should be more nucleophilic in virtue of the resonance properties of the methoxy group on the aromatic ring. Instead, as expected, a methoxy group in the MBH carbonate aromatic ring inhibits the reactivity, and no reaction was observed (**4l**). All the new benzylated products were isolated and fully characterised by ^{1}H, ^{13}C NMR and HRMS. The enantiomeric ratios were measured using chiral HPLC analysis on the purified samples. Specific optical rotation were measured for all the isolated benzylated products (**4a**-**4d** and **4f**-**4k**). Compound **4a** was crystallised and structure was resolved by XRD (CCDC 1960705). The absolute configuration of the benzylated products was determined as (*R*) by TD-DFT calculations of the electronic circular dichroism (ECD) spectrum (see Section4.9).

Chapter 3

Conclusions

Organocatalysis and photochemistry are gaining nowadays more and more attention for their lower impact on the environment and their lower hazardous nature. In this thesis project, the first light-triggered, Lewis-base catalysed allylic benzylation of isatin-derived MBH carbonates is reported.
The reaction affords a wide set of 3,3-disubstituted oxindoles bearing an *all-carbon* benzylated quaternary stereocenter with good yields up to 78% and moderate enantioselectivities around 40%. The reaction was optimised for batch and for microfluidic continuous synthesis. Remarkably, this represents one of the few examples of asymmetric light-triggered tranformations *via* covalent catalysis in flow.
The hypothesised dual activation by light and the chiral catalyst is proven. Light irradiation excites the 2-methylbenzophenone pronucleophile **1a** to generate the activated nucleophile **Ia**, while β-isocupreidine activates MBH carbonate **3a** towards the generation of the reactive electrophilic catalytic intermediate **IIIa** (*Figure 3.1*).

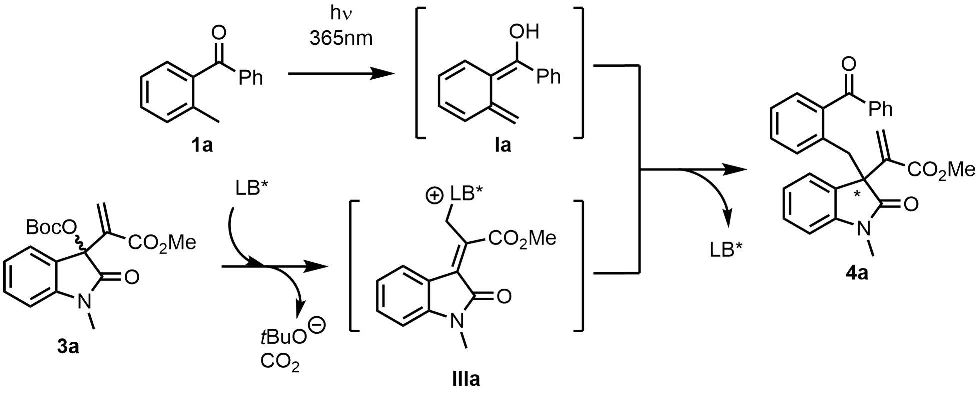

Figure 3.1: The dual activation mechanism of the present photoactivated asymmetric allylic benzylation.

Mechanistic investigation revealed that the reasons for the moderate asymmetric induction was the E/Z photoisomerisation of the intermediate **IIIa**, the catalytic resting state (*Figure 3.2*). The light-induced isomerisation and the decomposition of **IIIa** are verified by NMR experiments and are supported by the UV-vis spectrum of **IIIa**, that shows high absorption at the working wavelength.
Base-mediated isomerisation was ruled out after NMR experiments on a similar system with an inert counteranion instead of the strong base tBuO$^-$. Although allylic proton

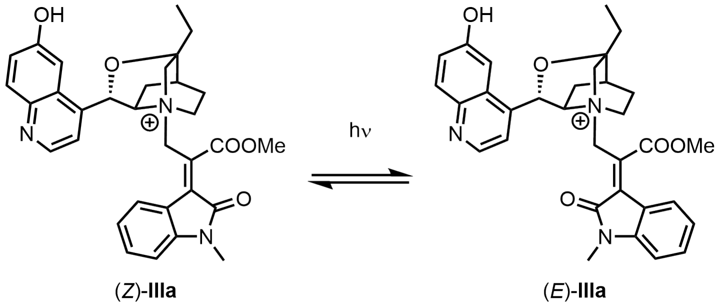

Figure 3.2: Isomerisation of the intermediate **IIIa**

exchange with the solvent is evidenced by the fact that in methanol-d_4 they slowly exchange with deuterium, the *t*BuO$^-$ ionised upon formation of **IIIa** is not the reason of the isomerisation.

There is still room for improvement. A recent study[58] used a 700nm laser to excite the 2-methylbenzaldehyde by two-photon absorption. This process generated the corresponding photoenol intermediate through an identical mechanism to the photoenolisation of 2-methylbenzophenone. The intermediate **XLIV** reacted in a [4+2] cycloaddition manifold with maleimides (*Figure 3.3*). Being the two-photon absorption a non-linear effect, a very intense light source was required. Therefore, this could be a possible solution to overcome the light-induced isomerisation of the intermediate **IIIa**, provided that the intermediate itself does not undergo two-photon absorption neither isomerisation upon laser illumination.

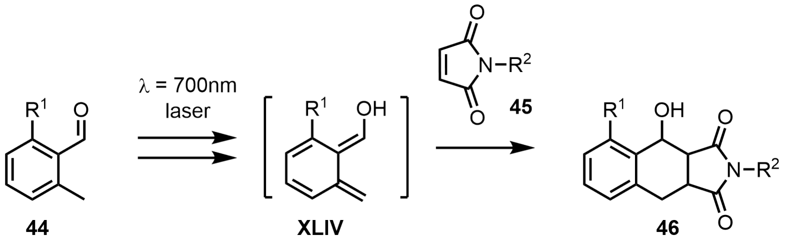

Figure 3.3: A double photon absorption of 2-methylbenzaldehyde **44** is used to generate the reactive photoenol **LXIV**.[58]

Chapter 4

Experimental

Instruments: NMR spectra were recorded on Bruker 400 Avance III HD equipped with a BBI-z grad probehead 5mm. The chemical shifts (δ) for ^{1}H and ^{13}C are given in ppm relative to residual signals of the solvents ($CDCl_3$@ 7.26 ppm ^{1}H NMR, 77.16 ppm ^{13}C NMR; MeOD@ 3.31 ppm, 4.87 ppm ^{1}H NMR, 49.00 ppm ^{13}C NMR). The following abbreviations are used to indicate the multiplicity: s, singlet; d, doublet; t, triplet; q,quartet; m, multiplet; bs, broad signal. NMR yields were calculated by using pyrazine as internal standard. High-Resolution Mass Spectra (HRMS) were obtained using Waters GCT gas chromatograph coupled with a time-of-flight mass spectrometer (GC/MS-TOF) with electron ionization (EI) or MicroTOF II (Bruker Daltonics): HPLC-MS-TOF (ESI). Chromatographic purification of products was accomplished using flash chromatography on silica gel (SiO_2, 0.04-0.063 mm) purchased from Machery-Nagel, with the indicated solvent system according to the standard techniques. Thin-layer chromatography (TLC) analysis was performed on pre-coated Merck TLC plates (silica gel 60 GF254, 0.25 mm). Visualization of the developed chromatography was performed by checking UV absorbance (254nm) as well as with aqueous potassium permanganate solutions. Organic solutions were concentrated under reduced pressure on a Büchi rotary evaporator.

Materials: Commercial grade reagents and solvents were purchased at the highest commercial quality from Sigma Aldrich, Alfa Aesar or Fluka and used as received, unless otherwise stated.

4.1 General procedure for preparation of substituted 2-methylbenzophenones

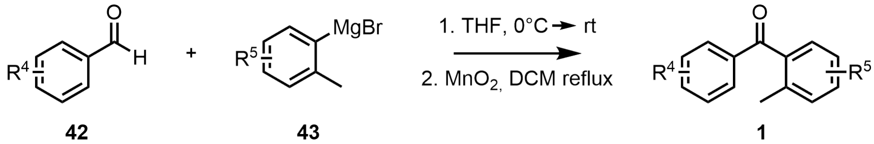

The benzaldehyde derivative **42** (1 eq.) is dissolved in dry THF under argon atmosphere. The mixture is cooled to 0°C and a 0.5M solution of **43** (1.2 eq.) is slowly added. The mixture is left to warm up to room temperature. After completion, the reaction is quenched with water and extracted with AcOEt. The organic phase is dried with $MgSO_4$ and dried in vacuum. The crude is then dissolved in dry DCM and MnO_2

(7 eq.) is added under Ar atmosphere. The mixture is refluxed for 10h. The mixture is then filtered, washed with DCM and purified by flash chromatography to afford compound **1**.[45]

4.2 General procedure for preparation of N-methyl-isatins

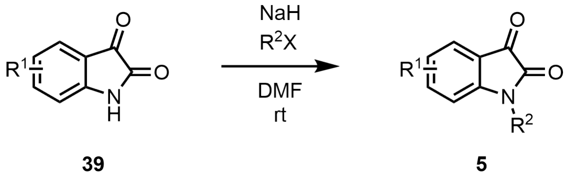

39 **5**

Substituted isatin **39** (1 eq.) is dissolved in DMF under N_2 atmosphere. NaH (1.2 eq.) is added at 0°C and stirred for 5 minutes. Methyl iodide (1.2 eq.) is then added slowly. After completion, the reaction is quenched with water and extracted with ethyl acetate. The organic layer is dried over $MgSO_4$ and dried in vacuum. The product **5** is precipitated from DMF by addition of water and filtered in vacuum.[59,60]

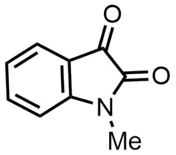

1-methyl-1H-indole-2,3-dione **5a**: ^{1}H NMR (400 MHz, Chloroform-d) δ 7.59 (qd, J = 7.5, 1.0 Hz, 2H), 7.12 (td, J = 7.5, 0.8 Hz, 1H), 6.90 (d, J = 7.9 Hz, 1H), 3.24 (s, 3H). The NMR peaks are in accordance with what previously reported in literature.[61]

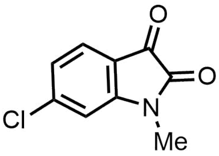

1-methyl-1H-6-chloro-indole-3-dione **5b**: ^{1}H NMR (300 MHz, Chloroform-d) δ 7.53 (d, J = 8.0 Hz, 1H), 7.09 (dd, J = 7.9, 1.7 Hz, 1H), 6.89 (d, J = 1.7 Hz, 1H), 3.23 (s, 3H). The NMR peaks are in accordance with what previously reported in literature.[62]

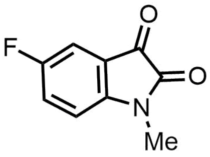

1-methyl-1H-5-fluoro-indole-3-dione **5c**: ^{1}H NMR (200 MHz, Chloroform-d) δ 7.42 – 7.27 (m, 2H), 6.86 (dd, J = 9.5, 3.4 Hz, 1H), 3.26 (s, 3H). The NMR peaks are in accordance with what previously reported in literature.[63]

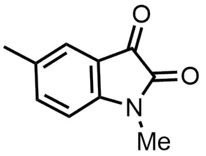

1,5-dimethyl-1H-indole-2,3-dione **5d**: ^{1}H NMR (200 MHz, Chloroform-d) δ 7.40 (d, J = 7.8 Hz, 2H), 6.78 (d, J = 8.1 Hz, 1H), 3.23 (s, 3H), 2.34 (s, 3H). The NMR peaks are in accordance with what previously reported in literature.[63]

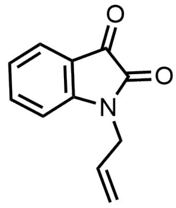

1-allyl-1H-indole-2,3-dione **5e**: ^{1}H NMR (200 MHz, Chloroform-d) δ 7.58 (qd, J = 7.8, 7.2, 1.2 Hz, 2H), 7.12 (t, J = 7.5 Hz, 1H), 6.89 (d, J = 7.9 Hz, 1H), 5.85 (ddd, J = 22.4, 10.4, 5.4 Hz, 1H), 5.47 – 5.14 (m, 2H), 4.37 (d, J = 5.2 Hz, 2H). The NMR peaks are in accordance with what previously reported in literature.[64]

4.3 General procedure for preparation of MBH alcohols

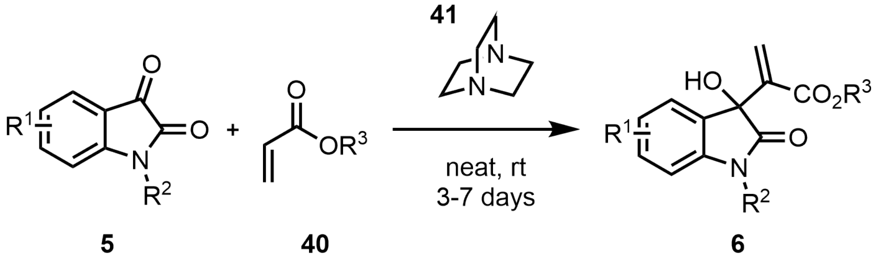

N-protected isatin **5** (1 eq.) is mixed with DABCO (0.5 eq.) and acrylate **40** (5 eq.) in a vial. After completion, the reaction mixture is purified by flash chromatography and dried in vacuum to afford the final product **6**.[65]

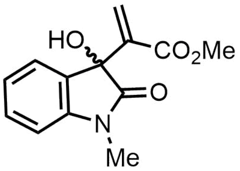

methyl 2-(3-hydroxy-1-methyl-2-oxoindolin-3-yl)acrylate **6a**: ^{1}H NMR (200 MHz, Chloroform-d) δ 7.35 (td, J = 7.7, 1.4 Hz, 1H), 7.24 – 7.14 (m, 1H), 7.04 (td, J = 7.5, 1.0 Hz, 1H), 6.87 (d, J = 7.8 Hz, 1H), 6.56 (s, 1H), 6.39 (s, 1H), 3.64 (s, 3H), 3.26 (s, 3H). The NMR peaks are in accordance with what previously reported in literature.[66]

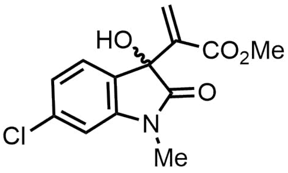

methyl 2-(6-chloro-3-hydroxy-1-methyl-2-oxoindolin-3-yl)acrylate **6b**: ^{1}H NMR (200 MHz, Chloroform-d) δ 7.11 (d, J = 8.2 Hz, 1H), 7.02 (dd, J = 8.2, 1.7 Hz, 1H), 6.87 (d, J = 1.9 Hz, 1H), 6.57 (s, 1H), 6.40 (s, 1H), 3.66 (s, 3H), 3.24 (s, 3H). The NMR peaks are in accordance with what previously reported in literature.[67]

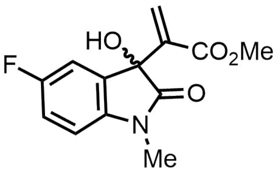

methyl 2-(5-fluoro-3-hydroxy-1-methyl-2-oxoindolin-3-yl)acrylate **6c**: ^{1}H NMR (300 MHz, Chloroform-d) δ 7.02 (td, J = 8.8, 2.6 Hz, 1H), 6.93 (dd, J = 7.6, 2.4 Hz, 1H), 6.77 (dd, J = 8.4, 4.1 Hz, 1H), 6.55 (s, 1H), 6.39 (s, 1H), 3.63 (s, 3H), 3.22 (s, 3H). The NMR peaks are in accordance with what previously reported in literature.[68]

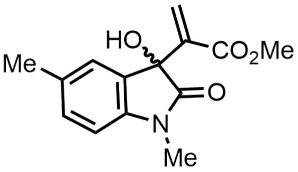

methyl 2-(5-methyl-3-hydroxy-1-methyl-2-oxoindolin-3-yl)acrylate **6d**: ^{1}H NMR (200 MHz, Chloroform-d) δ 7.14 (d, J = 9.3 Hz, 1H), 7.01 (s, 1H), 6.76 (d, J = 7.8 Hz, 1H), 6.56 (s, 1H), 6.39 (s, 1H), 3.65 (s, 3H), 3.24 (s, 3H), 2.30 (s, 3H). The NMR peaks are in accordance with what previously reported in literature.[69]

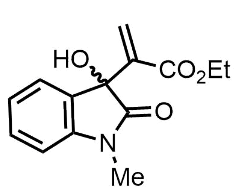

ethyl 2-(3-hydroxy-1-methyl-2-oxoindolin-3-yl)acrylate 6e: ^{1}H NMR (200 MHz, Chloroform-d) δ 7.34 (td, J = 7.5, 1.1 Hz, 1H), 7.20 (dd, J = 7.2, 1.0 Hz, 1H), 7.04 (td, J = 7.6, 0.9 Hz, 1H), 6.86 (d, J = 7.8 Hz, 1H), 6.58 (s, 1H), 6.38 (s, 1H), 4.06 (qd, J = 7.2, 2.0 Hz, 2H), 3.25 (s, 3H), 1.14 (t, J = 7.1 Hz, 3H). The NMR peaks are in accordance with what previously reported in literature.[70]

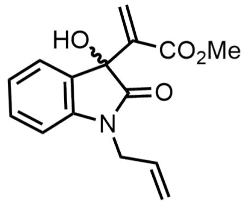

methyl 2-(3-hydroxy-1-allyl-2-oxoindolin-3-yl)acrylate 6f: ^{1}H NMR (200 MHz, Chloroform-d) δ 7.32 (d, J = 6.3 Hz, 1H), 7.20 (d, J = 7.0 Hz, 1H), 7.03 (t, J = 7.7 Hz, 1H), 6.87 (d, J = 7.6 Hz, 1H), 6.57 (s, 1H), 6.41 (s, 1H), 6.04 – 5.75 (m, 1H), 5.48 – 5.15 (m, 2H), 4.56 – 4.18 (m, 2H), 3.64 (s, 3H). The NMR peaks are in accordance with what previously reported in literature.[68]

4.4 General procedure for preparation of MBH carbonates

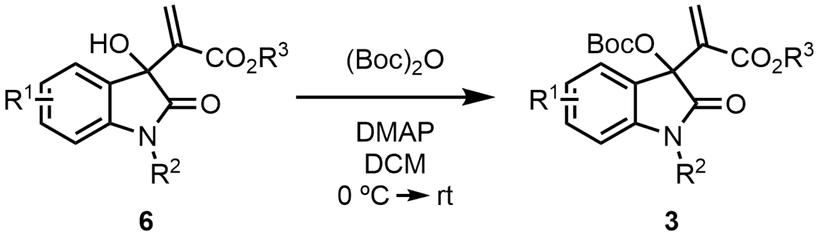

MBH alcohol **6** is dissolved in dry dichloromethane under N_2 atmosphere, in a round-bottomed flask. Di-tert-butyl dicarbonate (1.5 eq.) and DMAP (0.05 eq.) are mixed together in dichloromethane and then added to the reaction mixture at 0°C. The reaction is quenched with HCl 2M and extracted with dichloromethane. The organic layer is dried over $MgSO_4$ and subsequently purified by flash chromatography to afford the final product **3**.[71]

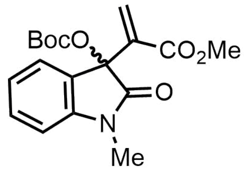

methyl 2-(1-methyl-3-tert-butoxycarbonyloxy-2-oxoindolin-3-yl)acrylate 3a: ^{1}H NMR (200 MHz, Chloroform-d) δ 7.33 (td, J = 7.7, 1.4 Hz, 1H), 7.18 (d, J = 7.5 Hz, 1H), 6.99 (td, J = 7.5, 1.0 Hz, 1H), 6.85 (d, J = 7.8 Hz, 1H), 6.60 – 6.54 (m, 1H), 6.53 (s, 1H), 3.57 (s, 3H), 3.29 (s, 3H), 1.34 (s, 9H). The NMR peaks are in accordance with what previously reported in literature.[71]

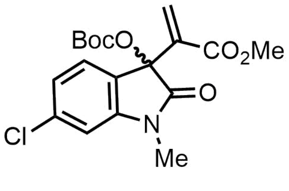

methyl 2-(3-((tert-butoxycarbonyl)oxy)-6-chloro-1-methyl-2-oxoindolin-3-yl)acrylate 3b: ^{1}H NMR (200 MHz, Chloroform-d) δ 7.09 (d, J = 7.7 Hz, 1H), 6.97 (dd, J = 7.9, 1.8 Hz, 1H), 6.85 (d, J = 1.6 Hz, 1H), 6.57 (s, 1H), 6.54 (s, 1H), 3.59 (s, 3H), 3.28 (s, 3H), 1.36 (s, 9H). The NMR peaks are in accordance with what previously reported in literature.[71]

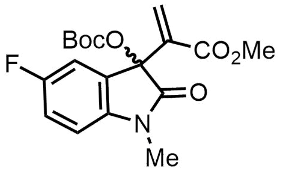

methyl 2-(3-((tert-butoxycarbonyl)oxy)-5-fluoro-1-methyl-2-oxoindolin-3-yl)acrylate **3c**: ^{1}H NMR (200 MHz, Chloroform-d) δ 7.11 – 6.91 (m, 2H), 6.83 – 6.72 (m, 1H), 6.59 (s, 1H), 6.54 (s, 1H), 3.60 (s, 3H), 3.29 (s, 3H), 1.37 (s, 9H). The NMR peaks are in accordance with what previously reported in literature.[65]

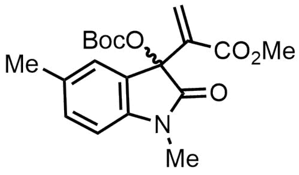

methyl 2-(1,5-dimethyl-3-tert-butoxycarbonyloxy-2-oxoindolin-3-yl)acrylate **3d**: ^{1}H NMR (200 MHz, Chloroform-d) δ 7.13 (d, J = 7.3 Hz, 1H), 7.00 (s, 1H), 6.74 (d, J = 8.1 Hz, 1H), 6.56 (s, 1H), 6.53 (s, 1H), 3.58 (s, 3H), 3.28 (s, 3H), 2.29 (s, 3H), 1.36 (s, 9H). The NMR peaks are in accordance with what previously reported in literature.[65]

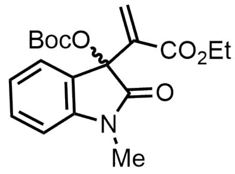

ethyl 2-(1-methyl-3-tert-butoxycarbonyloxy-2-oxoindolin-3-yl)acrylate **3e**: ^{1}H NMR (200 MHz, Chloroform-d) δ 7.33 (td, J = 7.8, 1.3 Hz, 1H), 7.18 (dd, J = 7.4, 0.8 Hz, 1H), 6.99 (td, J = 7.6, 0.9 Hz, 1H), 6.84 (d, J = 7.8 Hz, 1H), 6.57 (s, 1H), 6.51 (s, 1H), 3.98 (qd, J = 7.2, 4.5 Hz, 2H), 3.29 (s, 3H), 1.34 (s, 9H), 1.09 (t, J = 7.1 Hz, 3H). The NMR peaks are in accordance with what previously reported in literature.[71]

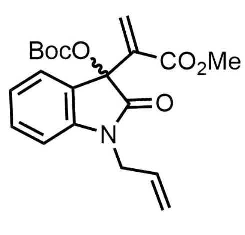

methyl 2-(3-((tert-butoxycarbonyl)oxy)-1-allyl-2-oxoindolin-3-yl)acrylate **3f**: ^{1}H NMR (200 MHz, Chloroform-d) δ 7.38 – 7.26 (m, 1H), 7.19 (d, J = 8.5 Hz, 1H), 6.98 (t, J = 7.5 Hz, 1H), 6.85 (d, J = 8.3 Hz, 1H), 6.54 (d, J = 7.6 Hz, 2H), 6.06 – 5.81 (m, 1H), 5.47 (d, J = 17.2 Hz, 1H), 5.26 (d, J = 10.4 Hz, 1H), 4.56 – 4.28 (m, 2H), 3.57 (s, 3H), 1.35 (s, 9H). The NMR peaks are in accordance with what previously reported in literature.[65]

4.5 General procedure for allylic benzylation

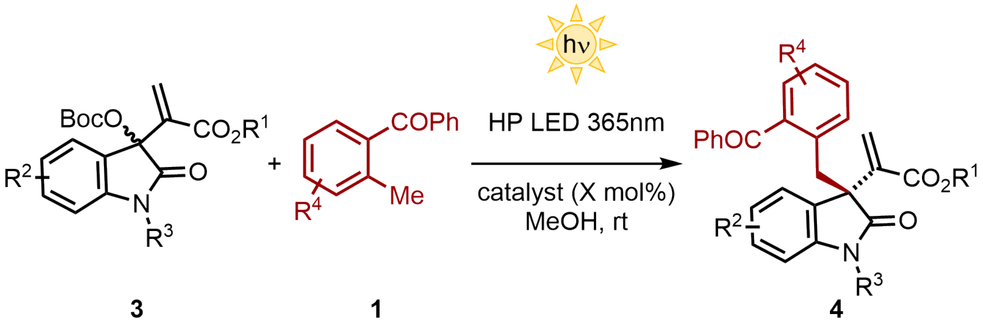
hν
BocO
CO$_2$R^1
R^2
O
N
R^3
+
COPh
Me
R^4
HP LED 365nm
catalyst (X mol%)
MeOH, rt
R^4
PhOC
CO$_2$R^1
R^2
O
N
R^3
3
1
4

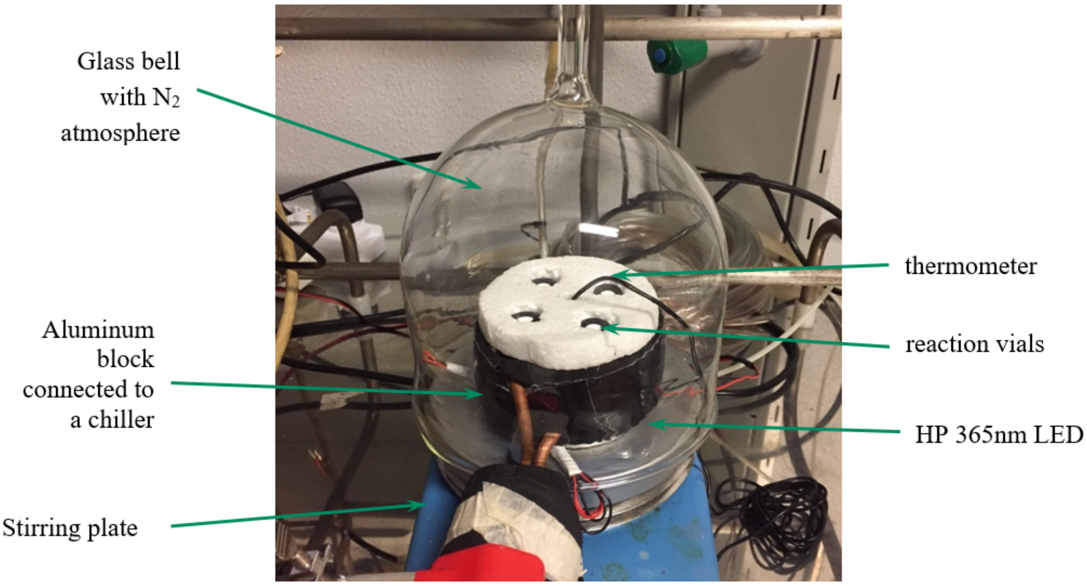
Glass bell with N$_2$ atmosphere
Aluminum block connected to a chiller
Stirring plate
thermometer
reaction vials
HP 365nm LED

Figure 4.1: Picture of the reaction setup used in this study

Racemic: MBH carbonate **3** (0.1 mmol, 1 eq.) and DABCO (0.2 eq.) are purged with Ar in a 4 ml an oven dried screw cap vial. Methanol (1 ml) is added and 2-methylbenzophenone **1** (5 eq.) is added. The mixture is put under UV light (High Power LED, 365nm, 0.35A) for 4h. The progress of reaction is checked by NMR with internal standard pyrazine. The crude is separated by flash chromatography to afford the final product. The product is dissolved in dichloromethane, filtered and injected in the chiral HPLC to see the retention time of the two enantiomers.

Chiral: MBH carbonate **3** (0.1 mmol, 1 eq.) and β-isocupreidine (0.1 eq.) are purged with Ar in an oven dried screw cap vial. Methanol (1 ml) and 2-methylbenzophenone **1** (5 eq.) are added. The mixture is put under light (High Power LED, max λ 365nm, 0.35A) and the reaction is followed by TLC. After completion, the crude is purified by flash chromatography to yield the final product. The product is dissolved in dichloromethane, filtered and injected in the chiral HPLC to evaluate the enantiomeric excess.

4.6 Screening of the reaction conditions for microfluidic setup

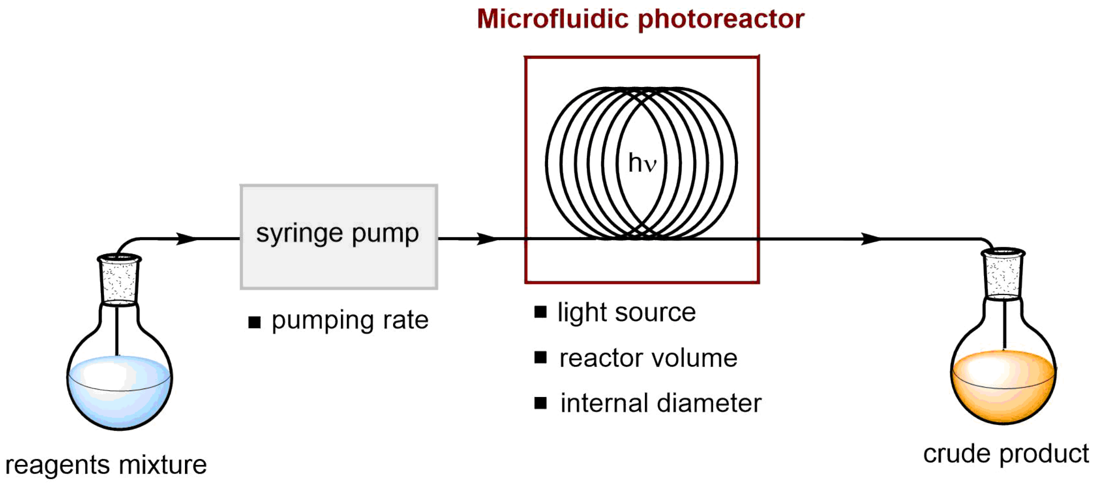
Microfluidic photoreactor
hν
syringe pump
■ pumping rate
■ light source
■ reactor volume
■ internal diameter
reagents mixture
crude product

Figure 4.2: Scheme of a microfluidic photoreactor

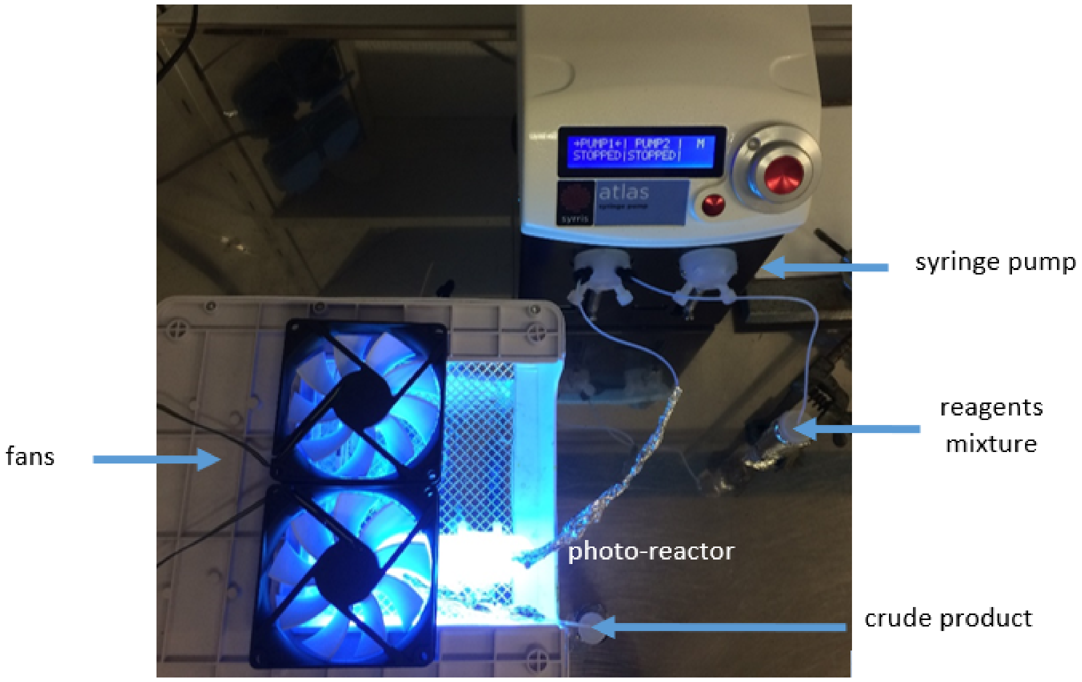
syringe pump
reagents mixture
fans
photo-reactor
crude product

Figure 4.3: Set-up of the microfluidic photoreactor used in this experiment

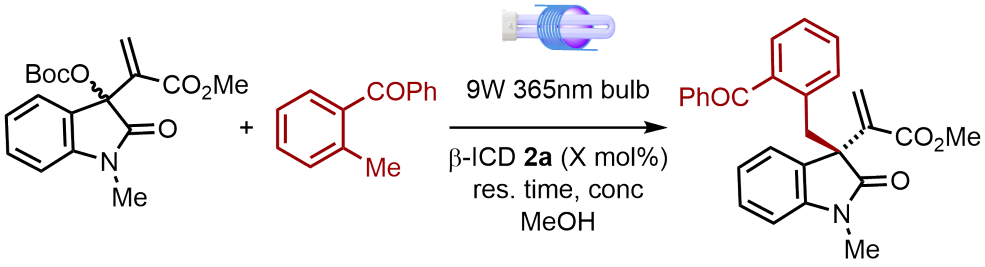
BocO
CO2Me
O
N
Me
+
COPh
Me
9W 365nm bulb
β-ICD 2a (X mol%)
res. time, conc
MeOH
PhOC
CO2Me
O
N
Me

3a **1a** **4a**

MBH carbonate **3** and β-isocupreidine **2a** are purged with Ar in a vial. Methanol (5 ml) and 2-methylbenzophenone **1** are added. The mixture is injected in a 400μL flow reactor in UV light (9W bulb, 365nm, 0.05A) varying the retention time. NMR is used to qualitatively determine the yield, with pyrazine as an internal standard. The results of the optimisation are shown in Table 4.1

Concentration	β-ICD **2a** (mol%)	2-MBP **1a**	Residence time	Conversion	NMR yield
0.1 M	20%	5 eq.	60 min	92%	39%
			40 min	89%	52%
			30 min	86%	50%
0.05 M	20%	5 eq.	40 min	f.c.	47%
			30 min	f.c.	55%
			15 min	71%	46%
			10 min	53%	34%
0.05 M	10%	5 eq.	50 min	89%	45%
			40 min	91%	44%
			30 min	67%	65% [65%][a]
0.05 M	5%	5 eq.	50 min	fc%	24%
			40 min	84%	25%
			30 min	68%	29%
			20 min	57%	29%
			10 min	36%	26%
0.05 M	20%	2 eq.	30 min	87%	58%
			25 min	51%	58%
			20 min	60%	39%
			15 min	82%	38%
0.05 M	10%	3 eq.	40 min	60%	46%
			35 min	60%	50%
			30 min	53%	43%
			20 min	48%	37%

Table 4.1: Screening of reaction conditions into a microfluidic photoreactor. Yield and conversion were calculated by integrating the NMR peaks of the reaction crude using pyrazine as internal standard. [a][Isolated yield].

4.6.1 Upscaling of flow reaction

MBH carbonate **3a** (3.5 mmol, 1 eq.) is mixed with β-isocupreidine **2a** (0.1 eq.) and 2-methylbenzophe-none **1a** (5 eq.) in a round-bottomed flask with 70 ml of methanol. Ar is bubbled inside the reaction mixture and after 30 minutes purging, the mixture is put in flow under light (9W 365 nm bulb, λ max=365 nm, 0.05A), with a retention time of 30 minutes. The crude is purified by flash chromatography, affording **4a** with 65% isolated yield.

4.7 Characterisation of the benzylated products

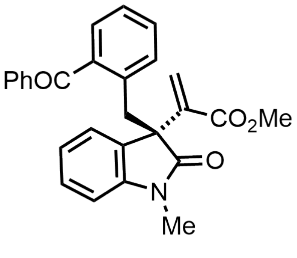

Methyl (R)-2-(3-(2-benzoylbenzyl)-1-methyl-2-oxoindolin-3-yl)acrylate **4a**: Synthesized following the general procedure described in Section 4.5. The product was obtained as a red solid after flash chromatography on silica gel using petroleum ether/EtOAc 9:1 as eluent. Yield 78%; e.r. 70:30 HRMS calculated for $[C_{27}H_{23}NO_4]$+H: 426.1705; found: 426.1705
$[\alpha]_D^{30} : (-15.7 \pm 1.9)^\circ$

^{1}H NMR (400 MHz, Chloroform-d) δ 7.48 – 7.40 (m, 1H), 7.29 – 7.17 (m, 6H),

7.07 – 6.99 (m, 2H), 6.83 (td, J = 7.7, 1.1 Hz, 1H), 6.65 – 6.61 (m, 1H), 6.52 (s, 1H), 6.43 (d, J = 7.7 Hz, 1H), 6.26 – 6.20 (m, 1H), 6.17 (s, 1H), 4.28 (d, J = 12.7 Hz, 1H), 3.42 (s, 3H), 3.37 (d, J = 12.7 Hz, 1H), 2.91 (s, 3H). **^{13}C NMR (101 MHz, Chloroform-d)** δ 197.38, 177.85, 165.32, 144.33, 140.38, 138.14, 137.32, 135.26, 132.68, 132.58, 130.63, 130.12, 129.93, 129.76, 128.35, 127.76, 127.53, 125.72, 123.54, 122.50, 107.36, 56.11, 51.96, 35.51, 26.10.
HPLC: Phenomenex Lux 5u Cellulose-5, Hex:iPrOH 80:20, 1ml/min, UV 254nm, t_r = 40.6 min, 47.0 min

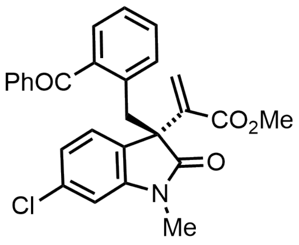

Methyl (R)-2-(3-(2-benzoylbenzyl)-6-chloro-1-methyl-2-oxoindolin-3-yl)acrylate **4b**: Synthesized following the general procedure described in Section 4.5. The product was obtained as a red solid after flash chromatography on silica gel using petroleum ether/EtOAc 9:1 as eluent. Yield 65%; e.r. 70:30
HRMS calculated for $[C_{27}H_{22}ClNO_4]$+H: 460.1316; found: 460.1299
$[\alpha]_D^{30}$: $(-16.6 \pm 0.5)°$

^{1}H NMR (400 MHz, Chloroform-d) δ 7.61 – 7.54 (m, 1H), 7.44 – 7.37 (m, 3H), 7.37 – 7.31 (m, 1H), 7.31 – 7.26 (m, 2H), 7.19 – 7.11 (m, 2H), 6.64 (s, 1H), 6.58 (d, J = 7.9 Hz, 1H), 6.51 (d, J = 1.8 Hz, 1H), 6.31 (s, 1H), 6.11 (dd, J = 7.9, 1.9 Hz, 1H), 4.51 (d, J = 12.7 Hz, 1H), 3.53 (s, 3H), 3.38 (d, J = 12.6 Hz, 1H), 2.98 (s, 3H). **^{13}C NMR (101 MHz, Chloroform-d)** δ 145.57, 139.92, 137.82, 136.97, 133.98, 132.94, 132.79, 130.32, 130.17, 128.12, 128.02, 127.97, 125.88, 124.49, 122.38, 108.22, 55.84, 52.11, 35.11, 26.21.
HPLC: Phenomenex Lux 5u Cellulose-4, Hex:iPrOH 80:20, 1ml/min, UV 254nm, t_r = 13.3 min, 17.0 min

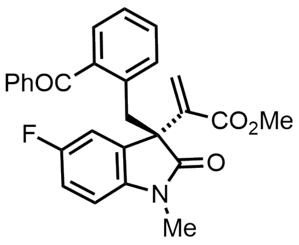

Methyl (R)-2-(3-(2-benzoylbenzyl)-5-fluoro-1-methyl-2-oxoindolin-3-yl)acrylate **4c**: Synthesized following the general procedure described in Section 4.5. The product was obtained as an orange solid after flash chromatography on silica gel using petroleum ether/EtOAc 9:1 as eluent. Yield 78%; e.r. 72:28
HRMS calculated for $[C_{27}H_{22}FNO_4]$+H: 444.1611; found: 444.1604
$[\alpha]_D^{30}$: $(-22.2 \pm 0.2)°$

^{1}H NMR (400 MHz, Chloroform-d) δ 7.48 (dt, J = 8.7, 4.4 Hz, 1H), 7.30 – 7.19 (m, 6H), 7.10 – 7.03 (m, 2H), 6.54 (s, 1H), 6.50 (td, J = 8.8, 2.6 Hz, 1H), 6.40 – 6.32 (m, 2H), 6.18 (s, 1H), 4.26 (d, J = 12.7 Hz, 1H), 3.44 (s, 3H), 3.34 (d, J = 12.7 Hz, 1H), 2.89 (s, 3H). **^{13}C NMR (101 MHz, Chloroform-d)** δ 197.28, 177.59, 165.18, 139.83, 138.07, 137.03, 134.83, 132.93, 132.71, 130.42, 130.16, 130.03, 128.14, 127.96, 125.91, 114.72, 114.48, 112.20, 111.95, 107.86, 107.78, 56.41, 52.10, 35.44, 26.27. **^{19}F NMR (376 MHz, Chloroform-d)** δ -120.84.
HPLC: Phenomenex Lux 5u Cellulose-4, Hex:iPrOH 80:20, 1ml/min, UV 254nm, t_r = 29.3 min, 33.7 min

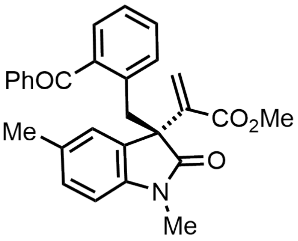

Methyl (R)-2-(3-(2-benzoylbenzyl)-1,5-dimethyl-2-oxoindolin-3-yl)acrylate **4d**: Synthesized following the general procedure described in Section 4.5. The product was obtained as a yellow solid after flash chromatography on silica gel using petroleum ether/EtOAc 9:1 as eluent. Yield 55%; e.r. 69:31
HRMS calculated for $[C_{28}H_{25}NO_4]$+H: 440.1862; found: 440.1831
$[\alpha]_D^{30}$: $(-9.4 \pm 0.4)°$

^{1}H NMR (400 MHz, Chloroform-d) δ 7.48 – 7.42 (m, 1H), 7.36 (d, J = 7.6 Hz, 1H), 7.26 – 7.18 (m, 3H), 7.14 (d, J = 7.2 Hz, 2H), 7.00 (ddd, J = 15.8, 7.4, 1.2 Hz, 2H), 6.58 (d, J = 7.8 Hz, 1H), 6.53 (s, 1H), 6.40 (s, 1H), 6.32 (d, J = 7.8 Hz, 1H), 6.20 (s, 1H), 4.45 (d, J = 12.5 Hz, 1H), 3.43 (s, 3H), 3.28 (d, J = 12.5 Hz, 1H), 2.89 (s, 3H), 1.38 (s, 3H). **^{13}C NMR (101 MHz, Chloroform-d)** δ 197.54, 165.35, 141.93, 140.45, 137.88, 137.35, 135.63, 133.02, 132.62, 132.49, 130.59, 130.41, 130.11, 128.68, 127.71, 127.56, 124.55, 107.12, 56.28, 52.00, 26.13, 20.21.
HPLC: Phenomenex Lux 5u Cellulose-4, Hex:iPrOH 80:20, 1ml/min, UV 254nm, t_r = 12.6 min, 18.4 min

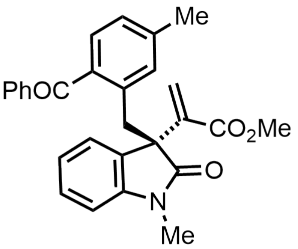

Methyl (R)-2-(3-(2-benzoyl-5-methylbenzyl)-1-methyl-2-oxoindolin-3-yl)acrylate **4f**: Synthesized following the general procedure described in Section 4.5. The product was obtained as a yellow solid after flash chromatography on silica gel using petroleum ether/EtOAc 9:1 as eluent. Yield 58%; e.r. 70:30
HRMS calculated for $[C_{28}H_{25}NO_4]$+H: 440.1862: found: 440.1853
$[\alpha]_D^{30}$: $(-2.9 \pm 0.2)°$

^{1}H NMR (400 MHz, Chloroform-d) δ 7.52 (tt, J = 7.8, 1.6 Hz, 1H), 7.37 – 7.27 (m, 4H), 7.13 (s, 1H), 7.03 – 6.89 (m, 3H), 6.73 (d, J = 7.3 Hz, 1H), 6.61 (s, 1H), 6.53 (d, J = 7.7 Hz, 1H), 6.36 (t, J = 7.5 Hz, 1H), 6.27 (s, 1H), 4.38 (d, J = 12.6 Hz, 1H), 3.51 (s, 3H), 3.42 (d, J = 12.6 Hz, 1H), 3.01 (s, 3H), 2.30 (s, 3H). **^{13}C NMR (101 MHz, Chloroform-d)** δ 197.54, 165.35, 141.93, 140.45, 137.88, 137.35, 135.63, 133.02, 132.62, 132.49, 130.59, 130.41, 130.11, 129.69, 128.68, 127.71, 127.56, 125.61, 124.55, 107.12, 56.28, 52.00, 26.13, 20.21.
HPLC: Phenomenex Lux 5u Cellulose-5, Hex:iPrOH 80:20, 1ml/min, UV 254nm, t_r = 34.9 min, 44.9 min

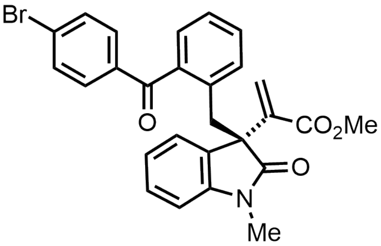

Methyl (R)-2-(3-(2-(4-bromobenzoyl)benzyl)-1-methyl-2-oxoindolin-3-yl)acrylate **4g**: Synthesized following the general procedure described in *Section 4.5.* The product was obtained as a white solid after flash chromatography on silica gel using petroleum ether/EtOAc 9:1 as eluent. Yield 47%; e.r. 69:31
HRMS calculated for $[C_{27}H_{22}BrNO_4+H]$: 504.0811; found: 504.0804
$[\alpha]_D^{30}$: $(-17.8 \pm 0.3)°$

^{1}H NMR (400 MHz, Chloroform-d) δ 7.46 (d, J = 8.5 Hz, 2H), 7.34 – 7.27 (m, 2H), 7.17 – 7.01 (m, 4H), 6.92 (t, J = 7.7 Hz, 1H), 6.71 (d, J = 7.3 Hz, 1H), 6.60 (s, 1H), 6.50 (d, J = 7.7 Hz, 1H), 6.34 (t, J = 7.5 Hz, 1H), 6.25 (s, 1H), 4.32 (d, J = 12.6 Hz, 1H), 3.49 (s, 3H), 3.44 (d, J = 12.6 Hz, 1H), 2.96 (s, 3H). **^{13}C NMR (101 MHz, Chloroform-d)** δ 196.28, 177.76, 144.45, 140.32, 137.62, 136.07, 135.36, 132.92, 132.11, 131.05, 130.20, 129.85, 129.81, 128.39, 127.76, 127.59, 125.80, 123.59, 122.46, 107.41, 56.12, 52.00, 35.41, 26.11.
HPLC: Phenomenex Lux 5u Cellulose-4, Hex:iPrOH 90:10, 1ml/min, UV 254nm, t_r = 16.1 min, 25.8 min

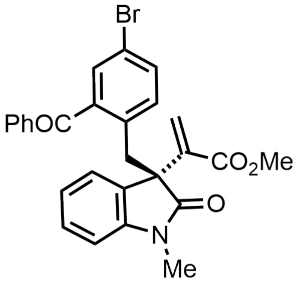

Methyl (R)-2-(3-(2-benzoyl-4-bromobenzyl)-1-methyl-2-oxoindolin-3-yl)acrylate **4h**: Synthesized following the general procedure described in Section 4.5. The product was obtained as a white solid after flash chromatography on silica gel using petroleum ether/EtOAc 9:1 as eluent. Yield 56%; e.r. 66:34
HRMS calculated for $[C_{27}H_{22}BrNO_4]$+H: 504.0811; found: 504.0804
$[\alpha]_D^{30}$: $(-8.8 \pm 1.2)^\circ$

^{1}H NMR (400 MHz, Chloroform-d) δ 7.54 (t, J = 7.3 Hz, 1H), 7.42 – 7.16 (m, 7H), 6.92 (td, J = 7.7, 1.0 Hz, 1H), 6.68 (d, J = 7.3 Hz, 1H), 6.59 – 6.52 (m, 2H), 6.30 (t, J = 7.5 Hz, 1H), 6.19 (s, 1H), 4.21 (d, J = 12.8 Hz, 1H), 3.48 (s, 3H), 3.38 (d, J = 12.8 Hz, 1H), 3.01 (s, 3H). **^{13}C NMR (101 MHz, Chloroform-d)** δ 195.76, 177.66, 165.23, 144.31, 140.25, 139.99, 136.58, 134.37, 134.27, 133.02, 132.84, 132.44, 130.57, 129.40, 128.58, 128.02, 123.57, 122.60, 119.87, 107.61, 52.02, 35.07, 26.23.
HPLC: Phenomenex Lux 5u Cellulose-1, Hex:iPrOH 95:5, 1ml/min, UV 254nm, t_r = 24.6 min, 38.1 min

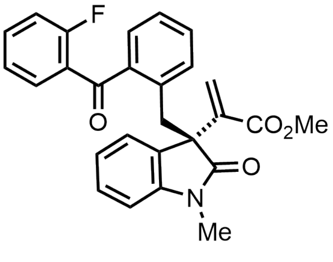

Methyl (R)-2-(3-(2-(2-fluorobenzoyl)benzyl)-1-methyl-2-oxoindolin-3-yl)acrylate **4i**: Synthesized following the general procedure described in *Section 4.5.* The product was obtained as a yellow solid after flash chromatography on silica gel using petroleum ether/EtOAc 9:1 as eluent. Yield 70%; e.r. 67:33
HRMS calculated for $[C_{27}H_{22}FNO_4]$+H: 444.1611; found: 444.1604
$[\alpha]_D^{30}$: $(-3.2 \pm 0.6)^\circ$

^{1}H NMR (400 MHz, Chloroform-d) δ 7.55 – 7.44 (m, 1H), 7.32 – 7.22 (m, 2H), 7.18 – 7.00 (m, 6H), 6.90 (d, J = 7.3 Hz, 1H), 6.57 (dd, J = 17.5, 7.7 Hz, 3H), 6.29 (s, 1H), 4.51 (d, J = 12.6 Hz, 1H), 3.54 (d, J = 11.7 Hz, 4H), 2.99 (s, 3H). **^{13}C (101 MHz, Chloroform-d)** δ 194.14, 177.81, 165.38, 144.53, 140.46, 138.22, 135.52, 133.82, 133.73, 132.66, 132.44, 130.66, 130.60, 129.90, 128.37, 127.49, 126.13, 123.76, 123.50, 123.46, 122.20, 116.51, 116.29, 107.62, 56.23, 51.98, 35.27, 26.09. **^{19}F NMR (376 MHz, Chloroform-d)** δ -109.74.
HPLC: Phenomenex Lux 5u Cellulose-4, Hex:iPrOH 80:20, 1ml/min, UV 254nm, t_r = 20.0 min, 33.4 min

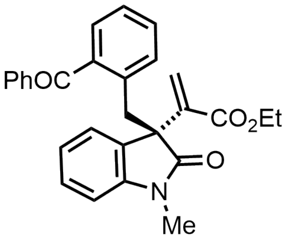

Ethyl (R)-2-(3-(2-benzoylbenzyl)-1-methyl-2-oxoindolin-3-yl)acrylate **4j**: Synthesized following the general procedure described in Section 4.5. The product was obtained as a white solid after flash chromatography on silica gel using petroleum ether/EtOAc 9:1 as eluent. Yield 57%; e.r. 69:31 HRMS calculated for $[C_{28}H_{25}NO_4]+H$: 440.1862; found: 440.1853
$[\alpha]_D^{30}$: $(-18.9 \pm 2.1)^\circ$

^{1}H (400 MHz, Chloroform-d) δ 7.53 (t, J = 6.9 Hz, 1H), 7.33 (dt, J = 11.0, 7.7 Hz, 6H), 7.12 (d, J = 6.2 Hz, 2H), 6.92 (t, J = 7.2 Hz, 1H), 6.73 (d, J = 7.3 Hz, 1H), 6.63 (s, 1H), 6.51 (d, J = 7.7 Hz, 1H), 6.33 (t, J = 7.5 Hz, 1H), 6.23 (s, 1H), 4.34 (d, J = 12.7 Hz, 1H), 3.98 – 3.82 (m, 2H), 3.47 (d, J = 12.6 Hz, 1H), 2.98 (s, 3H), 1.00 (t, J = 7.1 Hz, 3H). **^{13}C NMR (101 MHz, Chloroform-d)** δ 197.35, 177.82, 164.98, 140.53, 138.17, 137.33, 135.29, 132.66, 132.57, 130.64, 130.11, 129.94, 129.90, 128.28, 127.76, 127.51, 125.71, 123.58, 122.52, 107.25, 60.79, 56.06, 26.05, 13.74.
HPLC: Phenomenex Lux 5u Cellulose-4, Hex:iPrOH 80:20, 1ml/min, UV 254nm, t_r = 15.9 min, 25.2 min

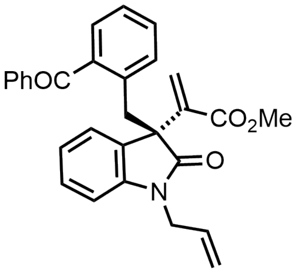

Methyl (R)-2-(1-allyl-3-(2-benzoylbenzyl)-2-oxoindolin-3-yl)acrylate **4k**: Synthesized following the general procedure described in Section 4.5. The product was obtained as an orange solid after flash chromatography on silica gel using petroleum ether/EtOAc 9:1 as eluent. Yield 52%; e.r. 70:30 HRMS calculated for $[C_{29}H_{25}NO_4]+H$: 452.1862; found: 440.1859
$[\alpha]_D^{30}$: $(-17.8 \pm 1.3)^\circ$

^{1}H NMR (400 MHz, Chloroform-d) δ 7.49 (tt, J = 5.7, 3.3 Hz, 1H), 7.35 – 7.24 (m, 6H), 7.16 – 7.07 (m, 2H), 6.81 (t, J = 7.3 Hz, 1H), 6.73 (d, J = 7.3 Hz, 1H), 6.59 (s, 1H), 6.49 (d, J = 7.8 Hz, 1H), 6.32 – 6.24 (m, 2H), 5.45 (ddt, J = 15.7, 10.4, 5.2 Hz, 1H), 5.07 – 4.99 (m, 1H), 4.84 – 4.76 (m, 1H), 4.41 – 4.27 (m, 2H), 3.97 (dd, J = 16.5, 5.5 Hz, 1H), 3.50 (s, 4H). **^{13}C NMR (101 MHz, Chloroform-d)** δ 197.35, 177.40, 165.28, 143.80, 140.64, 138.27, 137.18, 135.28, 133.34, 132.52, 131.56, 130.63, 130.30, 130.14, 129.51, 128.28, 127.72, 127.47, 125.72, 123.82, 122.32, 117.15, 108.47, 56.05, 51.94, 42.53.
HPLC: Phenomenex Lux 5u Cellulose-4, Hex:iPrOH 80:20, 1ml/min, UV 254nm, t_r = 16.1 min, 25.1 min

4.8 Synthesis and characterisation of intermediates IIIa and IIIa'

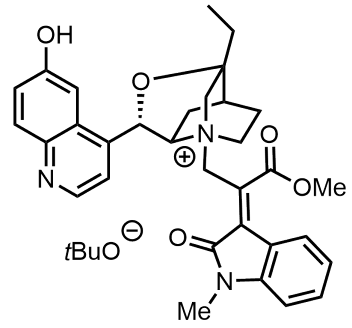

(3R)-3-ethyl-5-(6-hydroxyquinolin-4-yl)-1-(3-methoxy-2-((E)-1-methyl-2-oxoindolin-3-ylidene)-3-oxopropyl)-4-oxa-1-azatricyclo[4.4.0.0]decan-1-ium IIIa: Synthesized by mixing equimolar amount of methyl MBH carbonate **3a** (0.05 mmol, 1 equiv.) and β-isocupreidine (0.05 mmol, 1 equiv.) in methanol-d3 (0.5 mL, 0.1M) inside an NMR tube. Quantitative formation of (*E*)-**IIIa** after 15 min. HRMS calculated for $[C_{32}H_{33}N_3O_5]$+H: 540.2498, found: 540.2534

^{1}H NMR (400 MHz, Methanol-d$_3$) δ 8.31 (d, J = 4.5 Hz, 1H), 7.66 (d, J = 4.5 Hz, 1H), 7.40 – 7.31 (m, 3H), 7.27 (d, J = 2.5 Hz, 1H), 7.13 – 7.04 (m, 2H), 6.81 (s, 1H), 6.48 (m, 2H), 4.69 (d, J = 13.1 Hz, 1H), 4.43 (d, J = 6.4 Hz, 1H), 4.36 (d, J = 12.6, 1H), 4.15 (s, 3H), 3.93 – 3.83 (m, 1H), 3.57(d, J = 12.5 Hz, 1H), 3.46 (dd, J = 11.8, 8.0 Hz, 1H), 2.96 (s, 3H), 2.51 (dd, J = 7.1, 3.9 Hz, 1H), 2.12 – 1.95 (m, 3H), 1.85 (dd, J = 13.5, 6.5 Hz, 1H), 1.77 (q, J = 7.4 Hz, 2H), 1.02 (t, J = 7.4 Hz, 3H). **^{13}C NMR (101 MHz, Methanol-d$_3$)** δ 169.0, 167.6, 145.4, 141.9, 139.5, 137.7, 134.2, 130.8, 127.8, 126.5, 125.8, 124.1, 119.9, 119.8, 109.9, 103.8, 77.6, 71.7, 71.3, 69.4, 60.8, 56.9, 55.5, 54.1, 32.7, 27.4, 26.0, 26.0, 23.4, 23.1, 7.1.

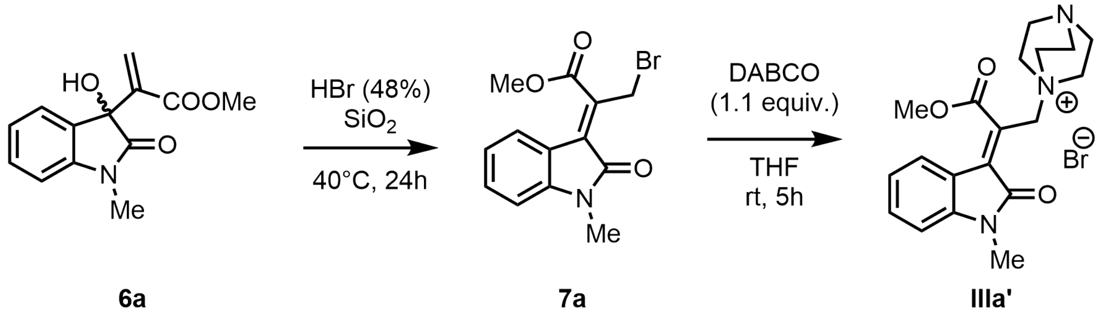

The MBH alcohol **6a** (2 mmol) was treated with aqueous HBr 48% (1.4 mL) in the presence of silica gel (670 mg) and heated at 40 °C for 24h. The mixture was then filtered through a bed of Celite and washed with CH_2Cl_2 (15 mL). The organic layer was collected, washed with brine and concentrated in vacuo to furnish the crude bromide **7a**. Purification by column chromatography on silica using hexane/EtOAc 7:3 as eluent afforded the pure bromide (*E*)-**7a** in 25% yield as a red solid. Subsequently, the bromide **7a** (3 mmol) was dissolved in THF (4 mL) and DABCO (1.1 equiv.) was added to the solution. The mixture was then stirred at room temperature for 5h, the salt **IIIa'** was purified by filtration and the filtrate was washed with Et_2O. (*E*)-**IIIa'** was obtained in 45% yield as an orange solid.[57]

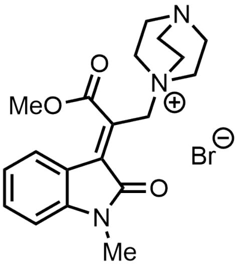

(E)-1-(3-methoxy-2-(1-methyl-2-oxoindolin-3-ylidene)-3-oxopropyl)-1,4-diazabicyclo[2.2.2] octan-1-ium **IIIa'**: **^{1}H NMR (400 MHz, Methanol-d$_3$)** δ 7.56 – 7.42 (m, 2H), 7.11 – 6.98 (m, 2H), 5.09 (s, H), 4.06 (s, 3H), 3.52 (t, J = 7.5 Hz, 6H), 3.25 – 3.16 (m, 9H). **^{13}C NMR (101 MHz, Methanol-d$_3$)** δ 168.88, 167.56, 146.16, 137.59, 134.41, 126.67, 126.06, 123.98, 120.15, 110.28, 54.21, 53.93, 46.12, 26.41. HRMS calculated for $[C_{19}H_{24}N_3O_3]$+H: 342.1812, found: 342.1821

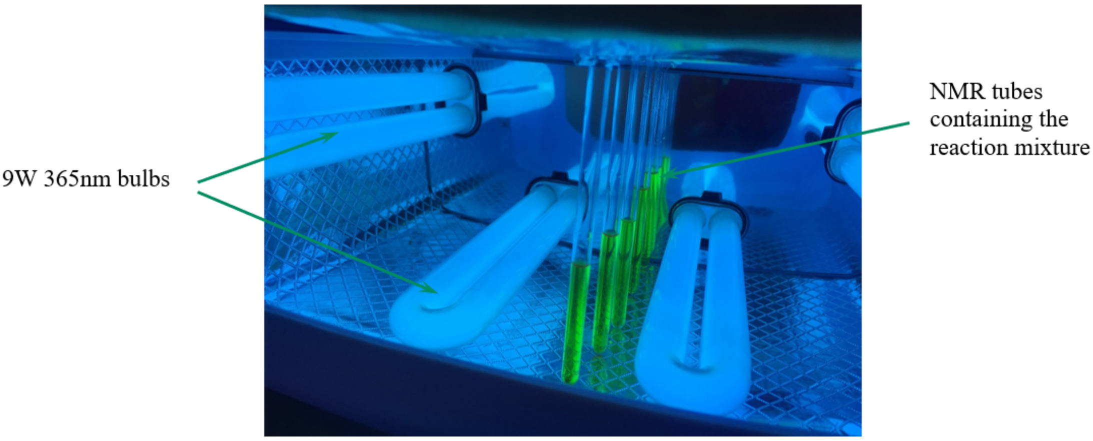

Figure 4.4: Setup for the photochemical semi-continuous ^{1}H NMR experiments used in this work to monitor the photoisomerization of the catalytic species.

4.9 X-Ray Structure and Absolute Configuration of Compound 4a

Crystals were prepared by dissolving compound **4a** in dichloromethane and freezing the solution. Three different vials were prepared with three different solvents: hexane, cyclohexane and toluene. Crystals were formed with hexane and cyclohexane and in particular the ones with hexane were used to resolve the crystal structure. The molecule crystallizes with a CH_2CL_2 molecule, as shown in *Figure 4.5*. X-ray structure was resolved thanks to Dr Marzio Rancan from University of Padova.
Data were collected using an Oxford Diffraction Gemini E diffractometer, equipped with a 2K×2K EOS CCD area detector using a sealed–tube Enhance (Mo) source. A suitable single crystal of the compound was fastened on the top of a Lindemann glass capillary. Data were collected by means of the ω-scans technique using graphite-monochromated radiation. Detector distance has been set at 45mm. The diffraction intensities were corrected for Lorentz/polarization effects as well as with respect to absorption. Empirical multi-scan absorption corrections using equivalent reflections were performed with the scaling algorithm SCALE3 ABSPACK. Data reduction, finalization and cell refinement were carried out through the CrysAlisPro software. Accurate unit cell parameters were obtained by least squares refinement of the angular settings of strongest reflections, chosen from the whole experiment. The structures were solved with Olex2 by using ShelXT structure solution program by Intrinsic Phasing and refined with the ShelXL refinement package using least-squares minimization. In the last cycles of refinement, non-hydrogen atoms were refined anisotropically. Hydrogen atoms were included in calculated positions, and a riding model was used for their refinement. A solvent molecule (CH_2Cl_2) was disordered over two sites, the occupancies of which were constrained to sum to 1.0. This disordered molecule was modelled using SADI and

RIGU restraints. EADP constrain was applied to atoms C28A/C28B and Cl1A/Cl1B. The specific refinement details have been deposited at the Cambridge Crystallographic Data Centre (CCDC 1960705).

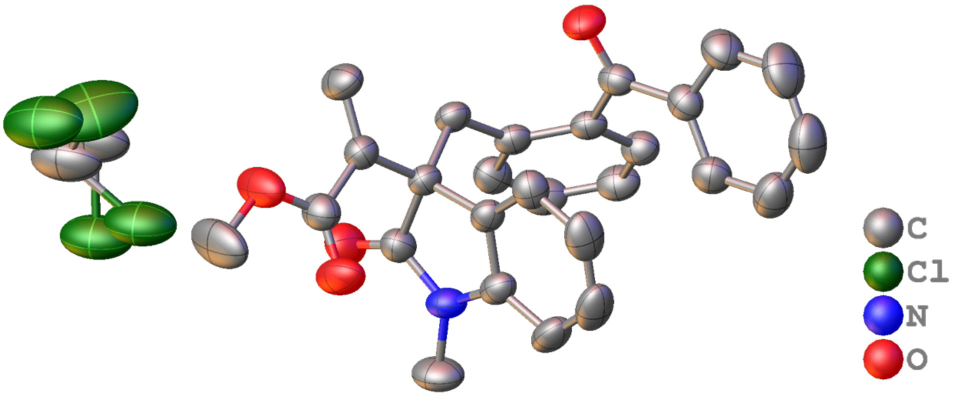

Figure 4.5: Crystal structure of compound **4a**. Thermal ellipsoids drawn at the 50% probability level. H atoms omitted for clarity.

It was not possible to obtain the absolute configuration by x-ray diffraction because the crystals obtained were racemates. The absolute configuration was determined thanks to Prof. Andrea Mazzanti from University of Bologna, by theoretical simulations of chiro-optical spectra (electronic circular dichroism, ECD). Comparing the measured circular dichroism of **4a** (e.r. 70:30) with the one calculated by DFT, the determination of the absolute configuration was possible. Results show that for **4a** the major enantiomer is the (*R*)-enantiomer, and so it is, for similarity, for all the other compounds. Comparison between the theoretical and the experimental ECD are shown in *Figure 4.7*.

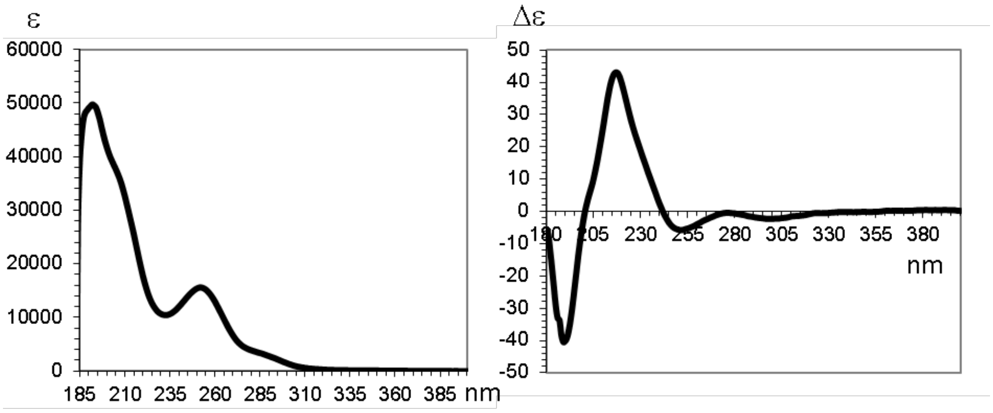

Figure 4.6: Measured UV and ECD spectra of **4a** 10^{-4}M in acetonitrile.

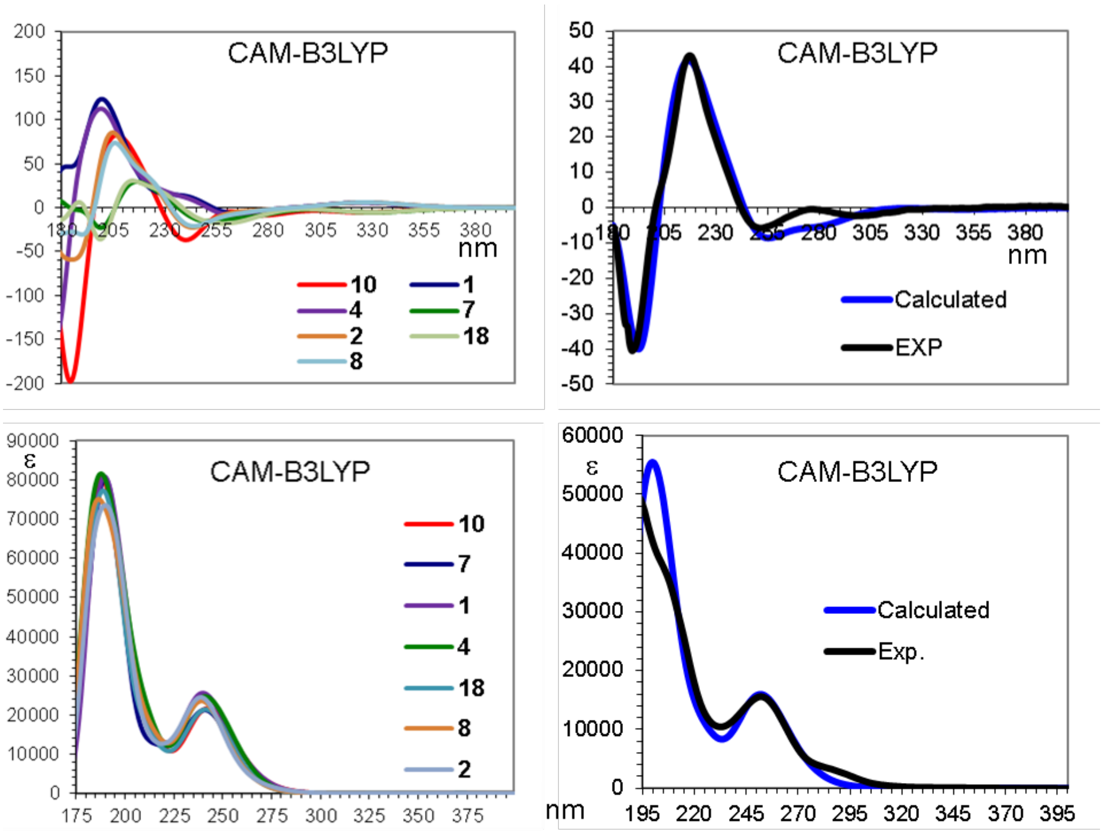

Figure 4.7: Left: TD-DFT simulated spectra calculated for the best seven conformations of **4a** (*R* absolute configuration) using CAM-B3LYP/6-311++G(2d,p) basis set. Right: comparison with the experimental spectrum (black traces) after Boltzmann averaging.

4.10 NMR Spectra

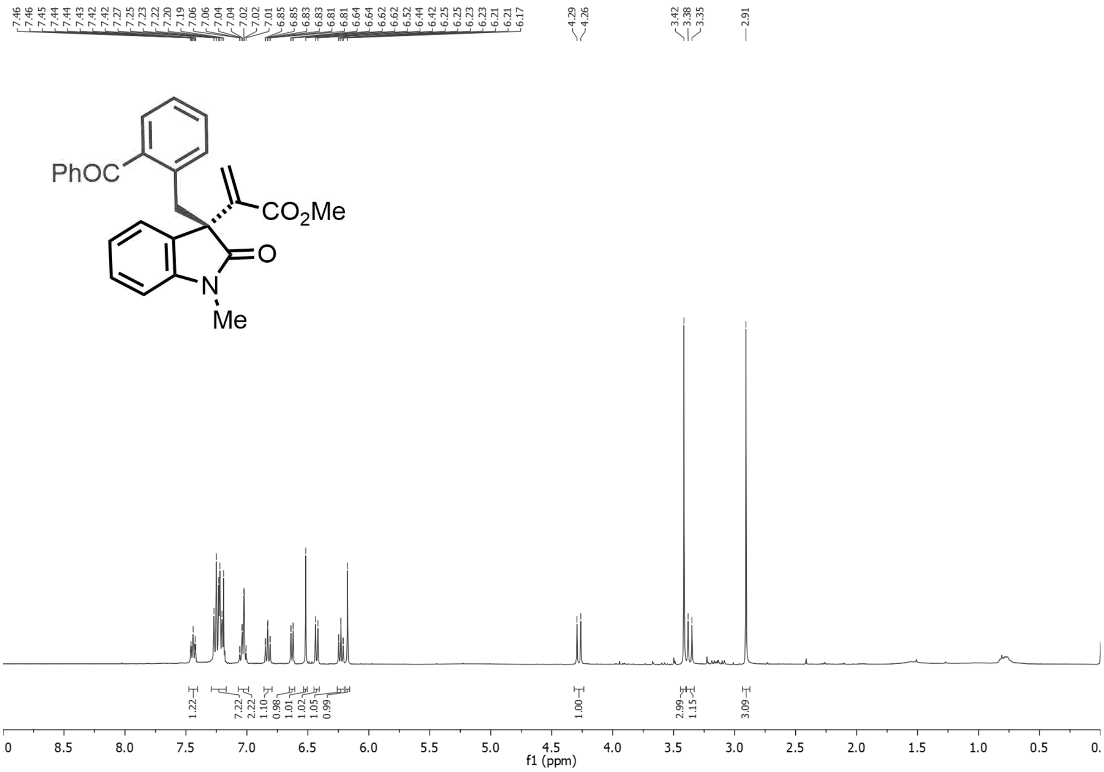

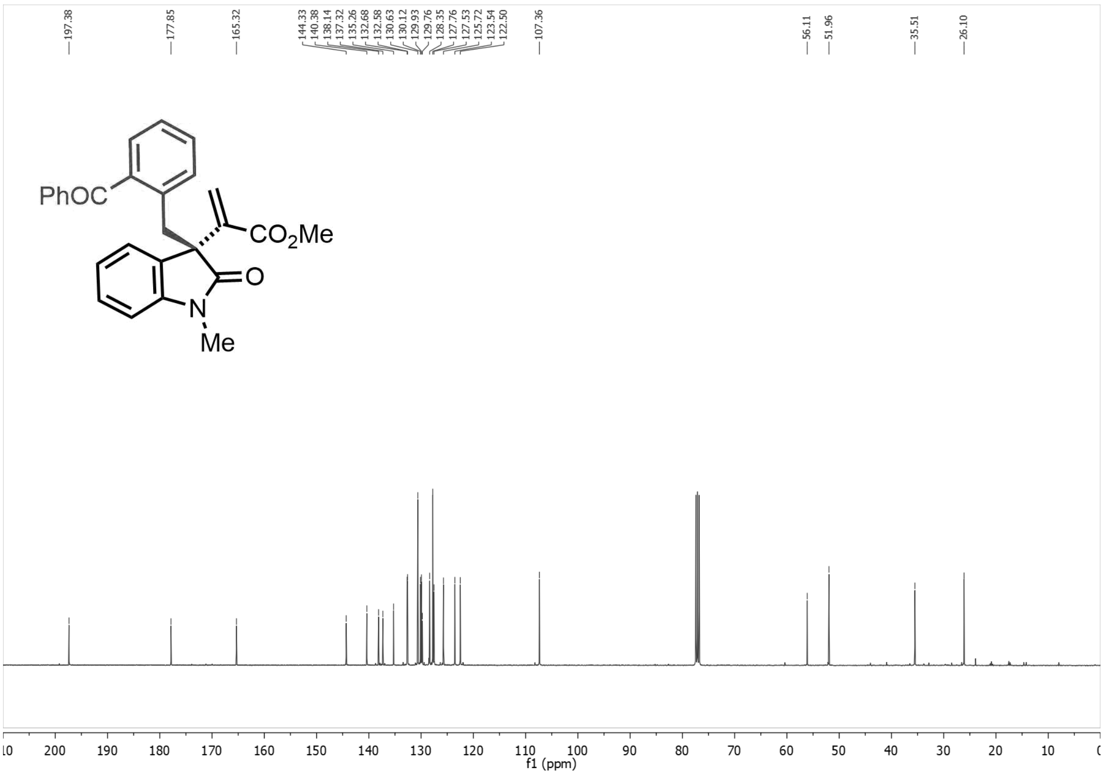

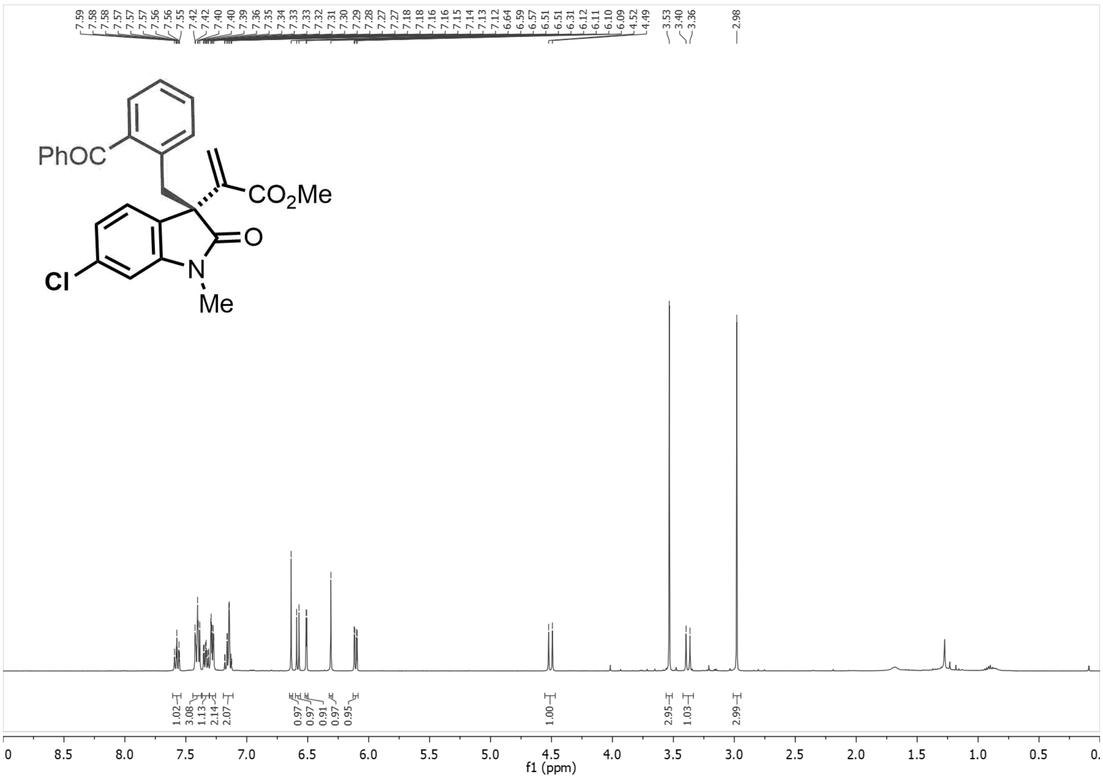

7.59
7.58
7.58
7.57
7.57
7.57
7.56
7.56
7.55
7.42
7.42
7.40
7.40
7.39
7.36
7.35
7.34
7.33
7.33
7.32
7.31
7.30
7.29
7.28
7.27
7.27
7.18
7.18
7.16
7.16
7.15
7.14
7.13
7.12
6.64
6.59
6.57
6.51
6.51
6.31
6.12
6.11
6.10
6.09
4.52
4.49
3.53
3.40
3.36
2.98
PhOC
CO2Me
O
Cl
N
Me
1.02
3.08
1.13
2.14
2.07
0.97
0.97
0.91
0.97
0.95
1.00
2.95
1.03
2.99
0
8.5
8.0
7.5
7.0
6.5
6.0
5.5
5.0
4.5
4.0
3.5
3.0
2.5
2.0
1.5
1.0
0.5
0.
f1 (ppm)

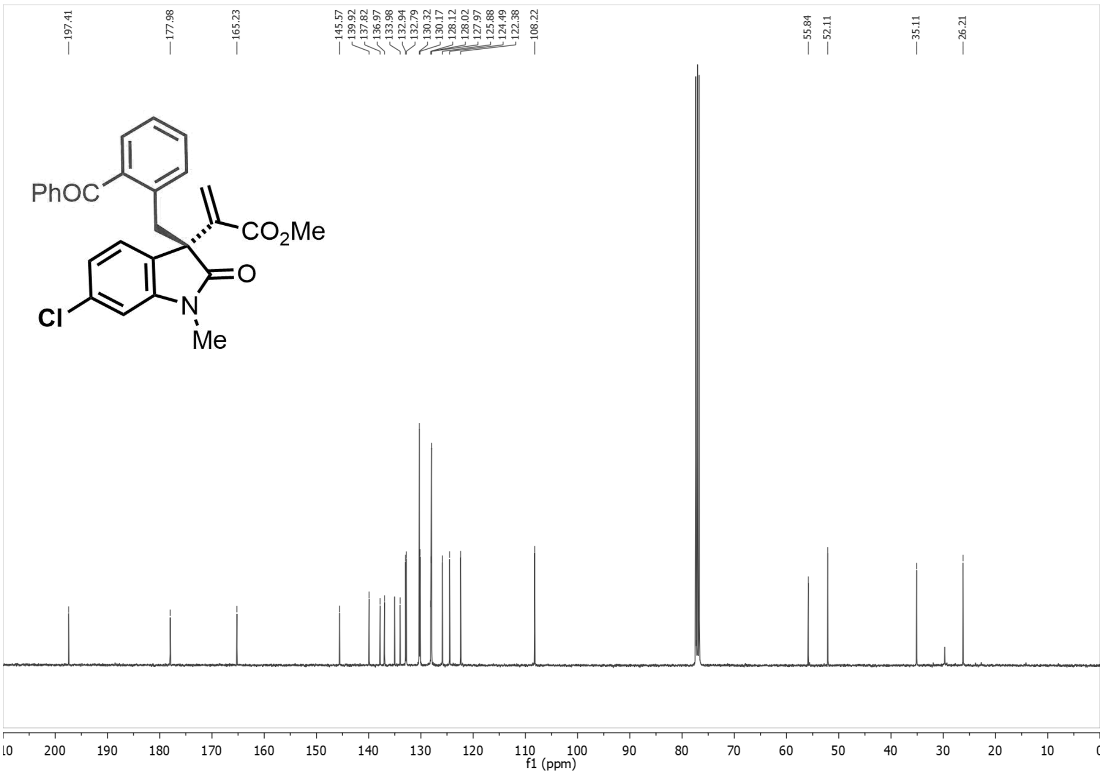

197.41
177.98
165.23
145.57
139.92
137.82
136.97
133.98
132.94
132.79
130.32
130.17
128.12
128.02
127.97
125.88
124.49
122.38
108.22
55.84
52.11
35.11
26.21
PhOC
CO2Me
O
Cl
N
Me
10
200
190
180
170
160
150
140
130
120
110
100
90
80
70
60
50
40
30
20
10
(
f1 (ppm)

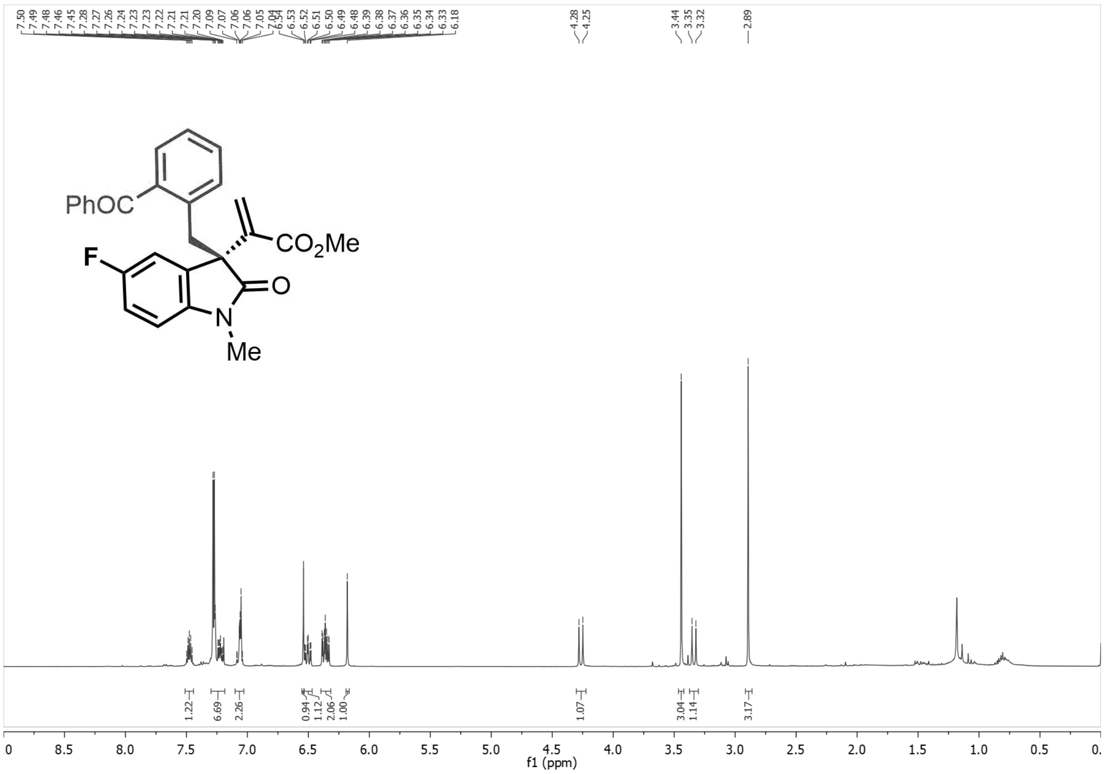
7.50
7.49
7.48
7.46
7.45
7.28
7.27
7.26
7.24
7.23
7.23
7.22
7.21
7.21
7.20
7.09
7.07
7.06
7.06
7.05
7.04
6.54
6.53
6.52
6.51
6.50
6.49
6.48
6.39
6.38
6.37
6.36
6.35
6.34
6.33
6.18
4.28
4.25
3.44
3.35
3.32
2.89
PhOC
CO2Me
F
O
N
Me
1.22
6.69
2.26
0.94
1.12
2.06
1.00
1.07
3.04
1.14
3.17
8.5
8.0
7.5
7.0
6.5
6.0
5.5
5.0
4.5
4.0
3.5
3.0
2.5
2.0
1.5
1.0
0.5
f1 (ppm)

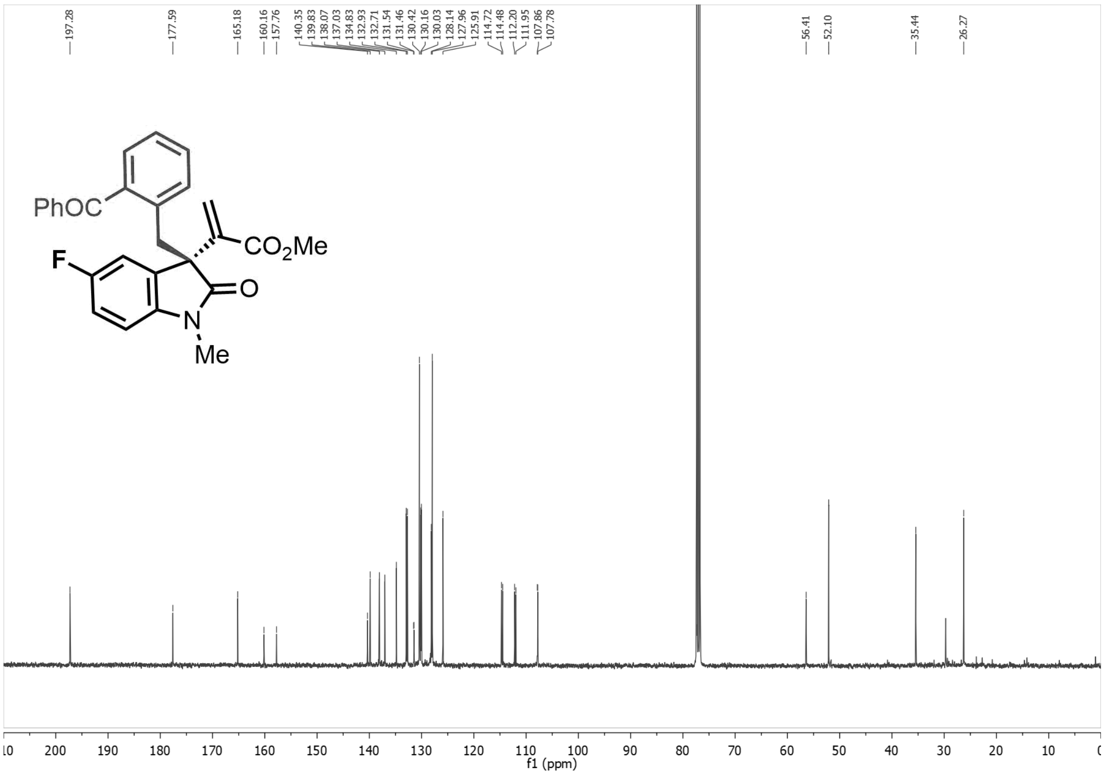
197.28
177.59
165.18
160.16
157.76
140.35
139.83
138.07
137.03
134.83
132.93
132.71
131.54
131.46
130.42
130.16
130.03
128.14
127.96
125.91
114.72
114.48
112.20
111.95
107.86
107.78
56.41
52.10
35.44
26.27
PhOC
CO2Me
F
O
N
Me
200
190
180
170
160
150
140
130
120
110
100
90
80
70
60
50
40
30
20
10
f1 (ppm)

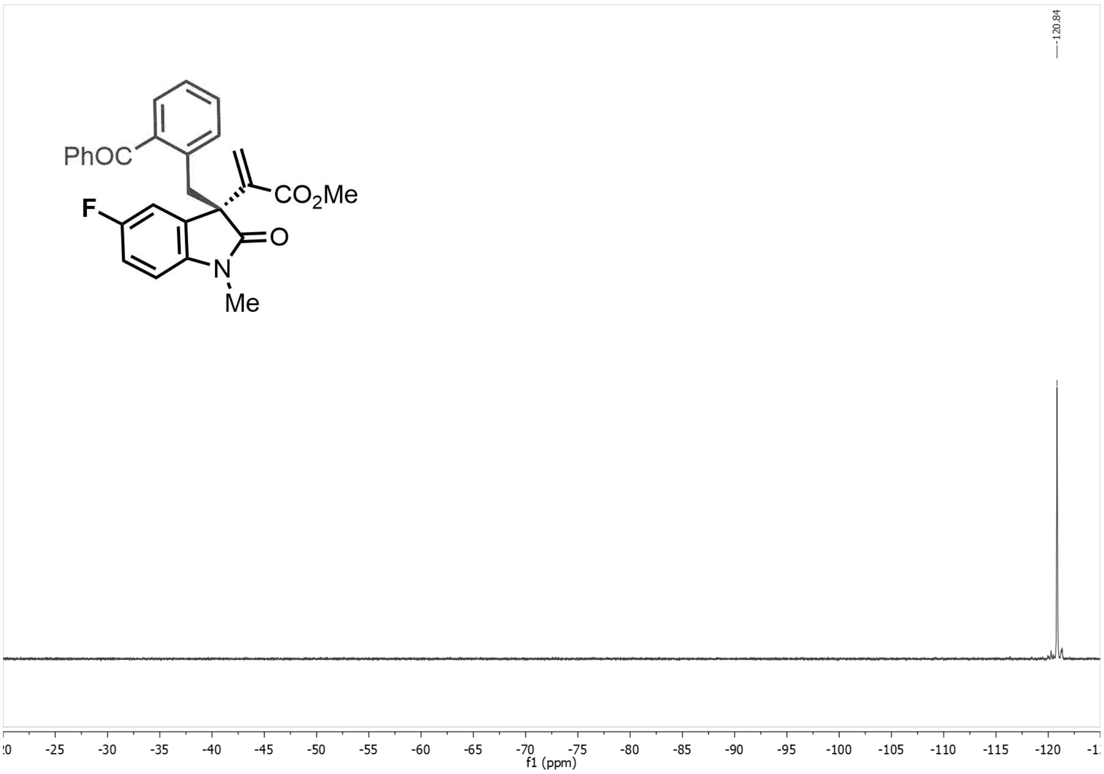
-120.84
PhOC
CO2Me
F
O
N
Me
-25
-30
-35
-40
-45
-50
-55
-60
-65
-70
-75
-80
-85
-90
-95
-100
-105
-110
-115
-120
f1 (ppm)

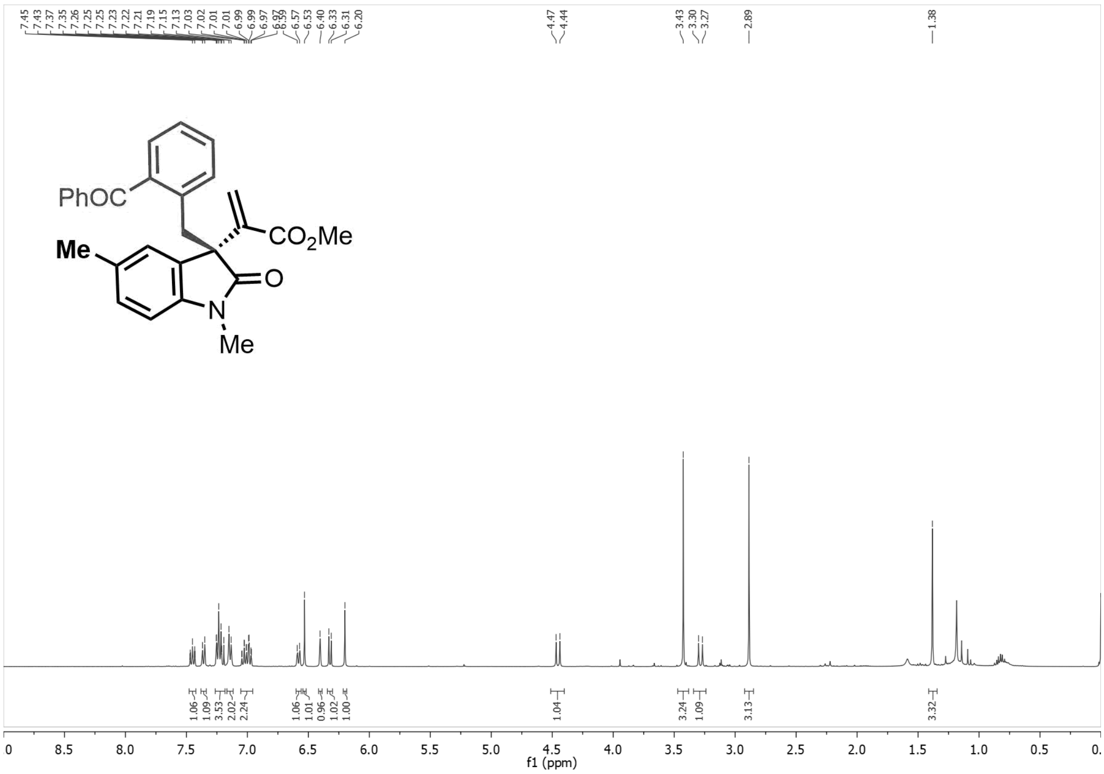
7.45
7.43
7.37
7.35
7.26
7.25
7.25
7.23
7.22
7.21
7.19
7.15
7.13
7.03
7.02
7.01
7.01
6.99
6.99
6.97
6.97
6.59
6.57
6.53
6.40
6.33
6.31
6.20
4.47
4.44
3.43
3.30
3.27
2.89
1.38
PhOC
CO2Me
Me
O
N
Me
1.06
1.09
3.53
2.02
2.24
1.06
1.01
0.96
1.02
1.00
1.04
3.24
1.09
3.13
3.32
0
8.5
8.0
7.5
7.0
6.5
6.0
5.5
5.0
4.5
4.0
3.5
3.0
2.5
2.0
1.5
1.0
0.5
0.
f1 (ppm)

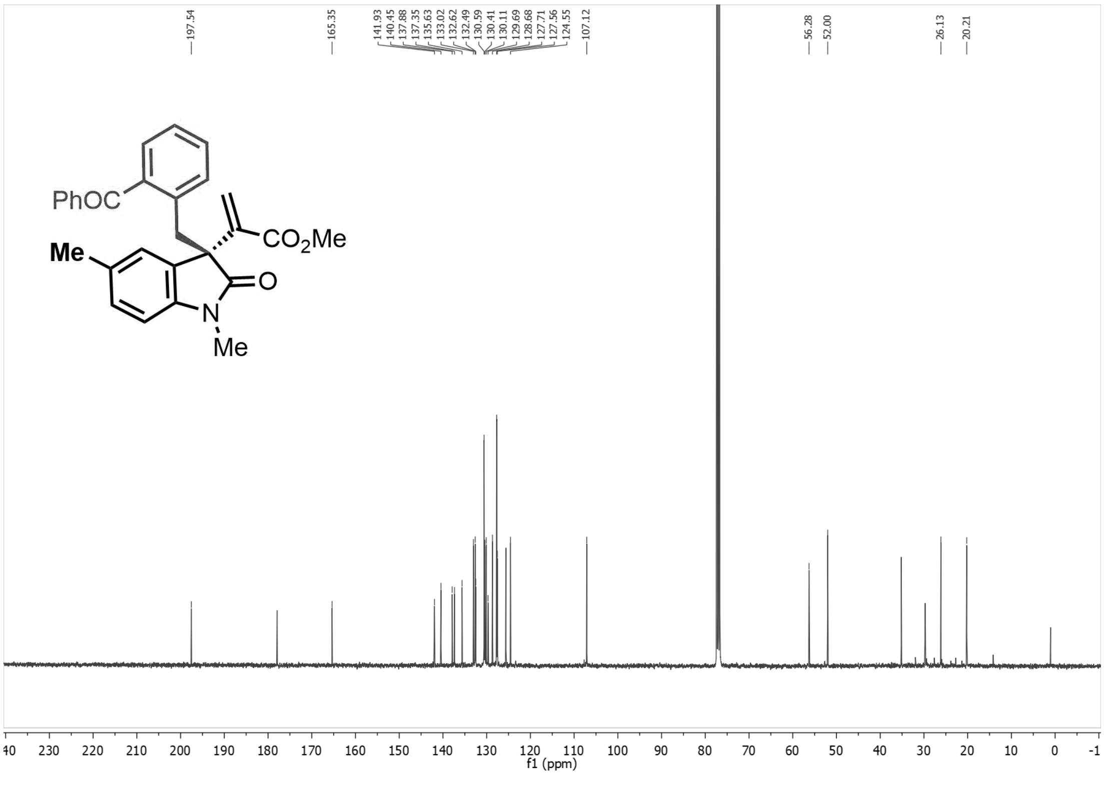
197.54
165.35
141.93
140.45
137.88
137.35
135.63
133.02
132.62
132.49
130.59
130.41
130.11
129.69
128.68
127.71
127.56
124.55
107.12
56.28
52.00
26.13
20.21
PhOC
CO2Me
Me
O
N
Me
40
230
220
210
200
190
180
170
160
150
140
130
120
110
100
90
80
70
60
50
40
30
20
10
0
-1
f1 (ppm)

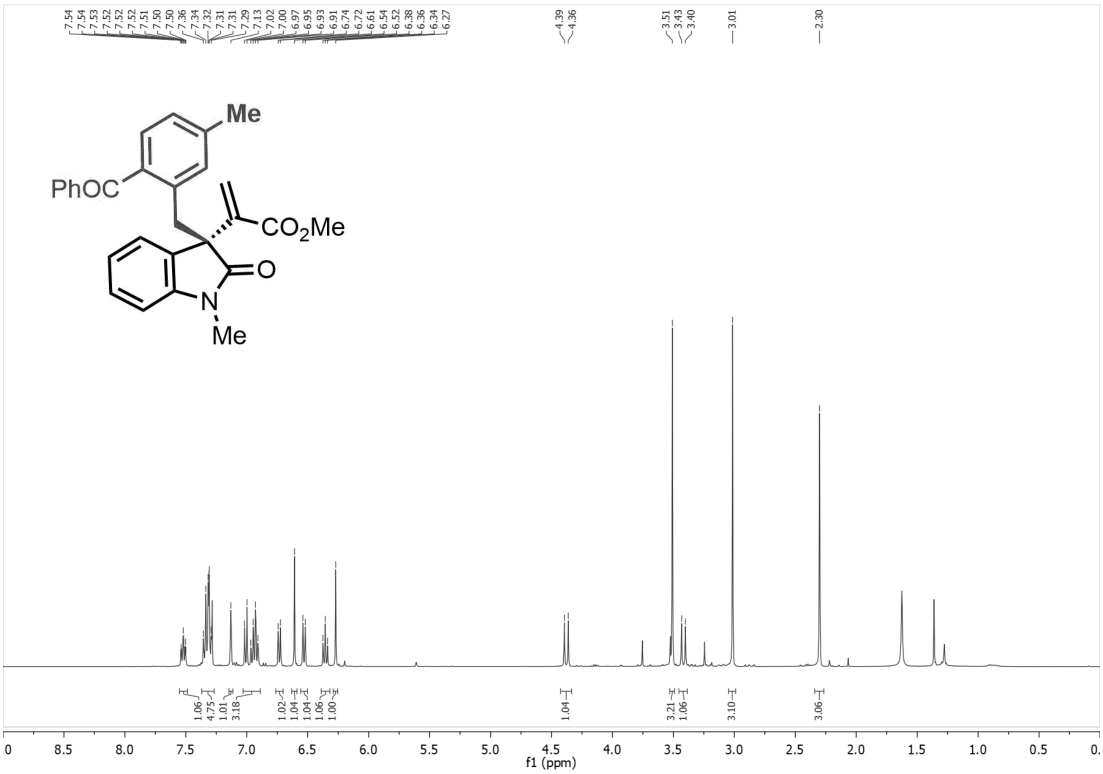
7.54
7.54
7.53
7.52
7.52
7.52
7.51
7.50
7.50
7.36
7.34
7.32
7.31
7.31
7.29
7.13
7.02
7.00
6.97
6.95
6.93
6.91
6.74
6.72
6.61
6.54
6.52
6.38
6.36
6.34
6.27
4.39
4.36
3.51
3.43
3.40
3.01
2.30
Me
PhOC
CO2Me
O
N
Me
1.06
4.75
1.01
3.18
1.02
1.04
1.04
1.06
1.00
1.04
3.21
1.06
3.10
3.06
0
8.5
8.0
7.5
7.0
6.5
6.0
5.5
5.0
4.5
4.0
3.5
3.0
2.5
2.0
1.5
1.0
0.5
0.
f1 (ppm)

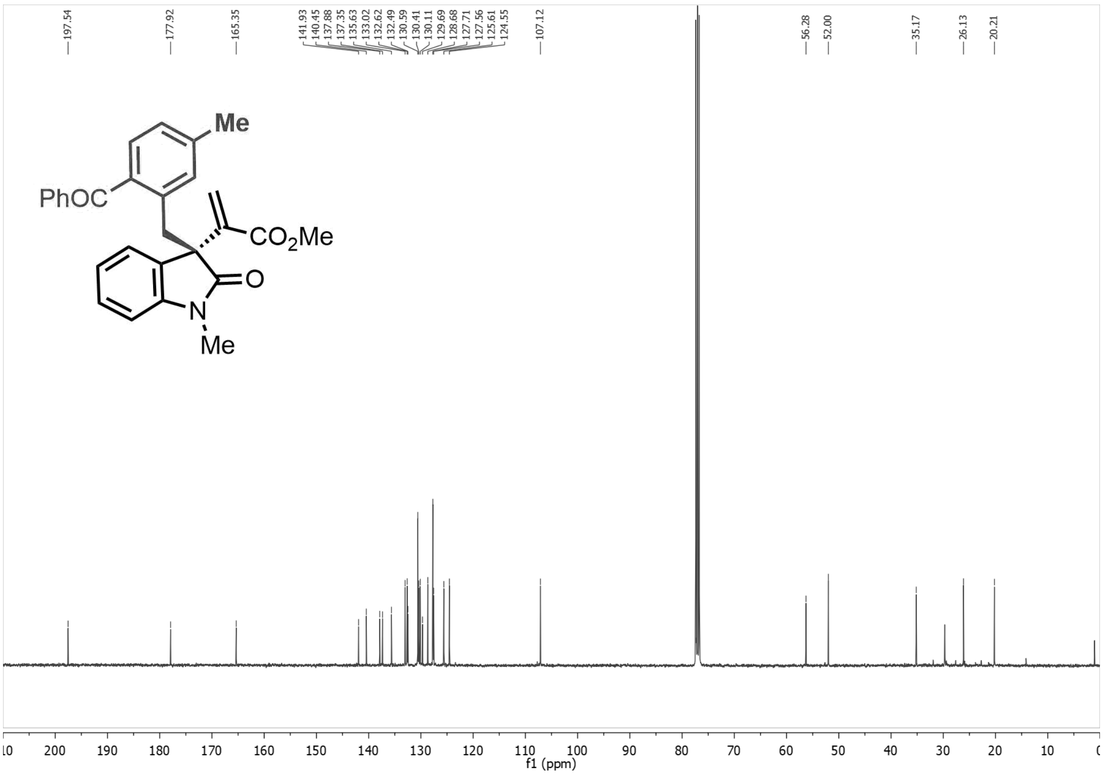
197.54
177.92
165.35
141.93
140.45
137.88
137.35
135.63
133.02
132.62
132.49
130.59
130.41
130.11
129.69
128.68
127.71
127.56
125.61
124.55
107.12
56.28
52.00
35.17
26.13
20.21
Me
PhOC
CO2Me
O
N
Me
10
200
190
180
170
160
150
140
130
120
110
100
90
80
70
60
50
40
30
20
10
0
f1 (ppm)

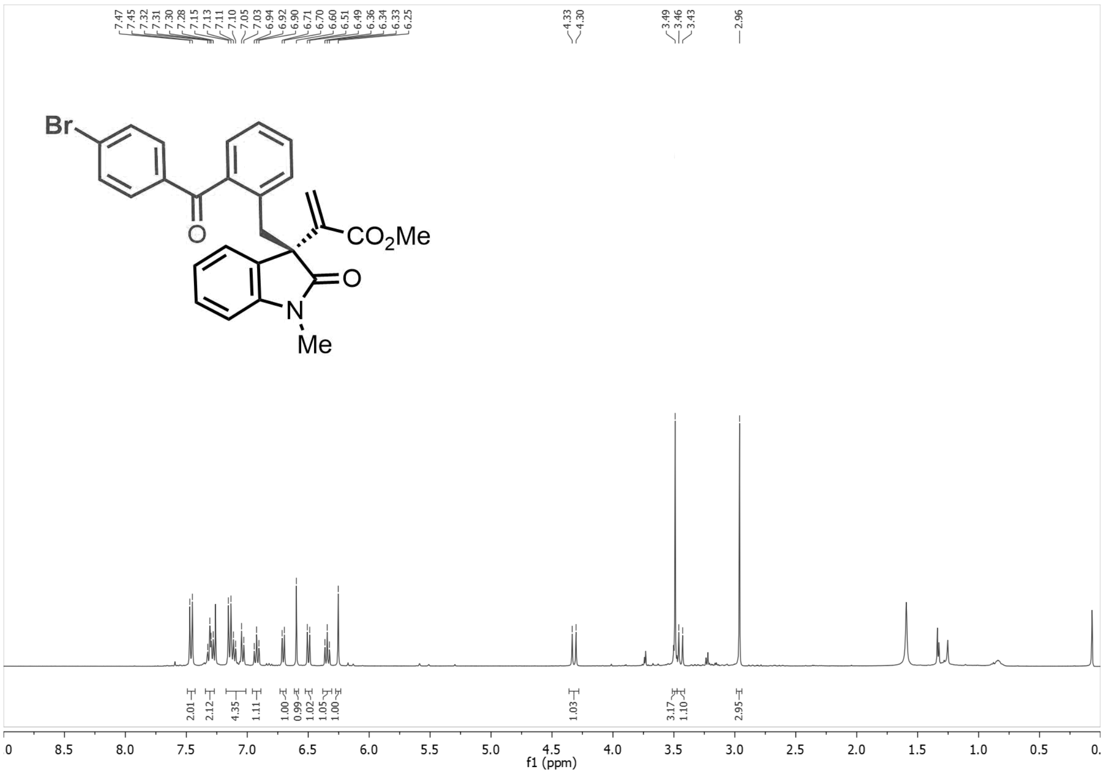
7.47
7.45
7.32
7.31
7.30
7.28
7.15
7.13
7.11
7.10
7.05
7.03
6.94
6.92
6.90
6.71
6.70
6.60
6.51
6.49
6.36
6.34
6.33
6.25
4.33
4.30
3.49
3.46
3.43
2.96
Br
O
CO2Me
O
N
Me
2.01
2.12
4.35
1.11
1.00
0.99
1.02
1.05
1.00
1.03
3.17
1.10
2.95
0
8.5
8.0
7.5
7.0
6.5
6.0
5.5
5.0
4.5
4.0
3.5
3.0
2.5
2.0
1.5
1.0
0.5
0.
f1 (ppm)

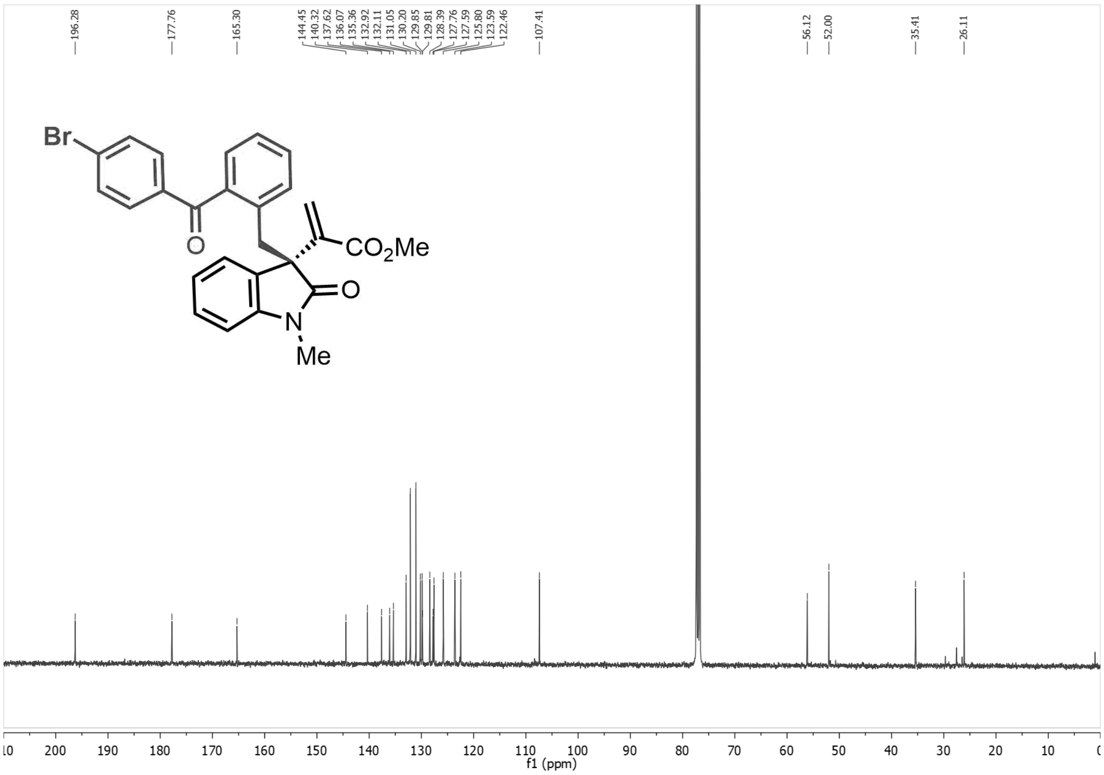
196.28
177.76
165.30
144.45
140.32
137.62
136.07
135.36
132.92
132.11
131.05
130.20
129.85
129.81
128.39
127.76
127.59
125.80
123.59
122.46
107.41
56.12
52.00
35.41
26.11
Br
O
CO2Me
O
N
Me
10
200
190
180
170
160
150
140
130
120
110
100
90
80
70
60
50
40
30
20
10
f1 (ppm)

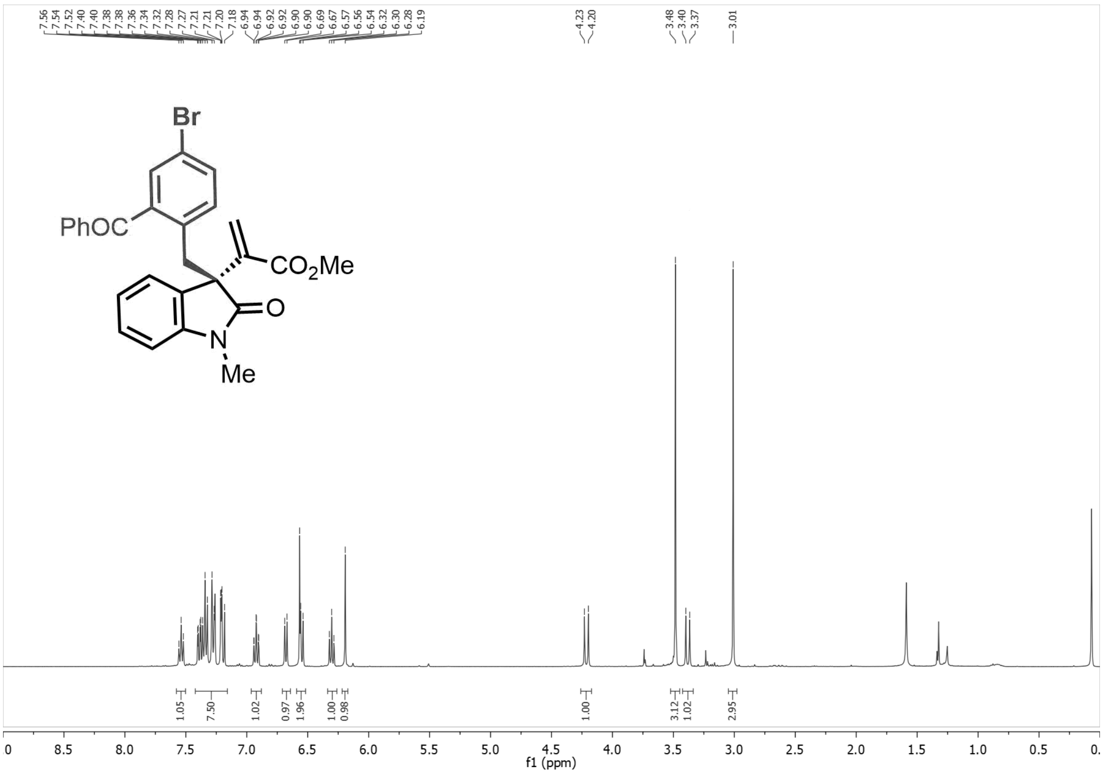
7.56
7.54
7.52
7.40
7.40
7.38
7.38
7.36
7.34
7.32
7.28
7.27
7.21
7.21
7.20
7.18
6.94
6.94
6.92
6.92
6.90
6.90
6.69
6.67
6.57
6.56
6.54
6.32
6.30
6.28
6.19
4.23
4.20
3.48
3.40
3.37
3.01
Br
PhOC
CO2Me
O
N
Me
1.05
7.50
1.02
0.97
1.96
1.00
0.98
1.00
3.12
1.02
2.95
8.5
8.0
7.5
7.0
6.5
6.0
5.5
5.0
4.5
4.0
3.5
3.0
2.5
2.0
1.5
1.0
0.5
f1 (ppm)

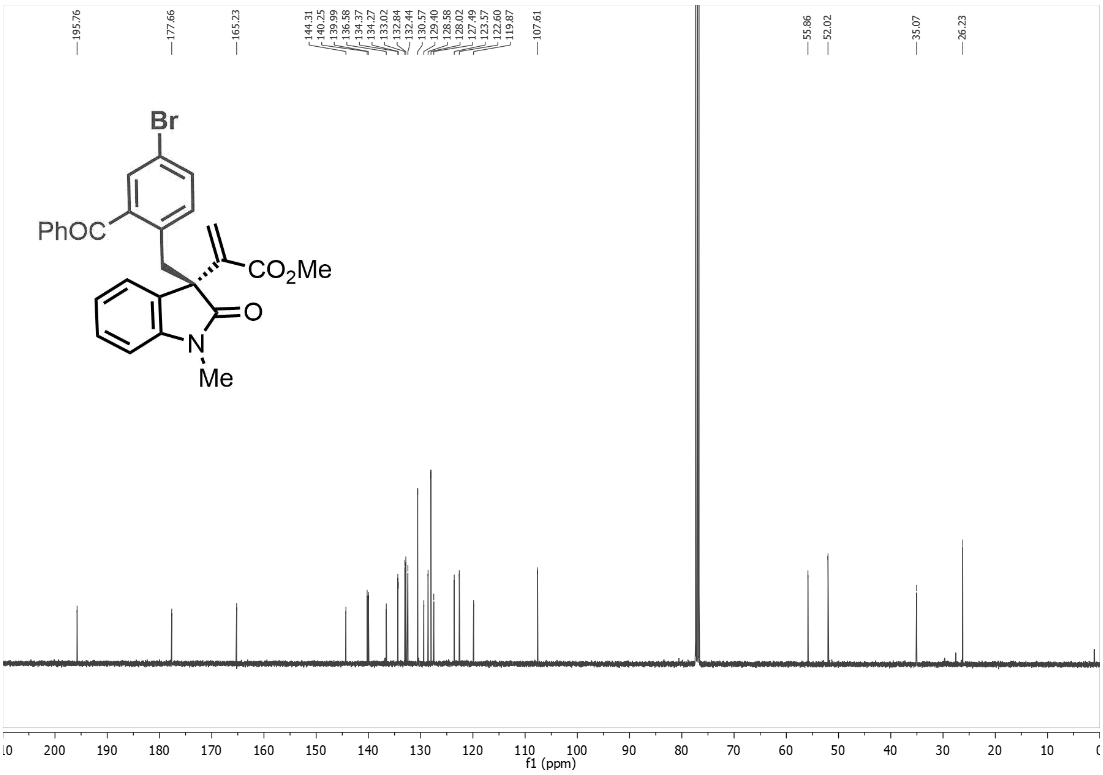
195.76
177.66
165.23
144.31
140.25
139.99
136.58
134.37
134.27
133.02
132.84
132.44
130.57
129.40
128.58
128.02
127.49
123.57
122.60
119.87
107.61
55.86
52.02
35.07
26.23
Br
PhOC
CO2Me
O
N
Me
200
190
180
170
160
150
140
130
120
110
100
90
80
70
60
50
40
30
20
10
f1 (ppm)

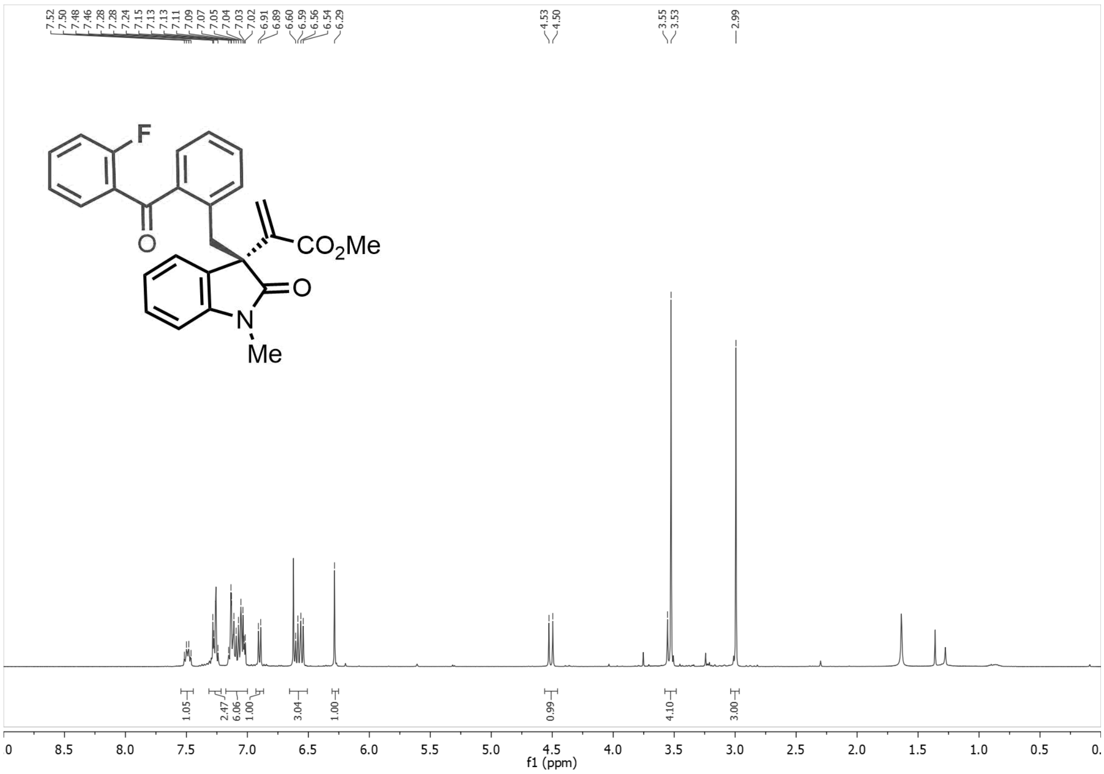
7.52
7.50
7.48
7.46
7.28
7.28
7.24
7.15
7.13
7.13
7.11
7.09
7.07
7.05
7.04
7.03
7.02
6.91
6.89
6.60
6.59
6.56
6.54
6.29
4.53
4.50
3.55
3.53
2.99
F
O
CO2Me
O
N
Me
1.05
2.47
6.06
1.00
3.04
1.00
0.99
4.10
3.00
8.5
8.0
7.5
7.0
6.5
6.0
5.5
5.0
4.5
4.0
3.5
3.0
2.5
2.0
1.5
1.0
0.5
f1 (ppm)

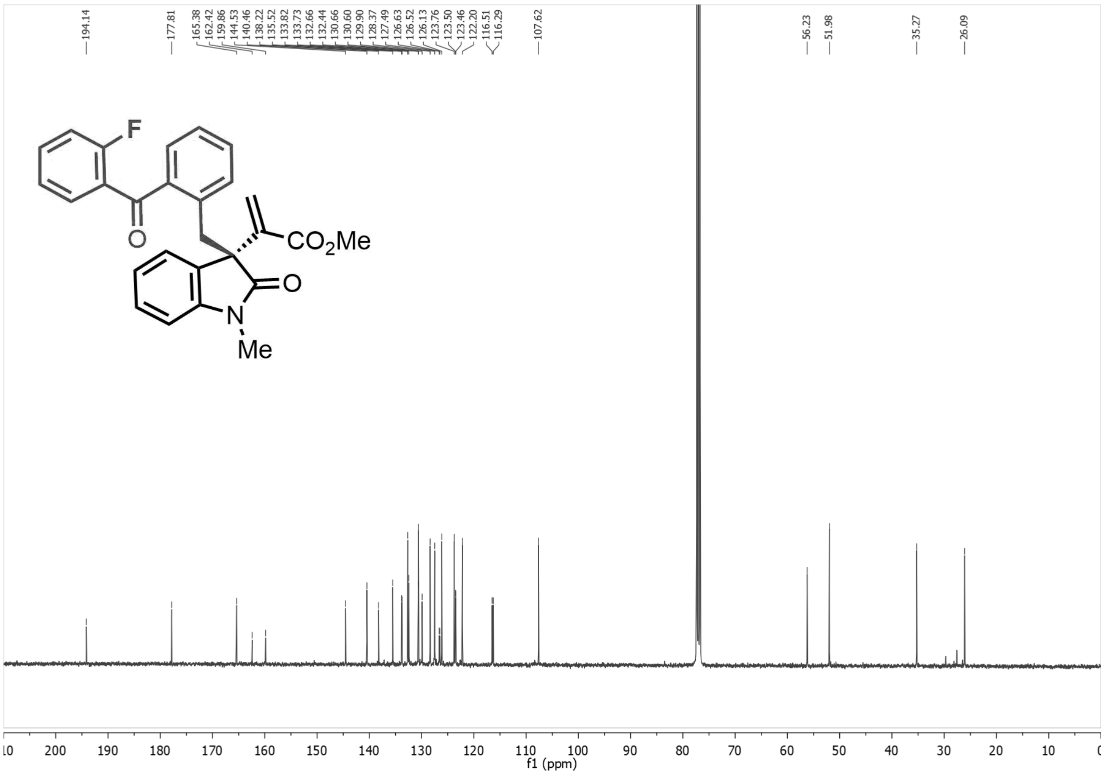
194.14
177.81
165.38
162.42
159.86
144.53
140.46
138.22
135.52
133.82
133.73
132.66
132.44
130.66
130.60
129.90
128.37
127.49
126.63
126.52
126.13
123.76
123.50
123.46
122.20
116.51
116.29
107.62
56.23
51.98
35.27
26.09
F
O
CO2Me
O
N
Me
200
190
180
170
160
150
140
130
120
110
100
90
80
70
60
50
40
30
20
10
f1 (ppm)

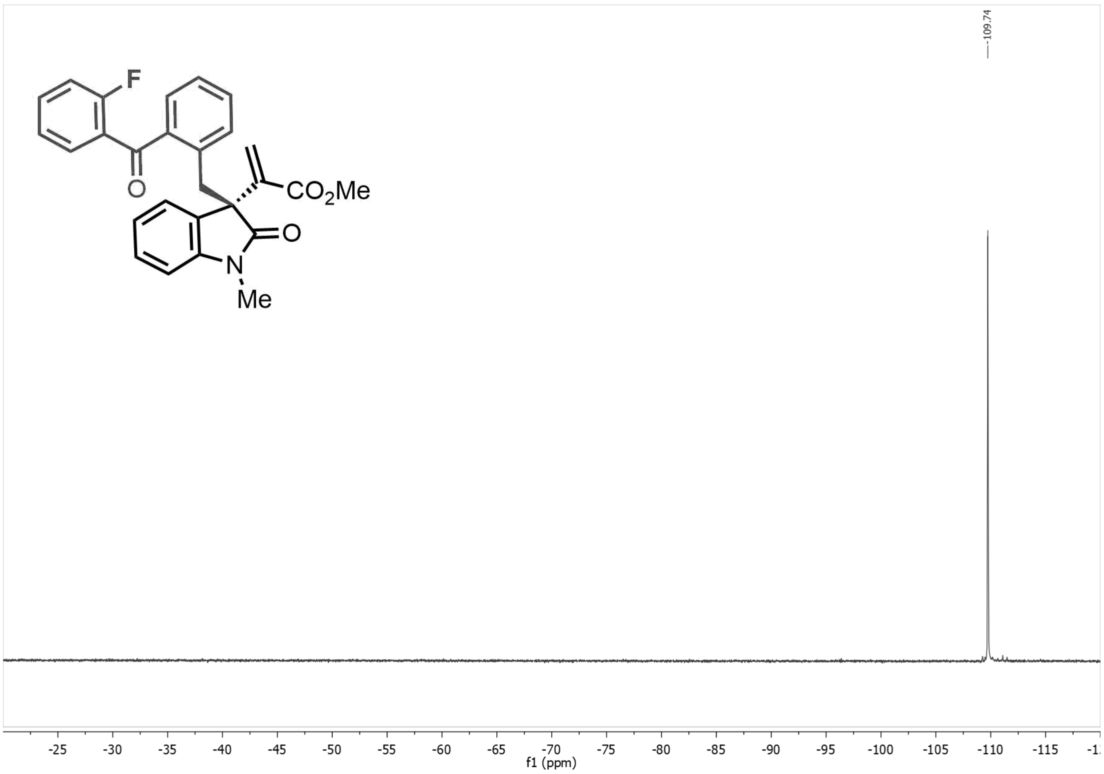
-109.74
F
O
CO$_2$Me
O
N
Me
-25
-30
-35
-40
-45
-50
-55
-60
-65
-70
-75
-80
-85
-90
-95
-100
-105
-110
-115
f1 (ppm)

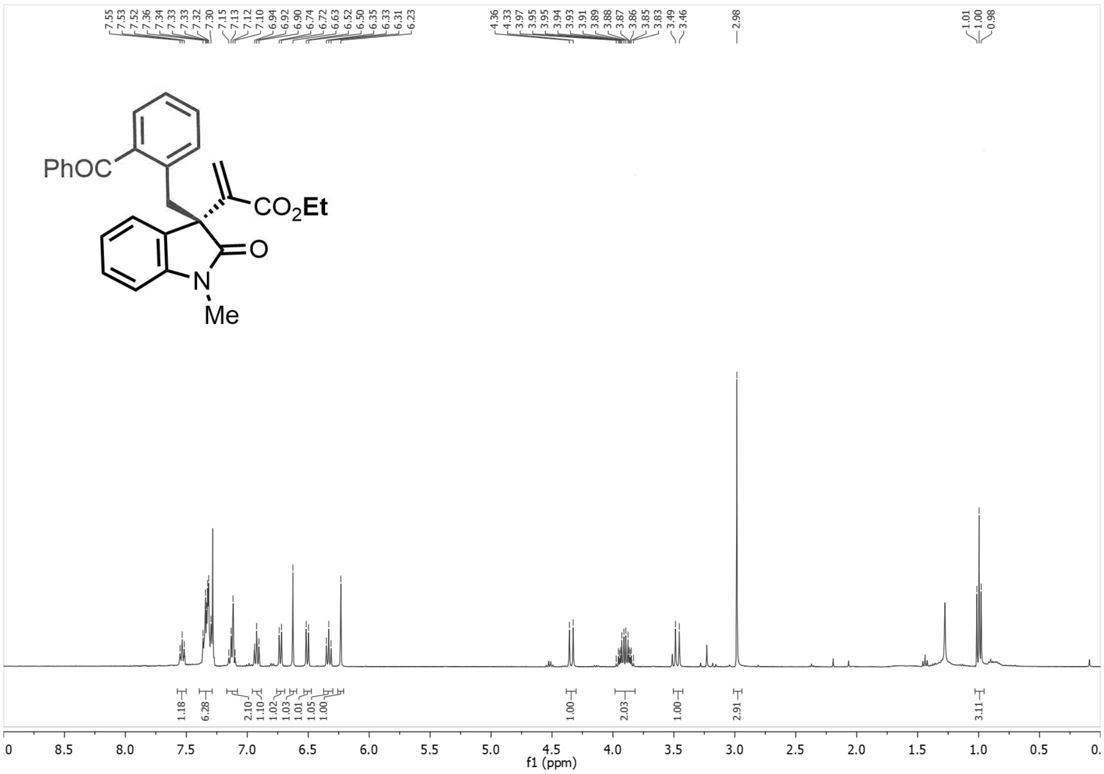
7.55
7.53
7.52
7.36
7.34
7.33
7.33
7.32
7.30
7.15
7.13
7.12
7.10
6.94
6.92
6.90
6.74
6.72
6.63
6.52
6.50
6.35
6.33
6.31
6.23
4.36
4.33
3.97
3.95
3.95
3.94
3.93
3.91
3.89
3.88
3.87
3.86
3.85
3.83
3.49
3.46
2.98
1.01
1.00
0.98
PhOC
CO2Et
O
N
Me
1.18
6.28
2.10
1.10
1.02
1.03
1.01
1.05
1.00
1.00
2.03
1.00
2.91
3.11
8.5
8.0
7.5
7.0
6.5
6.0
5.5
5.0
4.5
4.0
3.5
3.0
2.5
2.0
1.5
1.0
0.5
f1 (ppm)

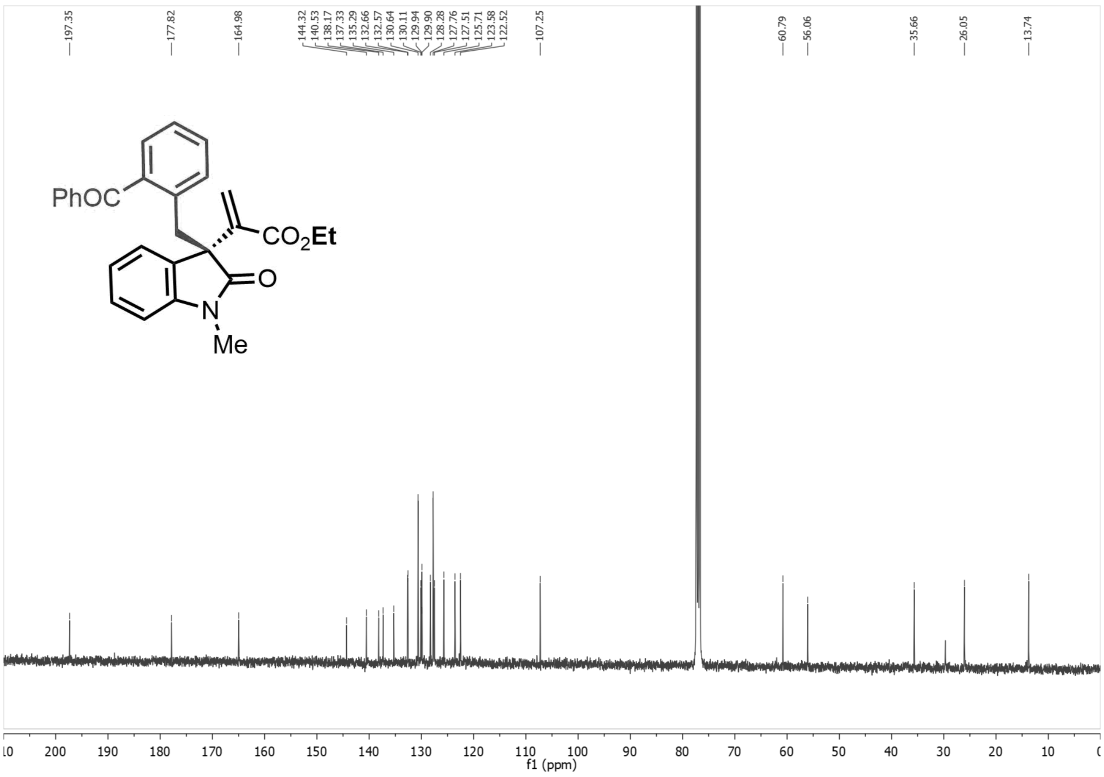
197.35
177.82
164.98
144.32
140.53
138.17
137.33
135.29
132.66
132.57
130.64
130.11
129.94
129.90
128.28
127.76
127.51
125.71
123.58
122.52
107.25
60.79
56.06
35.66
26.05
13.74
PhOC
CO2Et
O
N
Me
200
190
180
170
160
150
140
130
120
110
100
90
80
70
60
50
40
30
20
10
f1 (ppm)

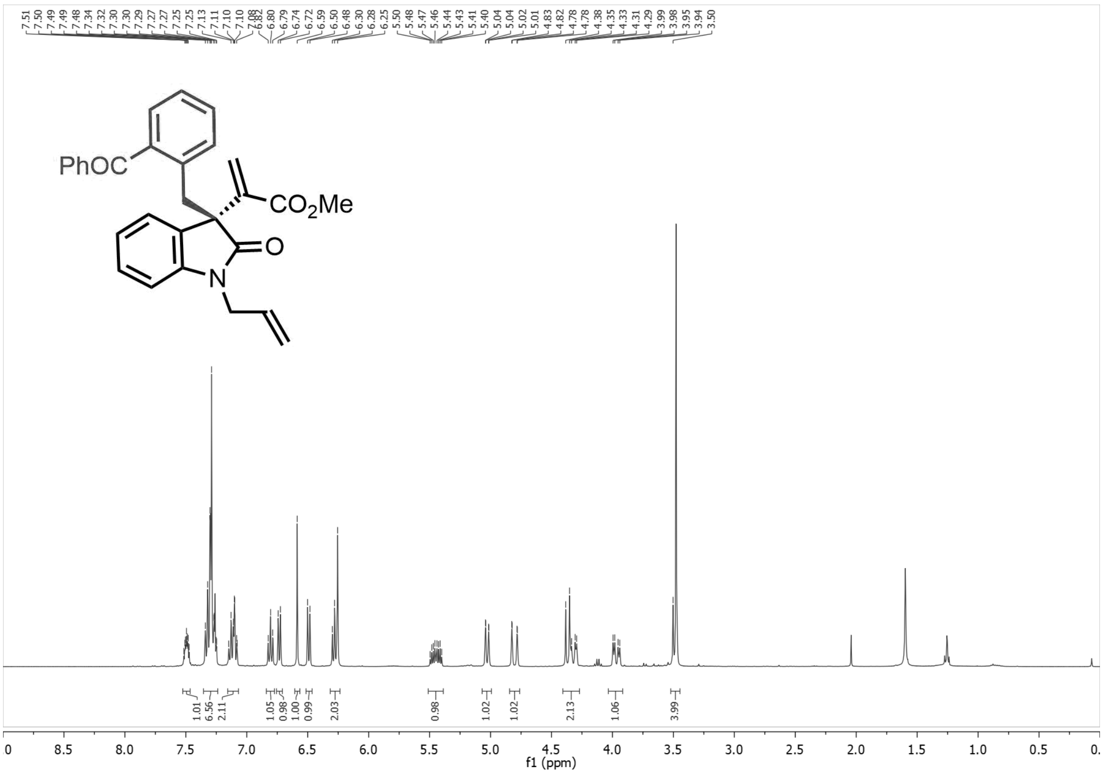
7.51 7.50 7.49 7.48 7.34 7.32 7.30 7.30 7.29 7.27 7.27 7.25 7.25 7.13 7.11 7.10 7.10 7.08 6.82 6.80 6.79 6.74 6.72 6.59 6.50 6.48 6.30 6.28 6.25 5.50 5.48 5.47 5.46 5.44 5.43 5.41 5.40 5.04 5.04 5.02 5.01 4.83 4.82 4.78 4.78 4.38 4.35 4.33 4.31 4.29 3.99 3.98 3.95 3.94 3.50
PhOC
CO2Me
O
N
1.01 6.56 2.11 1.05 0.98 1.00 0.99 2.03 0.98 1.02 1.02 2.13 1.06 3.99
8.5 8.0 7.5 7.0 6.5 6.0 5.5 5.0 4.5 4.0 3.5 3.0 2.5 2.0 1.5 1.0 0.5
f1 (ppm)

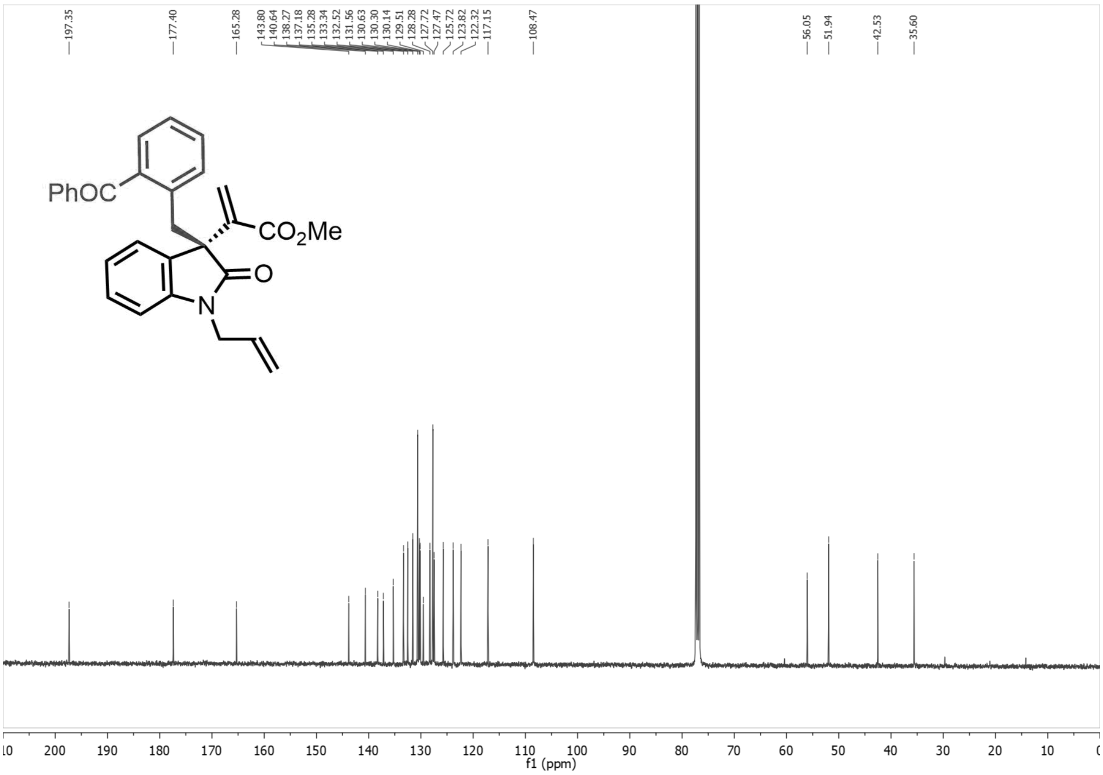
197.35 177.40 165.28 143.80 140.64 138.27 137.18 135.28 133.34 132.52 131.56 130.63 130.30 130.14 129.51 128.28 127.72 127.47 125.72 123.82 122.32 117.15 108.47 56.05 51.94 42.53 35.60
PhOC
CO2Me
O
N
200 190 180 170 160 150 140 130 120 110 100 90 80 70 60 50 40 30 20 10
f1 (ppm)

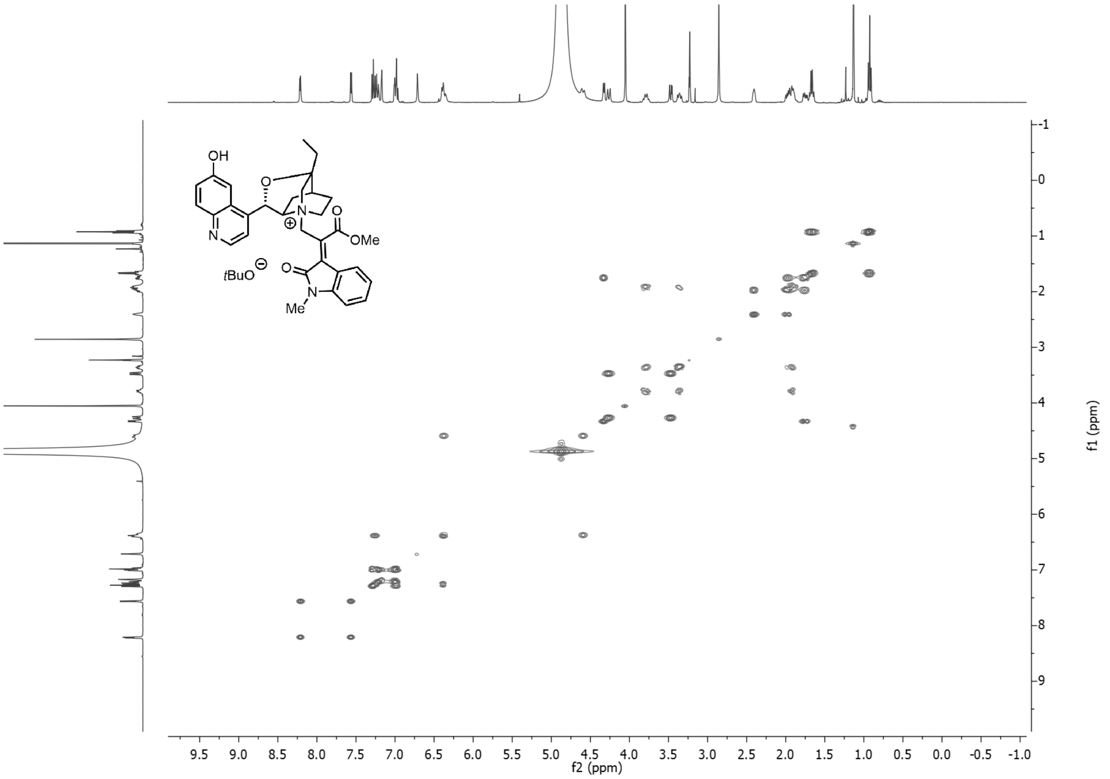

COSY experiment of **IIIa**

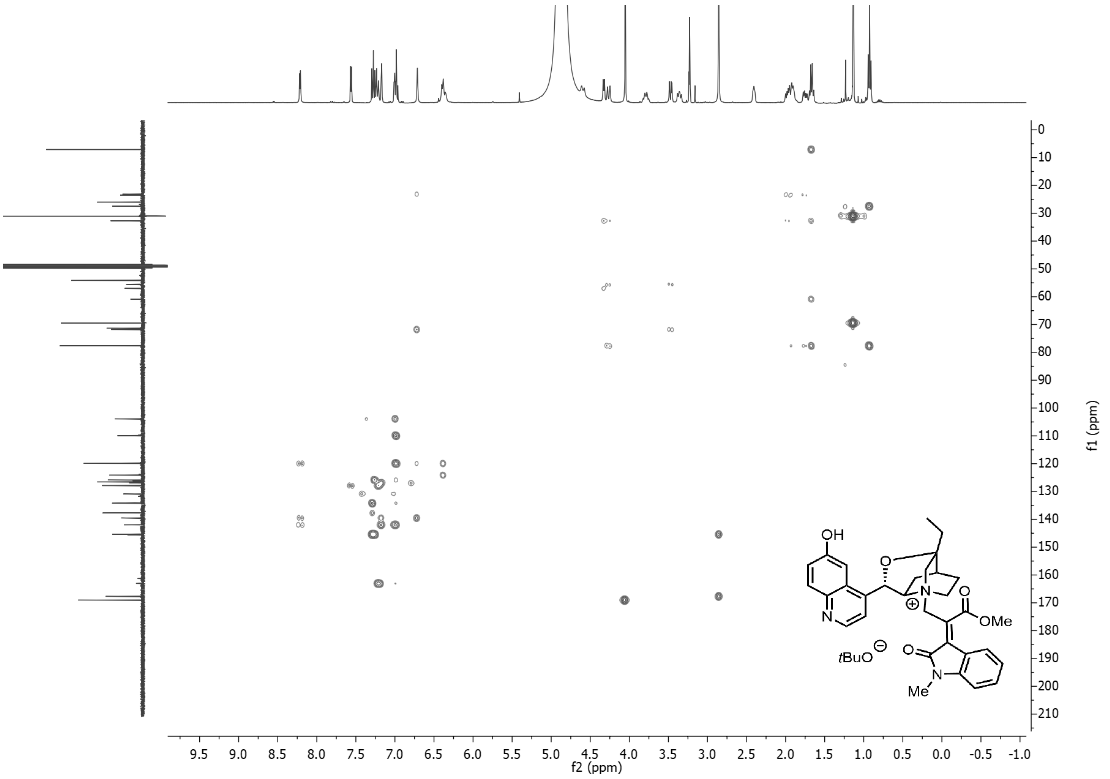

HMBC experiment of **IIIa**

4.11 HPLC Traces

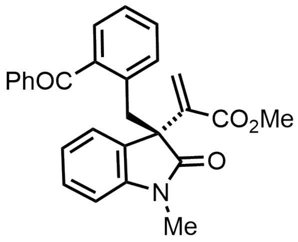

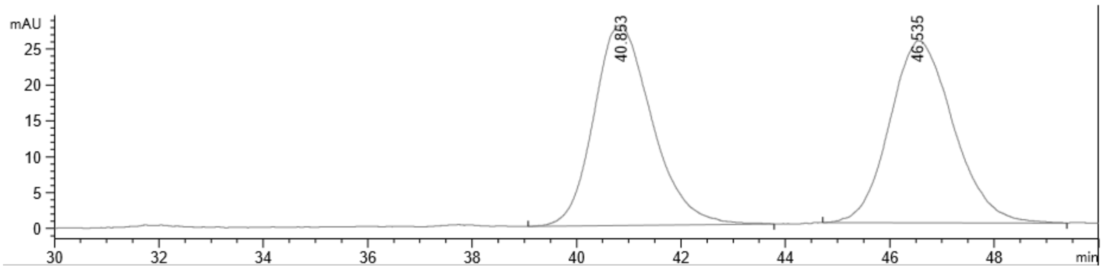

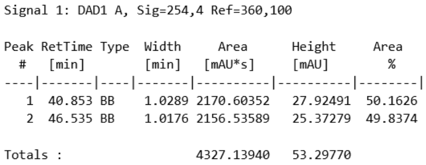

```
Signal 1: DAD1 A, Sig=254,4 Ref=360,100

Peak RetTime Type  Width     Area      Height     Area
  #   [min]        [min]   [mAU*s]     [mAU]        %
----|-------|----|-------|----------|----------|--------|
   1  40.853 BB    1.0289 2170.60352   27.92491  50.1626
   2  46.535 BB    1.0176 2156.53589   25.37279  49.8374

Totals :                  4327.13940   53.29770
```

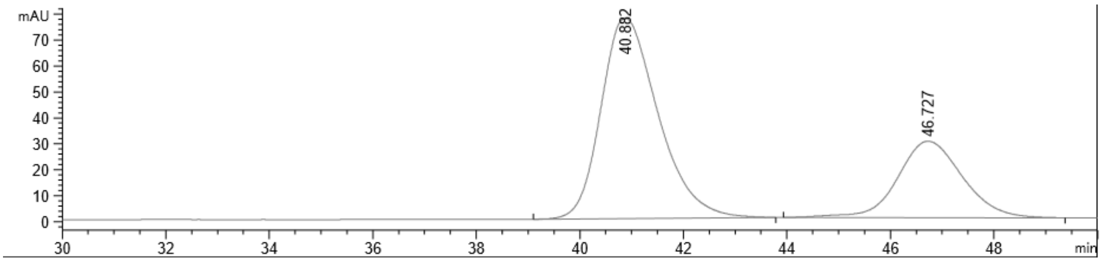

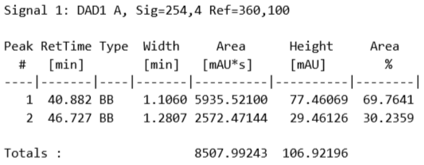

```
Signal 1: DAD1 A, Sig=254,4 Ref=360,100

Peak RetTime Type  Width     Area      Height     Area
  #   [min]        [min]   [mAU*s]     [mAU]        %
----|-------|----|-------|----------|----------|--------|
   1  40.882 BB    1.1060 5935.52100   77.46069  69.7641
   2  46.727 BB    1.2807 2572.47144   29.46126  30.2359

Totals :                  8507.99243  106.92196
```

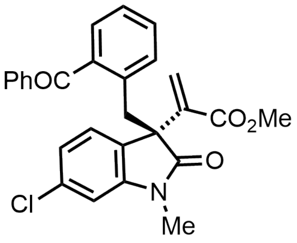

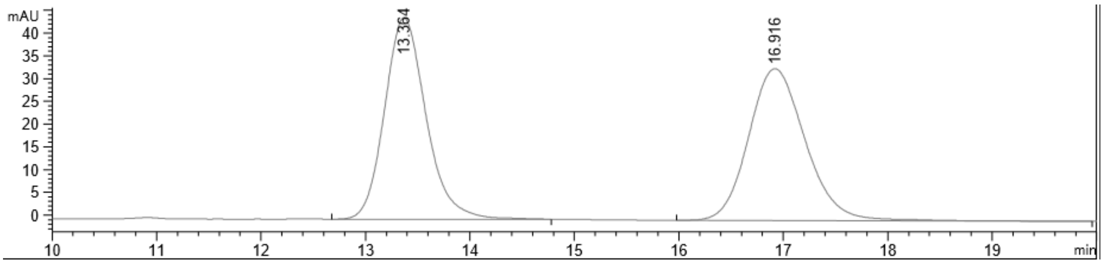

```
Signal 1: DAD1 A, Sig=254,4 Ref=360,100

Peak RetTime Type  Width     Area      Height     Area
  #   [min]        [min]   [mAU*s]     [mAU]        %
----|-------|----|-------|----------|----------|--------|
   1  13.364 BB    0.4238 1221.61768   44.29236  49.1867
   2  16.916 BB    0.5912 1262.01489   33.37462  50.8133

Totals :                  2483.63257   77.66698
```

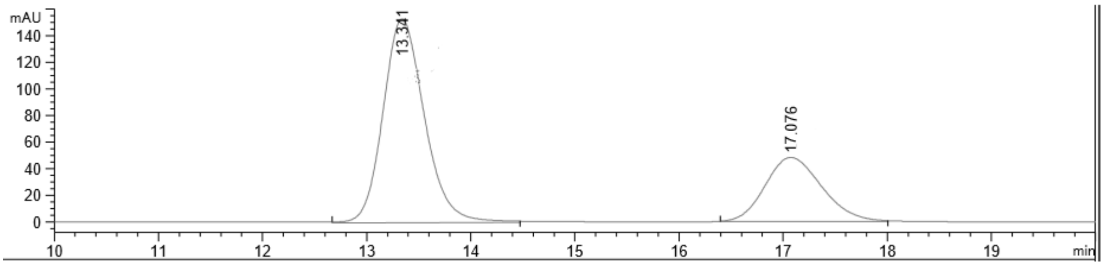

```
Signal 1: DAD1 A, Sig=254,4 Ref=360,100

Peak RetTime Type  Width     Area      Height     Area
  #   [min]        [min]   [mAU*s]     [mAU]        %
----|-------|----|-------|----------|----------|--------|
   1  13.341 MM    0.4613 4239.04736  153.15678  70.1062
   2  17.076 MM    0.6277 1807.55994   47.99307  29.8938

Totals :                  6046.60730  201.14986
```

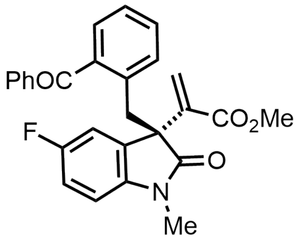

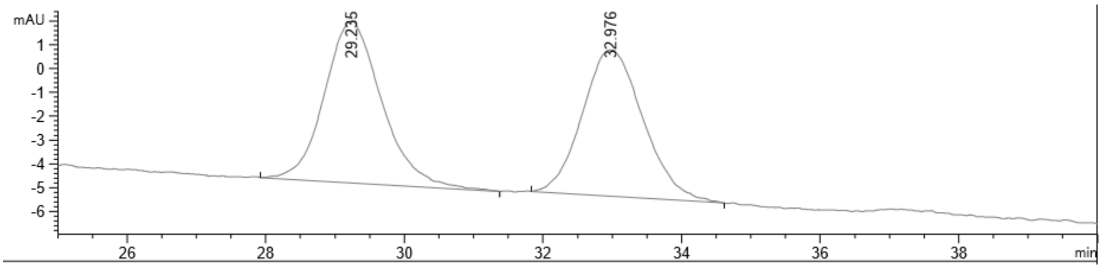

```
Signal 1: DAD1 A, Sig=254,4 Ref=360,100

Peak RetTime Type  Width     Area      Height     Area
  #   [min]        [min]   [mAU*s]     [mAU]       %
----|-------|----|-------|----------|----------|--------|
   1  29.235 BB    0.8374  391.40472    6.80111  51.0273
   2  32.976 BB    0.8350  375.64484    6.14667  48.9727

Totals :                   767.04956   12.94778
```

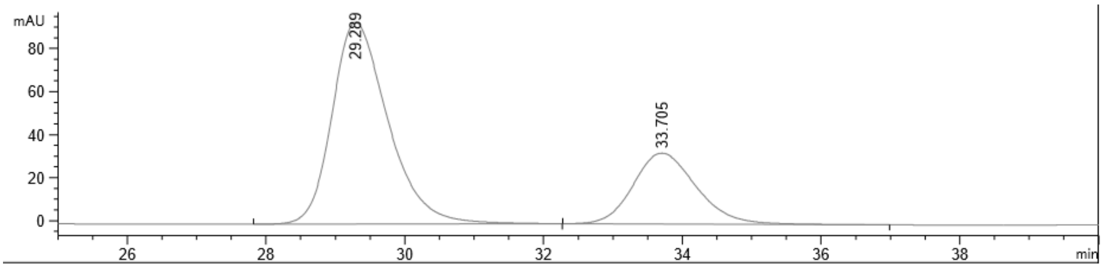

```
Signal 1: DAD1 A, Sig=254,4 Ref=360,100

Peak RetTime Type  Width     Area      Height     Area
  #   [min]        [min]   [mAU*s]     [mAU]       %
----|-------|----|-------|----------|----------|--------|
   1  29.289 BB    0.8552 5254.84521   93.85522  71.5620
   2  33.705 BB    0.9572 2088.22144   32.95712  28.4380

Totals :                  7343.06665  126.81234
```

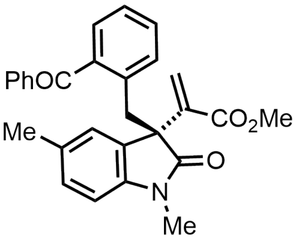

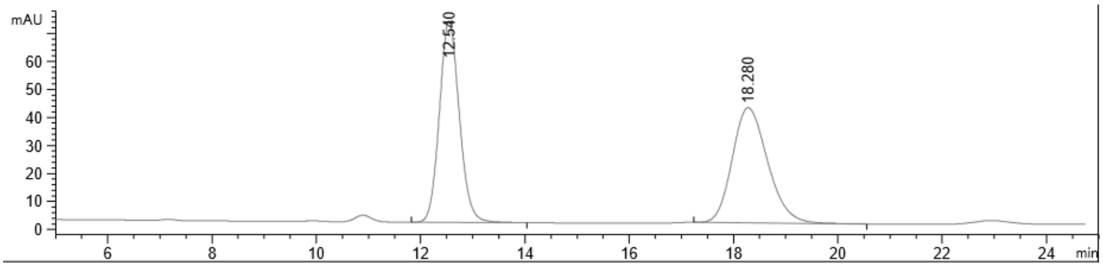

```
Signal 1: DAD1 A, Sig=254,4 Ref=360,100

Peak RetTime Type  Width     Area      Height     Area
  #   [min]        [min]   [mAU*s]     [mAU]       %
----|-------|----|-------|----------|----------|--------|
   1  12.540 BB    0.4103 1911.80835   71.87636  49.6427
   2  18.280 BB    0.7366 1939.32861   41.09378  50.3573

Totals :                  3851.13696  112.97014
```

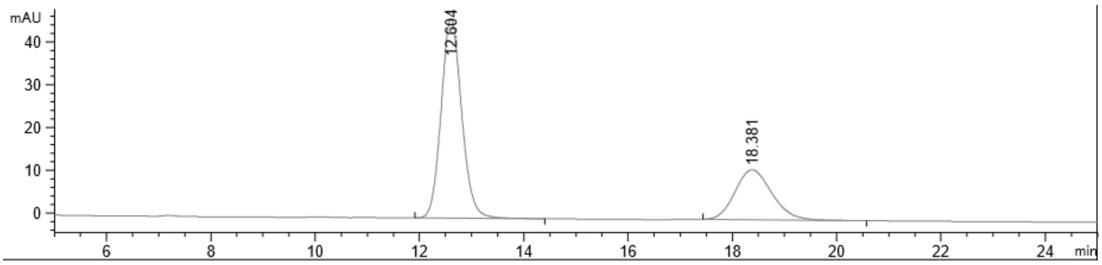

```
Signal 1: DAD1 A, Sig=254,4 Ref=360,100

Peak RetTime Type  Width     Area      Height     Area
  #   [min]        [min]   [mAU*s]     [mAU]       %
----|-------|----|-------|----------|----------|--------|
   1  12.604 BB    0.4237 1274.77075   46.52517  69.0034
   2  18.381 BB    0.7653  572.63123   11.65276  30.9966

Totals :                  1847.40198   58.17792
```

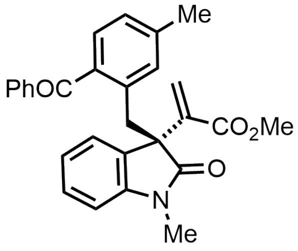

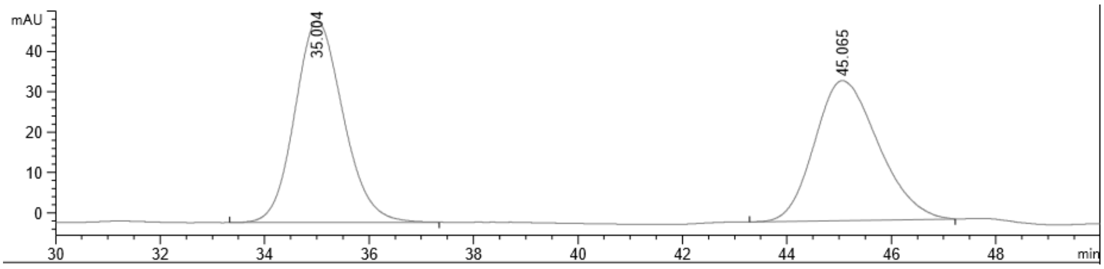

```
Signal 1: DAD1 A, Sig=254,4 Ref=360,100

Peak RetTime Type  Width     Area      Height     Area
  #   [min]        [min]   [mAU*s]     [mAU]        %
----|-------|----|-------|----------|----------|--------|
   1  35.004 BB    0.9789 3212.99292   49.92331  52.1703
   2  45.065 BB    1.1745 2945.67358   34.69617  47.8297

Totals :                  6158.66650   84.61947
```

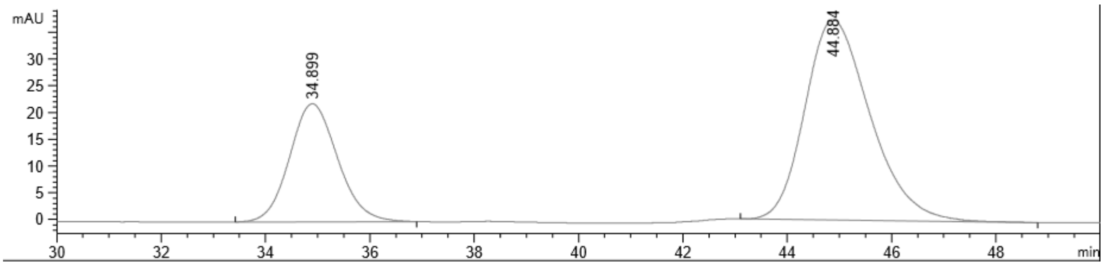

```
Signal 1: DAD1 A, Sig=254,4 Ref=360,100

Peak RetTime Type  Width     Area      Height     Area
  #   [min]        [min]   [mAU*s]     [mAU]        %
----|-------|----|-------|----------|----------|--------|
   1  34.899 BB    0.9497 1415.66064   22.08766  30.2489
   2  44.884 BB    1.3253 3264.38184   37.43648  69.7511

Totals :                  4680.04248   59.52414
```

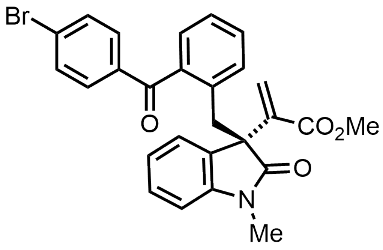

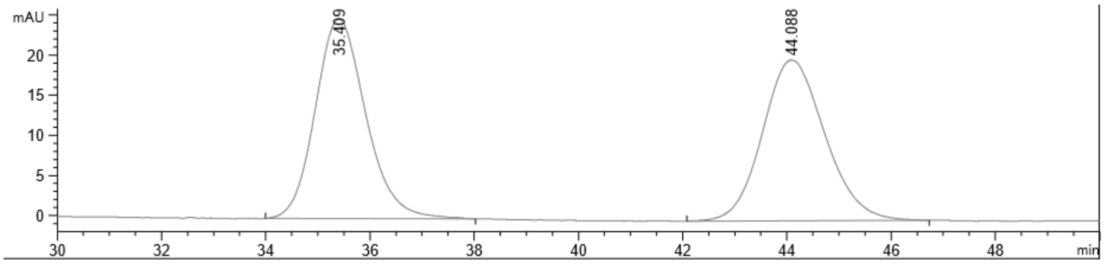

```
Signal 1: DAD1 A, Sig=254,4 Ref=360,100

Peak RetTime Type  Width     Area      Height     Area
  #   [min]        [min]   [mAU*s]     [mAU]        %
----|-------|----|-------|----------|----------|--------|
   1  35.409 BB    0.9943 1681.88196   24.95560  50.1287
   2  44.088 BB    1.1634 1673.24414   20.05376  49.8713

Totals :                  3355.12610   45.00936
```

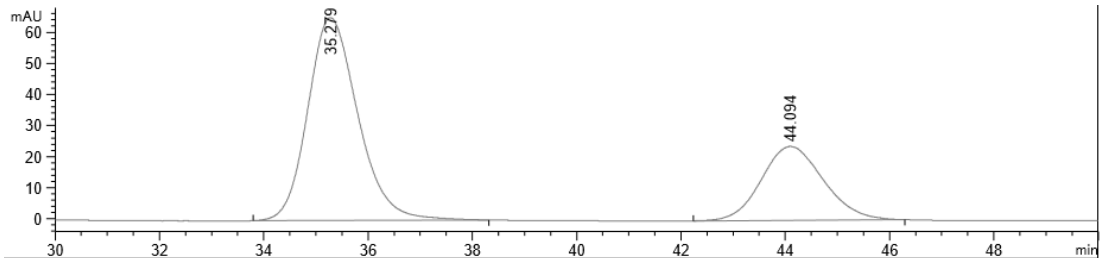

```
Signal 1: DAD1 A, Sig=254,4 Ref=360,100

Peak RetTime Type  Width     Area      Height     Area
  #   [min]        [min]   [mAU*s]     [mAU]        %
----|-------|----|-------|----------|----------|--------|
   1  35.279 BB    1.0071 4370.07813   65.27428  68.9522
   2  44.094 BB    1.1609 1967.76135   23.79143  31.0478

Totals :                  6337.83948   89.06572
```

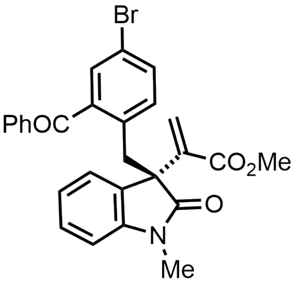

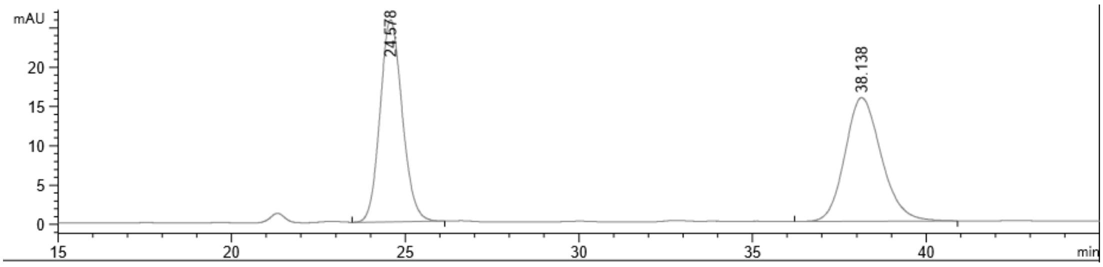

```
Signal 1: DAD1 A, Sig=254,4 Ref=360,100

Peak RetTime Type  Width     Area      Height     Area
  #   [min]        [min]   [mAU*s]     [mAU]        %
----|-------|----|-------|----------|----------|--------|
   1  24.578 BB    0.6584 1141.74390   25.69363  49.9291
   2  38.138 BB    1.0206 1144.98779   15.74059  50.0709

Totals :                  2286.73169   41.43422
```

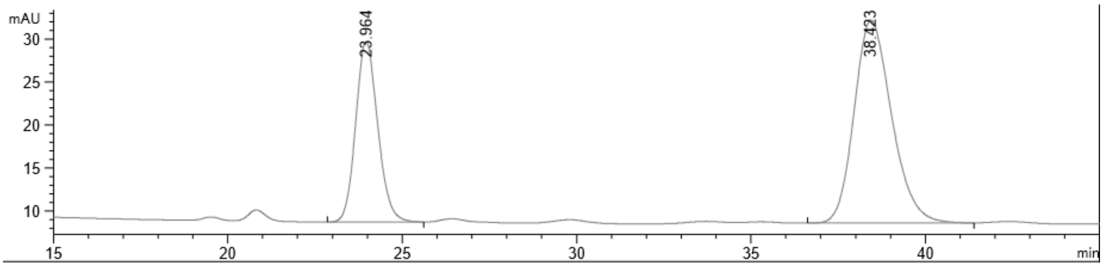

```
Signal 1: DAD1 A, Sig=254,4 Ref=360,100

Peak RetTime Type  Width     Area      Height     Area
  #   [min]        [min]   [mAU*s]     [mAU]        %
----|-------|----|-------|----------|----------|--------|
   1  23.964 BB    0.6808  924.30701   20.94804  34.3835
   2  38.423 BB    0.9852 1763.92322   23.62043  65.6165

Totals :                  2688.23022   44.56846
```

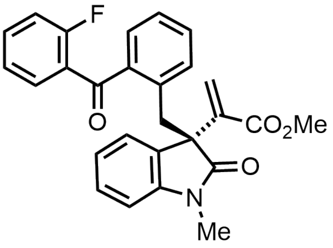

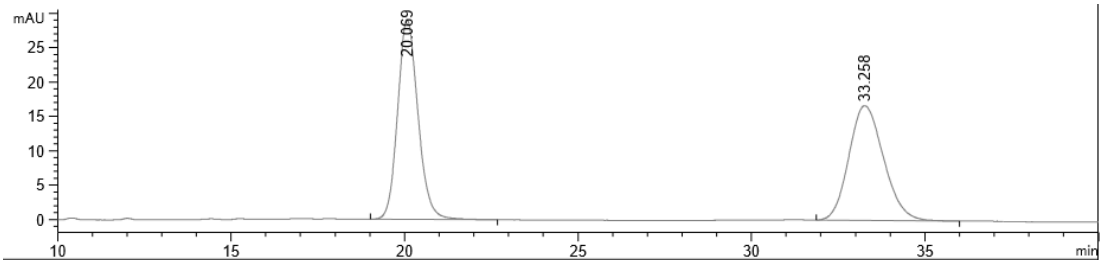

```
Signal 1: DAD1 A, Sig=254,4 Ref=360,100

Peak RetTime Type  Width     Area      Height     Area
  #   [min]        [min]   [mAU*s]     [mAU]        %
----|-------|----|-------|----------|----------|--------|
   1  20.069 BB    0.6304 1187.71082   29.08329  50.4956
   2  33.258 BB    1.0637 1164.39771   16.69535  49.5044

Totals :                  2352.10852   45.77864
```

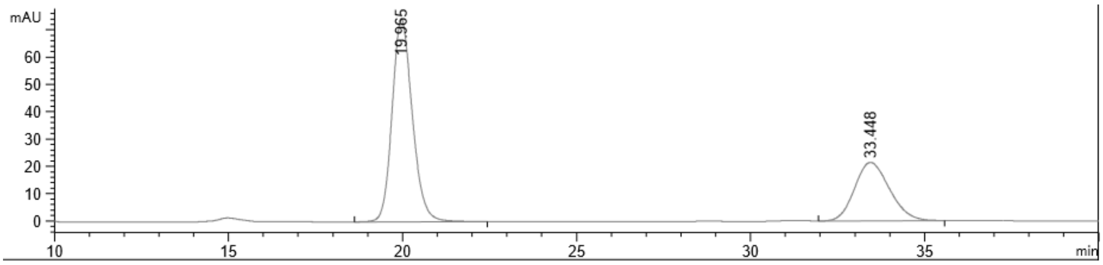

```
Signal 1: DAD1 A, Sig=254,4 Ref=360,100

Peak RetTime Type  Width     Area      Height     Area
  #   [min]        [min]   [mAU*s]     [mAU]        %
----|-------|----|-------|----------|----------|--------|
   1  19.965 BB    0.6156 3008.31372   74.41463  66.8549
   2  33.448 BB    1.0463 1491.45032   21.36810  33.1451

Totals :                  4499.76404   95.78273
```

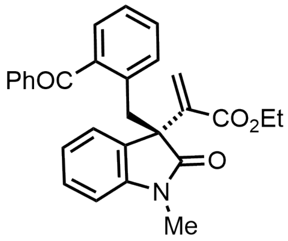

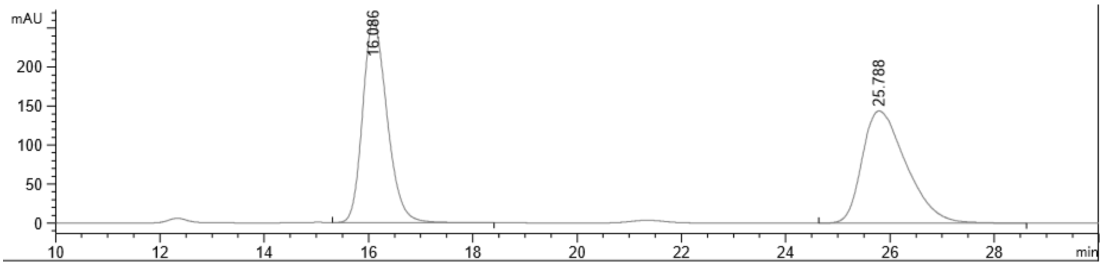

```
Signal 1: DAD1 A, Sig=254,4 Ref=360,100

Peak RetTime Type  Width     Area      Height     Area
  #   [min]        [min]   [mAU*s]     [mAU]        %
----|-------|----|-------|----------|----------|--------|
   1  16.086 BB    0.5101 8434.07129  260.27405  49.9872
   2  25.788 BB    0.7636 8438.38281  144.02235  50.0128

Totals :                  1.68725e4   404.29640
```

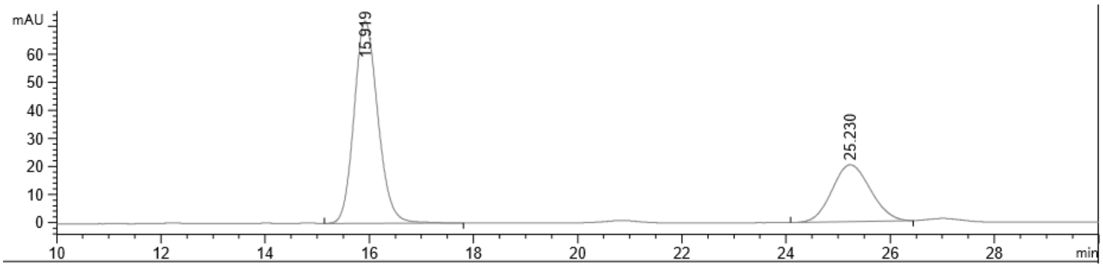

```
Signal 1: DAD1 A, Sig=254,4 Ref=360,100

Peak RetTime Type  Width     Area      Height     Area
  #   [min]        [min]   [mAU*s]     [mAU]        %
----|-------|----|-------|----------|----------|--------|
   1  15.919 BB    0.4920 2288.85938   72.18044  68.7630
   2  25.230 BB    0.7938 1039.76160   20.29088  31.2370

Totals :                  3328.62097   92.47132
```

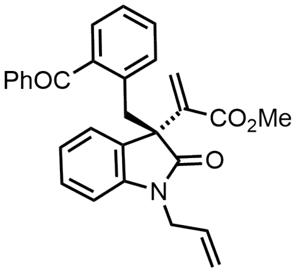

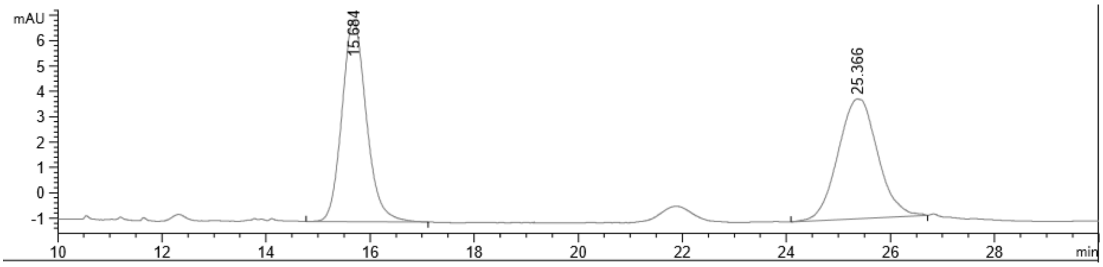

```
Signal 1: DAD1 A, Sig=254,4 Ref=360,100

Peak RetTime Type  Width     Area      Height     Area
  #   [min]        [min]   [mAU*s]     [mAU]        %
----|-------|----|-------|----------|----------|--------|
   1  15.684 BB    0.5050  260.16006    7.96574  50.9707
   2  25.366 BB    0.7218  250.25070    4.72569  49.0293

Totals :                   510.41077   12.69143
```

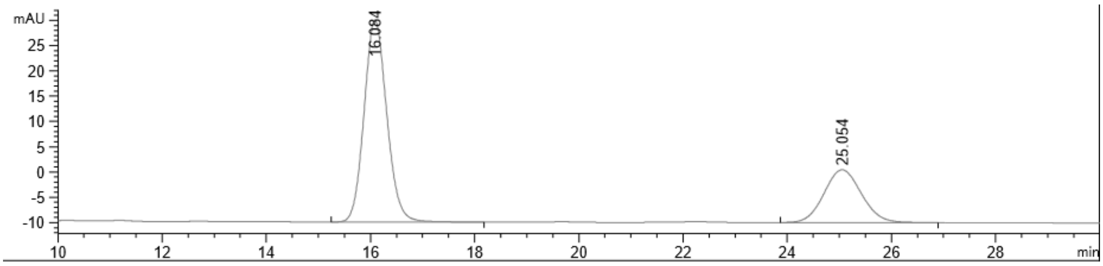

```
Signal 1: DAD1 A, Sig=254,4 Ref=360,100

Peak RetTime Type  Width     Area      Height     Area
  #   [min]        [min]   [mAU*s]     [mAU]        %
----|-------|----|-------|----------|----------|--------|
   1  16.084 BB    0.4677 1212.86743   40.00750  69.9291
   2  25.054 BB    0.7692  521.55707   10.43426  30.0709

Totals :                  1734.42450   50.44176
```

References

(1) Prudhomme, M., *Advances in Anticancer Agents in Medicinal Chemistry*; Bentham Science Publishers: 2013.

(2) Varun; Sonam; Kakkar, R. *Med. Chem. Commun.* **2019**, *10*, 351–368.

(3) Stalder, R.; Mei, J.; Graham, K. R.; Estrada, L. A.; Reynolds, J. R. *Chemistry of Materials* **2014**, *26*, 664–678.

(4) Liu, X.-L.; Jing, D.-H.; Yao, Z.; Zhang, W.-H.; Liu, X.-W.; Yang, Z.-J.; Zhao, Z.; Zhou, Y.; Li, X.-N. *Tetrahedron Letters* **2015**, *56*, 5637 –5645.

(5) Zhou, F.; Liu, Y.-L.; Zhou, J. *Advanced Synthesis & Catalysis* **2010**, *352*, 1381–1407.

(6) Lovering, F.; Bikker, J.; Humblet, C. *Journal of Medicinal Chemistry* **2009**, *52*, 6752–6756.

(7) Clayden, J.; Greeves, N.; Warren, S., *Organic Chemistry*; OUP Oxford: 2012.

(8) Heravi, M. M.; Dehghani, M.; Zadsirjan, V. *Tetrahedron: Asymmetry* **2016**, *27*, 513 –588.

(9) Taussig, H. B.; Baltimore, M. D. *JAMA* **1962**, *180*, 1106–1114.

(10) Dalko, P. I.; Moisan, L. *Angewandte Chemie International Edition* **2004**, *43*, 5138–5175.

(11) Bredig, G; Fiske, P. *Biochem. Z* **1912**, *46*.

(12) Melchiorre, P.; Marigo, M.; Carlone, A.; Bartoli, G. *Angewandte Chemie International Edition* **2008**, *47*, 6138–6171.

(13) Hajos, Z. G.; Parrish, D. R. *The Journal of Organic Chemistry* **1974**, *39*, 1615–1621.

(14) Eder, U.; Sauer, G.; Wiechert, R. *Angewandte Chemie International Edition in English* **1971**, *10*, 496–497.

(15) List, B.; Lerner, R. A.; Barbas, C. F. *Journal of the American Chemical Society* **2000**, *122*, 2395–2396.

(16) Ahrendt, K. A.; Borths, C. J.; MacMillan, D. W. *Journal of the American Chemical Society* **2000**, *122*, 4243–4244.

(17) MacMillan, D. W. C. *Nature* **2008**, *455*, 304—308.

(18) Abbasov, M. E.; Romo, D. *Nat. Prod. Rep.* **2014**, *31*, 1318–1327.

(19) Palumbo, C.; Guidotti, M. *ScienceOpen Research* **2015**, 1–14.

(20) Doyle, A. G.; Jacobsen, E. N. *Chemical Reviews* **2007**, *107*, 5713–5743.

(21) Hoffmann, H. M. R.; Frackenpohl, J. *European Journal of Organic Chemistry* **2004**, *2004*, 4293–4312.

(22) Marcelli, T.; van Maarseveen, J. H.; Hiemstra, H. *Angewandte Chemie International Edition* **2006**, *45*, 7496–7504.

(23) Tsuji, J.; Takahashi, H.; Morikawa, M. *Tetrahedron Letters* **1965**, *6*, 4387 –4388.

(24) Trost, B. M.; Fullerton, T. J. *Journal of the American Chemical Society* **1973**, *95*, 292–294.

(25) Trost, B. M.; Strege, P. E. *Journal of the American Chemical Society* **1977**, *99*, 1649–1651.

(26) Trost, B. M.; Van Vranken, D. L. *Chemical Reviews* **1996**, *96*, 395–422.

(27) Kim, J. N.; Lee, H. J.; Gong, J. H. *Tetrahedron Letters* **2002**, *43*, 9141–9146.

(28) Cho, C.-W.; Kong, J.-R.; Krische, M. J. *Organic Letters* **2004**, *6*, 1337–1339.

(29) Chung, Y. M.; Gong, J. H.; Kim, T. H.; Kim, J. N. *Tetrahedron Letters* **2001**, *42*, 9023 –9026.

(30) Peng, J.; Huang, X.; Cui, H.-L.; Chen, Y.-C. *Organic Letters* **2010**, *12*, 4260–4263.

(31) Kamlar, M.; Císařová, I.; Hybelbauerová, S.; Veselý, J. *European Journal of Organic Chemistry* **2017**, *2017*, 1926–1930.

(32) Zhao, S.; Chen, Z.-L.; Rui, X.; Gao, M.-M.; Chen, X. *Synlett* **2019**, *30*, 703–708.

(33) Rios, R. *Catalysis Science & Technology* **2012**, *2*, 267–278.

(34) Wang, B.; Companyó, X.; Li, J.; Moyano, A.; Rios, R. *Tetrahedron Letters* **2012**, *53*, 4124 –4129.

(35) Ceban, V.; Tauchman, J.; Meazza, M.; Gallagher, G.; Light, M. E.; Gergelitsová, I.; Veselỳ, J.; Rios, R. *Scientific reports* **2015**, *5*, 16886.

(36) Zhu, D.; Lv, L.; Li, C.-C.; Ung, S.; Gao, J.; Li, C.-J. *Angewandte Chemie International Edition* **2018**, *57*, 16520–16524.

(37) Mao, J.; Zhang, J.; Jiang, H.; Bellomo, A.; Zhang, M.; Gao, Z.; Dreher, S. D.; Walsh, P. J. *Angewandte Chemie International Edition* **2016**, *55*, 2526–2530.

(38) Wardle, B., *Principles and Applications of Photochemistry*; Wiley: 2009.

(39) Ciamician, G. *Science* **1912**, *36*, 385–394.

(40) Ravelli, D.; Protti, S.; Fagnoni, M. *Chemical Reviews* **2016**, *116*, 9850–9913.

(41) Albini, A.; Fagnoni, M., *Photochemically- generated intermediates in synthesis*; Wiley: 2013, pp 1–372.

(42) Yang, N. C.; Rivas, C. *Journal of the American Chemical Society* **1961**, *83*, 2213–2213.

(43) Nicolaou, K. C.; Gray, D.; Tae, J. *Angewandte Chemie International Edition* **2001**, *40*, 3675–3678.

(44) Masuda, Y.; Ishida, N.; Murakami, M. *Journal of the American Chemical Society* **2015**, *137*, 14063–14066.

(45) Dell'Amico, L.; Vega-Peñaloza, A.; Cuadros, S.; Melchiorre, P. *Angewandte Chemie International Edition* **2016**, *55*, 3313–3317.

(46) Dell'Amico, L.; Fernández-Alvarez, V. M.; Maseras, F.; Melchiorre, P. *Angewandte Chemie International Edition* **2017**, *56*, 3304–3308.

(47) Yuan, X.; Dong, S.; Liu, Z.; Wu, G.; Zou, C.; Ye, J. *Organic Letters* **2017**, *19*, 2322–2325.

(48) Hepburn, H. B.; Magagnano, G.; Melchiorre, P. *Synthesis* **2017**, *49*, 76–86.

(49) Cuadros, S.; Dell'Amico, L.; Melchiorre, P. *Angewandte Chemie International Edition* **2017**, *56*, 11875–11879.

(50) Plutschack, M. B.; Pieber, B.; Gilmore, K.; Seeberger, P. H. *Chemical Reviews* **2017**, *117*, 11796–11893.

(51) Cambié, D.; Bottecchia, C.; Straathof, N. J. W.; Hessel, V.; Noël, T. *Chemical Reviews* **2016**, *116*, 10276–10341.

(52) Mateos, J.; Cherubini-Celli, A.; Carofiglio, T.; Bonchio, M.; Marino, N.; Companyó, X.; Dell'Amico, L. *Chem. Commun.* **2018**, *54*, 6820–6823.

(53) Mateos, J.; Rigodanza, F.; Vega, A.; Sartorel, A.; Natali, M.; Bortolato, T.; Pelosi, G.; Companyo, X.; Bonchio, M.; Dell'Amico, L. *Angewandte Chemie International Edition*, *n/a*, just accepted.

(54) Mato, R.; Manzano, R.; Reyes, E.; Carrillo, L.; Uria, U.; Vicario, J. L. *Journal of the American Chemical Society* **2019**, *141*, 9495–9499.

(55) Chen, G.-Y.; Zhong, F.; Lu, Y. *Organic Letters* **2012**, *14*, 3955–3957.

(56) Zhang, H.; Zhang, S.-J.; Zhou, Q.-Q.; Dong, L.; Chen, Y.-C. *Beilstein Journal of Organic Chemistry* **2012**, *8*, 1241–1245.

(57) Baidya, M.; Remennikov, G.; Mayer, P.; Mayr, H. *Chemistry – A European Journal* **2010**, *16*, 1365–1371.

(58) Mueller, P.; Zieger, M. M.; Richter, B.; Quick, A. S.; Fischer, J.; Mueller, J. B.; Zhou, L.; Nienhaus, G. U.; Bastmeyer, M.; Barner-Kowollik, C.; Wegener, M. *ACS Nano* **2017**, *11*, 6396–6403.

(59) Du, Y.; Yu, A.; Jia, J.; Zhang, Y.; Meng, X. *Chem. Commun.* **2017**, *53*, 1684–1687.

(60) Liu, Y.-Y.; Duan, S.-W.; Zhang, R.; Liu, Y.-H.; Chen, J.-R.; Xiao, W.-J. *Org. Biomol. Chem.* **2016**, *14*, 5224–5228.

(61) Gui, J.; Chen, G.; Cao, P.; Liao, J. *Tetrahedron: Asymmetry* **2012**, *23*, 554–563.

(62) Liao, Y.-Y.; Gao, Y.-C.; Zheng, W.; Tang, R.-Y. *Advanced Synthesis & Catalysis* **2018**, *360*, 3391–3400.

(63) Zhang, Y.; Luo, L.; Ge, J.; Yan, S.-Q.; Peng, Y.-X.; Liu, Y.-R.; Liu, J.-X.; Liu, C.; Ma, T.; Luo, H.-Q. *The Journal of Organic Chemistry* **2019**, *84*, 4000–4008.

(64) Ilangovan, A.; Satish, G. *The Journal of Organic Chemistry* **2014**, *79*, 4984–4991.

(65) Fan, X.; Yang, H.; Shi, M. *Advanced Synthesis & Catalysis* **2017**, *359*, 49–57.

(66) Wu, L.; Zhang, Q.-R.; Huang, J.-R.; Li, Y.; Su, F.; Dong, L. *Tetrahedron* **2017**, *73*, 3966 –3972.

(67) Min, B. K.; Seo, D. Y.; Ryu, J. Y.; Lee, J.; Kim, J. N. *Bulletin of the Korean Chemical Society* **2018**, *39*, 115–118.

(68) Dong, Z.; Yan, C.; Gao, Y.; Dong, C.; Qiu, G.; Zhou, H.-B. *Advanced Synthesis & Catalysis* **2015**, *357*, 2132–2142.

(69) Vaithiyanathan, V.; Ravichandran, G.; Thirumailavan, V. *Tetrahedron Letters* **2019**, *60*, 507 –510.

(70) Garden, S.; Skakle, J. *Tetrahedron Letters* **2002**, *43*, 1969–1972.

(71) Min, B. K.; Lee, S.; Roh, H. J.; Ryu, J. Y.; Lee, J.; Kim, J. N. *Tetrahedron Letters* **2017**, *58*, 3251 –3255.

Acknowledgements

Il percorso che ho intrapreso cinque anni fa non è mai stato una passeggiata. Ho spesso avuto dubbi sulle mie capacità (e li ho tuttora), ma alla fine ce l'ho fatta: sono arrivata all'ultima pagina. Perciò la voglio dedicare a tutte le persone che mi hanno accompagnata, aiutata, incoraggiata a dare sempre il meglio di me in questi cinque anni in cui sono diventata un po' più esperta in chimica, pur restando l'idiota di sempre.

Il mio primo grazie va al gruppo NanoMolCat che mi ha accolta e mi ha resa partecipe dei loro innumerevoli progetti (non solo di ricerca): grazie al mio relatore Luca per essere stato sempre presente e disponibile, grazie ad *amazing* Suva, per il suo entusiasmo e i preziosi consigli, grazie al mio dolcissimo compagno di cappa "pinche" Alberto e alle canzoni mariachi, a Javi, il connubio perfetto di genio e follia, per avere sempre la risposta giusta, al mio compagno di sventure Carletto, alla mia spalla Pietro, a Tommi che è il Clayden ma con il dono della parola, a Francesco Rigodanza (scritto bene) e Domenico Bini, a Philip e le sue playlist da laboratorio, al mio erede Alessio per avermi fatto sbellicare dalle risate. Ultimo, il migliore di tutti: Xavi, che con gli stornelli cantati alle reazioni (100% metodo scientifico) e le chiacchirate motivazionali, si è preso cura di me e del mio progetto nonostante i suoi mille impegni. Grazie anche per avermi corretto la tesi nonostante la mia ostinazione a scrivere in Latex, "perché è più elegante".

Un grazie ancora più grande va ai miei sponsor ufficiali dal 1995, nonché miei più grandi fan: la mia famiglia, che mi ha sempre dato supporto e fiducia incondizionati, anche da lontano, anche nonostante le mie rare dimostrazioni di affetto e la mia scarsa inclinazione a farmi viva ogni tanto. Mamma, papà, mio fratello, le nonne, gli zii: nessuno sa esattamente cosa sto facendo, ma sono tutti fieri di me. Grazie per essere sempre pronti a darmi una mano, anche (soprattutto) quando penso di potercela fare da sola.

Un grazie lo devo anche a Silvia e Silvia che mi conoscono e mi sostengono da una vita e che rendono Conegliano un posto un po' più interessante; un grazie a tutti gli amici e coinquilini di cinque anni padovani e agli amici dell'Erasmus perché ora, ovunque vada nel mondo, potrò sentirmi quasi come a casa mia.

Infine, gran parte del mio successo accademico è dovuto a quella strana accozzaglia di compagni di corso che, cinque anni or sono, hanno scoperto che stare insieme era estremamente divertente. A qualsiasi ora del giorno e della notte. È così che sono nati gli Alchimisti Anonimi, che in questi cinque anni sono cresciuti e si sono arricchiti di nuovi compagni di studio, spritz, pause pranzo e vacanze memorabili. Grazie a voi ora vanto delle impareggiabili e assolutamente spendibili soft skills in trash, meme, tressette, spritz e alta cucina. Grazie, perché avete reso questi cinque anni padovani un'avventura unica e indimenticabile.

Michi